Progress in Aerospace Sciences 138 (2023) 100897

Contents lists available at ScienceDirect

Progress in Aerospace Sciences

journal homepage: www.elsevier.com/locate/paerosci

Advancements and prospects of boundary layer ingestion propulsion concepts

Nicolas G.M. Moirou [*,1], Drewan S. Sanders[2], Panagiotis Laskaridis[3]

Centre for Propulsion and Thermal Power Engineering, Cranfield University, Cranfield, MK43 0AL, United Kingdom

ARTICLE INFO

Keywords:
Boundary layer ingestion
Conceptual aircraft
Distributed propulsion
Engine-airframe integration
Performance accounting
Propulsive fuselage

ABSTRACT

The aviation sector is experiencing an increasing pressure to reduce emissions via long-term strategies for a ceaselessly growing number of flight passengers. Aircraft currently in operation have typically been designed by considering the airframe somewhat separately from the propulsion system. In doing so, conventional aero-engine architectures are approaching their limits in terms of propulsive efficiency, with technological advancements yielding diminishing returns. A promising alternative architecture for improving the overall performance of the next generation of commercial aircraft relies upon boundary layer ingestion (BLI). This technology aerodynamically couples the airframe with a strategically positioned propulsion system to purposely ingest the airframe's boundary layer flow. Nonetheless, there is a lack in consensus surrounding the interpretation and quantification of BLI benefits. This is primarily because conventional performance accounting methods breakdown in scenarios of strong aerodynamic coupling. Subsequently, there is a major challenge in defining appropriate performance metrics to provide a consistent measurement and comparison of the potential benefits. This review examines the various accounting methods and metrics that have been applied in evaluating BLI performance. These are discussed and critiqued in the context of both numerical and experimental models. Numerically, the geometric, aerodynamic and propulsive models are sorted by their orders of fidelity along with the plenitude of methods used for flow feature identification enabling a phenomenological understanding of BLI. Particular attention is then given to experimental BLI models with their different set-ups, methods and associated limitations and uncertainties. Finally, the numerous unconventional BLI aircraft concepts are categorised, compared and critiqued with reference to their associated design exploration and optimisation studies.

1. Introduction

Turbojet engines and their development initiated back in the 1930s with Frank Whittle and Hans von Ohain whose latter, contributed to the first turbojet-propelled aircraft, the Heinkel He 178, in 1939 after the conception of his continuous cycle combustion engine. Through the years, the position, size and shape of the turbojets evolved into more capable and powerful engines before the introduction of the turbofan concept as a means to greater fuel efficiency. These engines continue to be the workhorse of modern day commercial aviation but the improvements in propulsive efficiency enabled by ingesting greater amounts of mass-flow enlarges the fan diameter and ipso facto increases the weight and drag of the aircraft.

Despite their constant technological advancements, diminishing returns have been achieved [1]. In addition, the ceaseless growth in passengers necessitates the civil aerospace industry to pay heed to aircraft emissions. To respond to this demand and to lean towards more sustainable strategies, stringent regulations are emerging. The European Commission (E.C.), National Aeronautics and Space Administration (NASA) and the European Union Aviation Safety Agency (EASA) have set different targets [2–7] to drastically reduce the fuel consumption and emissions whilst enhancing acoustic performance. A summary of these strategies and goals are given in Table 1 whereof CO_2 and noise emissions reductions of *only* 38 and 37%, respectively, were achieved by 2015. Whilst this represents significant progress compared to an aircraft from 2000, efforts must be strengthened to meet the challenging goals set for 2050.

To achieve these ambitious objectives, it is notwithstanding that revolutionary aircraft concepts are necessary, whereby the pursuit of

* Corresponding author.
E-mail addresses: nicolas.g.moirou@cranfield.ac.uk (N.G.M. Moirou), d.s.sanders@cranfield.ac.uk (D.S. Sanders), p.laskaridis@cranfield.ac.uk (P. Laskaridis).
[1] Ph.D. Researcher.
[2] Research Fellow.
[3] Professor.

https://doi.org/10.1016/j.paerosci.2023.100897
Received 16 November 2022; Received in revised form 20 February 2023; Accepted 23 February 2023
Available online 23 March 2023
0376-0421/© 2023 The Author(s). Published by Elsevier Ltd. This is an open access article under the CC BY license (http://creativecommons.org/licenses/by/4.0/).

Nomenclature

Abbreviations

AD	Actuator Disc
ARF	Absolute Reference Frame
BC	Boundary Condition
BFM	Body-Force Model
BLI	Boundary Layer Ingestion
BPR	By-Pass Ratio
BWB	Blended-Wing Body
CDI	Circumferential Distortion Index
CFD	Computational Fluid Dynamics
CV	Control Volume
DPC	Disruptive Propulsive Concept
EIS	Entry-Into-Service
EWC	Exergy Waste Coefficient
FPR	Fan Pressure Ratio
HWB	Hybrid-Wing Body
IPR	Intake Pressure Recovery
NPF	Net Propulsive Force
NVF	Net Vehicle Force
ORFEC	Over- and Rear-Fuselage Engines Concept
PER	Potential for Energy Recovery
PFC	Propulsive Fuselage Concept
PIV	Particle Image Velocimetry
PSC	Power Saving Coefficient
RDI	Radial Distortion Index
RRF	Relative Reference Frame
TeDP	Turbo-electric Distributed Propulsion
TS	Thrust-Split
TSFC	Thrust-Specific Fuel Consumption

Greek Symbols

ζ	Shock wave identifier, –
η	Efficiency, –
Θ	Rate of volumetric pressure work, J s^{-1}
θ	Force in the thrust domain, N
μ	Dynamic viscosity, Pa s
ξ	Shear-layer identifier, –
ρ	Density, kg m^{-3}
$\overline{\overline{\tau}}$	Viscous stress tensor, Pa
Υ	Jet-plume identifier, –
Φ	Rate of volumetric viscous dissipation, J s^{-1}
ϕ	Force in the drag domain, N
Ψ	Surfacic force, N
Ω	Flux force, N

Roman Symbols

$\dot{\mathcal{A}}_{tot}$	Rate of total anergy generation, J s^{-1}
$\mathcal{D}$	Drag, N
e	Mass-specific internal energy, J kg^{-1}
$\dot{\mathcal{E}}_m$	Rate of mechanical energy, J s^{-1}
$\dot{\mathcal{E}}_p$, $\dot{E}_p$	Rate of pressure-defect energy, J s^{-1}
$\dot{\mathcal{E}}_{\mathrm{P}}$	Rate of energy from the propulsor, J s^{-1}
$\dot{\mathcal{E}}_\tau$	Rate of viscous boundary-work, J s^{-1}
$\dot{\mathcal{E}}_{th}$	Rate of thermal exergy, J s^{-1}
$\dot{\mathcal{E}}_u$, $\dot{E}_u$	Rate of stream-wise mechanical energy, J s^{-1}
$\dot{\mathcal{E}}_v$, $\dot{E}_v$	Rate of transverse mechanical energy, J s^{-1}
$\boldsymbol{f}$	Volume-specific body force vector, N m^{-3}
$\mathcal{F}$	Force, N
$\dot{h}$	Rate of change in altitude, m s^{-1}
H	Total enthalpy, J
$\dot{I}$	Momentum flux force, N
L	Lift, N
$\hat{\boldsymbol{n}}$	Unit normal vector, –
P	Total pressure, Pa
p	Static pressure, Pa
P_K	Mechanical energy inflow rate, J s^{-1}
P_S	Net propulsor shaft power, J s^{-1}
P_V	Rate of volumetric pressure work, J s^{-1}
$\boldsymbol{q}$	Heat conduction flux vector, J m^{-2} s^{-1}
$\dot{q}$	Volumetric heat addition/removal, J m^{-3} s^{-1}
q	Dynamic head, Pa
$\mathcal{R}$	Range, m
$\mathcal{S}$	Control surface, –
$\mathcal{T}$	Thrust, N
$\boldsymbol{V}$	Velocity vector, m s^{-1}
$\mathcal{V}$	Control volume, –
W	Weight, N

Sub-/Super-scripts

∞	Quantity at free-stream
$\bar{(\,)}$	Area-averaged quantity
$\tilde{(\,)}$	Ideally expanded quantity
A/C	Quantity on aircraft
A	Quantity in the absolute reference frame
B	Quantity on body surface
BP	Quantity on by-pass
FE	Quantity at fan-exit
FF	Quantity at fan-face
FS	Quantity on free-stream surface
G	Gauge/Gross quantity
int, std, ov	Intrinsic, standard and overall quantities
N	Net quantity
nac	Quantity on nacelle
NZ	Quantity at nozzle
P	Quantity on propulsor
post	Quantity on post-exit stream-tube
pre	Quantity on pre-entry stream-tube
ref	Reference quantity
SC	Quantity on side cylinder
TE	Quantity at trailing-edge
TP	Quantity on Trefftz plane

innovative designs and technologies is now required. A potential solution is the concept of boundary layer ingestion (BLI), which focuses on synergies between airframe and propulsion system in a more holistic aircraft design approach to fully exploit the aerodynamic benefits of closer integration. The concept originates from the marine sector, whereby the submersible vehicles' propulsor takes advantages of the flow travelling around the body [8,9], hence making that technology also applicable to airborne systems. Through the introduction of a

Table 1
EU Vision 2020, EU Flightpath 2050 and NASA N + 3 environmental goals.

	EU Vision 2020	EU Flightpath 2050	NASA N + 3 2025	NASA N + 3 2035+
Reference technology year	2000	2000	2005	2005
CO_2	−50%	−75%	Neutral growth	−50%
NO_x	−80%	−90%	−80%	>−80%
Perceived noise	−50%	−65%	−40%	>−50%

power saving coefficient (PSC), Smith demonstrated significant power savings originating from the filling of the boundary layer (BL) momentum deficit at a lower fuel consumption whilst attenuating the aircraft's wake [10]. However, improved aircraft aerodynamic design will try to minimise drag whilst maximising lift, i.e. maximise the lift-to-drag ratio. Minimising drag through optimisation, flow control [11,12] with laminarisation [13], surface plasma [14,15] and their applications [16] will result in a reduced energy content of the BL, and subsequently reduce its harvesting and ultimately benefits. Therefore, caution should be taken not to try and maximise BLI benefits by inadvertently penalising the airframe lift-to-drag ratio.

Commonly, the aircraft's aerodynamics are assessed as a still vehicle around which air is moving, like in wind-tunnel testing. This is referred to herein as the relative reference frame (RRF). However, to enable more physically intuitive interpretations, the absolute reference frame (ARF) is preferred whereby the aircraft moves through an initially quiescent atmosphere [17,18] as illustrated with moving control volumes (moving in space but fix relative to the aircraft) in Fig. 1. The aircraft motion through the air displaces the air particles to satisfy the no-slip condition on the airframe wall surfaces, whereby constricting their near-wall velocity, imparting energy to the surrounding flow, and developing a BL. A strategic propulsor integration enables the boundary layer's energy to be harvested, rather than wasted within the aircraft's wake, increasing the vehicle's efficiency. Those power benefits are reported to vary between 5 and 13% [19–21] and the fuel burn to be reduced by between 12 and 36% [20,22] despite presenting numerous challenges [23], notably:

- the aircraft configurations and architectures need to ensure the aircraft operability and safety at any point along its mission (on- and off-design) even if an engine becomes inoperable,
- the different aircraft concepts integrate propulsion systems in different fashions facing different levels of distortion and potentially aggravating the aircraft's performance and operability,
- the transmission architectures that can be of the form of turbo-mechanical, turbo-electric or hybrid-electric distributed propulsions present other thermal management concerns or additional weight penalties.

It is noteworthy that the close engine-airframe integration [24–28] makes the distinction between the positive (thrust) and negative (drag) forces challenging because of their strong interaction. Therefore, the well-established thrust-drag bookkeepings set out by the MIDAP (Ministry-Industry Drag Analysis Panel) Study Group [29] and the SAE (Society of Automotive Engineers) Committee [30] become invalid, because the assumptions upon which they are based no longer hold. Yet, the momentum-based principle can still be considered if treated cautiously with control volumes defined around the vehicle and propulsion system but still do not enable a meaningful distinction between thrust and drag [31,32]. Consequently, a favoured approach is to consider the system more holistically [33]. From this approach, further developments are enabled [17,34,35] leading to unifications of these approaches [36–38] to gain a wider understanding of the different BLI aircraft configurations and performance.

The renewed interest in BLI has led to a profusion of publications and reviews of the state of the art [23,32,39–44]. Hendricks gathered NASA's efforts in the modelling approaches and introduced the degree of coupling between the vehicle aerodynamic and propulsion

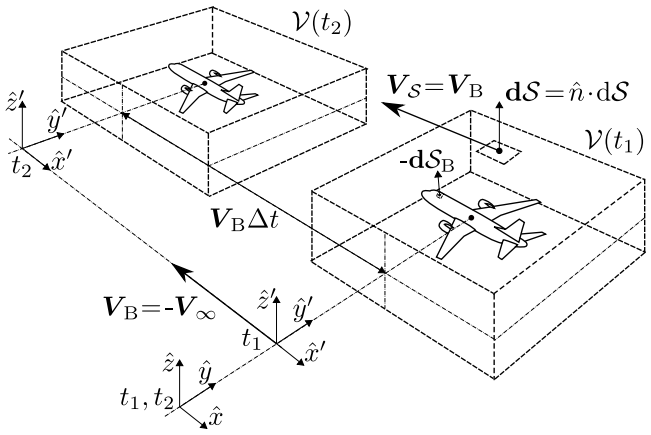


Fig. 1. Motion of a flying aircraft from t_1 to t_2 with its control volume in the ARF ($\hat{x}$, $\hat{y}$, $\hat{z}$) and the RRF ($\hat{x}'$, $\hat{y}'$, $\hat{z}'$).
Source: Adapted from Ref. [18].

system models. In search of proposing a unified momentum-based book-keeping to treat BLI, Habermann et al. [32] first reviewed and categorised part of the literature based on the different performance book-keeping methods. A division between momentum-, energy- and exergy-based accounting was presented along with their associated metrics, precautions and requirements. However, these were solely evaluated to suit the universality and applicability to the conceptual design phase. Additional analogous reviews from Refs. [43,44] treat the different conceptual BLI aircraft which are split into three distinctive architectures (tube-and-wing, lifting fuselage and unconventional airframes) with an emphasis on the former. The diverse concepts are summarised in both publications where the former authors' focus are on the numerical modelling and the benefits offered by the configurations whereas the latter work offers a more in-depth analysis of the results and the main contributions of the works. Notwithstanding the multiple reviews available, limited opinions and critiques are provided on the methods and models chosen by the researchers community leading to their work and results obtained.

This paper therefore seeks to assess the theoretical, numerical and experimental progress related to BLI. From the conservation equations, the different book-keeping approaches are derived in Section 2. The close integration of the engine within the airframe prevents the aerodynamic to be studied in isolation from the propulsion system raising an ambiguity and discrepancies between the methods. Unlike previous reviews solely assessing the suitability to the conceptual design phase, a primary contribution of this paper lies in a comprehensive review of the existing approaches to evaluate the aircraft performance at any phase of the design process. Notably, the book-keeping schemes and metrics are discussed with their applicability to both numerical and experimental investigations.

Additionally, it is noted from the previous reviews introduced a definite lack of review in experimental practices despite the recent efforts. Consequently, in tandem with the theoretical and numerical development of methods and their applications that are reviewed and critiqued in Section 3, an emphasis is given to experimental studies and specifically to their challenges and risks. The different apparatuses and techniques are discussed in Section 4 to contribute to this review and highlight the current difficulties emanating from BLI.

A thorough survey of various studies in Section 5 gives prominence to the assumptions, methods and models used to mitigate the results claimed. Unlike previous reviews only mentioning discrepancies amidst all studies, this paper seeks to share the authors' opinions on the models and methods used to discuss the BLI-related and synergistic benefits offered by the peculiar architectures and therefore the underlying reasons that have led to those discrepancies.

Overall, the paper aims at addressing the gaps unfilled by previous work and contrasting the plenitude of studies based on the methodologies and approaches followed that yield sometimes important divergences in the benefits reported. In doing so, one is provided with a comparison of the different schemes features, degrees of fidelity in the modellings and common practices in experimental investigations but also their unresolved challenges. Further, recommendations are given on the direction of the BLI investigations and complementary technologies.

2. Performance accounting and metrics

In retrospect, to investigate the behaviour and performance of aircraft before their test flight, sub-scaled mock-ups were assessed in wind-tunnels [45]. Nonetheless, in the course of time, a growing interest emanated from the rise of new technologies and particularly with the development of computer-based solvers that replicate the flow physics — computational fluid dynamics (CFD) [46]. Whether the formulations use low- or high-order models, the cost represented by the simulations was drastically reduced compared to the manufacturing and testing of scaled aircraft. An interest still exists in performing wind-tunnel testing to ensure that the computations accurately predict the flow phenomena but regardless of the nature of the testing, the evaluation of the aircraft performance is based on equivalent book-keepings which are reviewed, hereafter.

2.1. Performance accounting

Regardless of whether the tests are experimental or numerical, a robust analysis and hence accounting needs to be developed to assess the vehicle performance in a consistent manner. AGARD [29] and SAE [30] appear as pioneers in that respect with the development of a standardised thrust-drag accounting method. This book-keeping considers stream-tubes delimited by fictitious transverse surfaces at thermodynamic stations of interest. The stream-tubes can also be referred as control volumes whereby the momentum conservation aids in determining the net forces experienced by either surface integrations of pressure and skin-friction forces on all physical surfaces or, momentum flux integrations over a transverse control surfaces positioned behind the body. These two approaches are referred to as *near-field* and *far-field*, respectively. Although this accounting has been long established, in the performance evaluation of BLI aircraft, its applicability is discussed by Ref. [33]. The distinction between thrust and drag becomes complex and some Refs. [10,47–49] introduce an ingested drag quantity highlighting that drag cannot be evaluated separately as it becomes part of the re-accelerated flow. Alternative means of by-passing this ambiguity have come forth such as revised momentum-based approaches [31,32,48], energy- and exergy-based methods with Refs. [17,33] and Ref. [35] respectively, and vortical-based approaches [50,51].

2.1.1. Fundamental laws and control volume theory

To rigorously examine the aerodynamic performance of an aircraft, it is essential to evoke control volume (CV) theory to which the fundamental laws of mass, momentum and energy conservation may be applied. Broadly speaking, and considering steady flight, the outer bounds ($\mathcal{S}_{\text{FS}} \cup \mathcal{S}_{\text{SC}} \cup \mathcal{S}_{\text{TP}}$) of the control volume (Fig. 2) are typically considered to be fixed in space relative to the aircraft and observer positioned in the same inertial reference frame. This has been referred

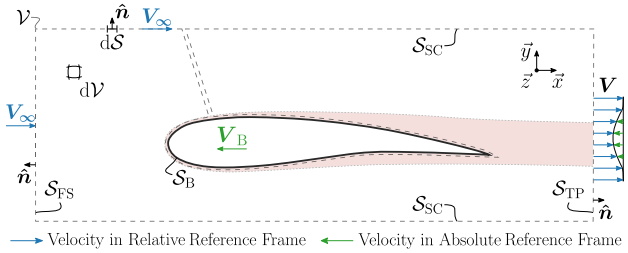


Fig. 2. Two-dimensional cutaway of a three-dimensional control volume encapsulating an aerofoil with its boundary layer development (shaded region).

to herein as the RRF, where the flow is viewed as passing over the *stationary* aircraft, and is of practical advantage in numerical modelling and wind-tunnel testing experiments.

The integral forms of the fundamental equations are usually derived with respect to this reference frame, and the closed surface integrals are expanded via the summation rule of integration to allow them to be split and rearranged into *near-field* and *far-field* contributions. The *far-field* integration is simplified through substitutions that express velocity and pressure terms relative to the free-stream conditions (Table 2). This is convenient because the integrations on those surfaces sufficiently ahead $\mathcal{S}_{\text{FS}}$, above, below, or out to the sides $\mathcal{S}_{\text{SC}}$ of the aircraft become zero, and the only surface integral remaining is that behind the aircraft $\mathcal{S}_{\text{TP}}$, which is across an area commonly referred to at the Trefftz plane.

Reducing the *far-field* surface integrals to the Trefftz plane, is a seemingly pure mathematical manipulation for convenience, and is a feature of almost all *far-field* decomposition methods, including momentum- [50], energy- [33], exergy- [35] and vortical-based [51] methods. However, this mathematical manipulation has inadvertently, and seemingly unwittingly to the authors of the aforementioned references, been a transformation to the ARF, whereby the aircraft is perceived as moving through the flow instead of the other way round. This was first pointed out by Sanders and Laskaridis [17], in their contributions to further developing the mechanical energy-based approach of Drela [33]. Subsequently, [18,18] show this by re-deriving the fundamental equations for a general control volume in motion (but still fixed in space relative to the aircraft), alike Fig. 1 with respect to the ARF by means of the Leibniz–Reynolds general transport theorem. Assuming that the control volume remains fixed in space relative to the aircraft, the generalised fundamental equations may be simplified by assuming steady flow, and applying them to the RRF and ARF, respectively. These forms of the equations are summarised in Table 2.

Mass and momentum conservation

Considering a simple representation of an aerofoil as given in Fig. 2 and assuming steady conditions, the mass and momentum conservation equations can be written in integral form over an arbitrary volume $\mathcal{V}$ enclosed by a surface $\mathcal{S} = \mathcal{S}_{\text{FS}} \cup \mathcal{S}_{\text{SC}} \cup \mathcal{S}_{\text{TP}}$, as given by Eqs. (1) to (4) where ρ is the fluid density, $\boldsymbol{V}$ the velocity vector at any given point of the volume, p the static pressure of the fluid, $\bar{\bar{\tau}}$ the viscous stress tensor, $\boldsymbol{f}$ the net body force per unit mass exerted on the fluid within the volume $\mathcal{V}$ and $\hat{\boldsymbol{n}}$ the unit normal vector along a surface $\mathcal{S}$ and pointing out of the volume $\mathcal{V}$ by convention [52].

Energy conservation

The total energy conservation within a control volume $\mathcal{V}$, is given by Eqs. (7) and (8) [53] where e is the mass-specific internal energy, $\boldsymbol{q}$ the heat flux due to thermal conduction and $\dot{q}$ a volumetric source term. The internal energy, i.e. energy associated with the atoms and molecules of a system, is obtained from the first law of thermodynamics [54] and subtracting it from the total energy (Eqs. (7) and (8)) yields the mechanical energy (Eqs. (5) and (6)) which can also be derived

Table 2
Conservation equations in the relative (RRF) and absolute (ARF) reference frames, respectively.

	Change of reference frame	
RRF	$V \quad \vert \quad p = p_G + p_\infty$	
ARF	$V = V_A + V_\infty \quad \vert \quad p = p_G + p_\infty$	
	Mass conservation	
RRF	$\oiint_S \rho(\boldsymbol{V}\cdot\hat{\boldsymbol{n}})\ \mathrm{d}S = 0$	(1)
ARF	$\oiint_S \rho(\boldsymbol{V}\cdot\hat{\boldsymbol{n}})\ \mathrm{d}S = 0$	(2)
	Momentum conservation	
RRF	$\oiint_S \rho(\boldsymbol{V}\boldsymbol{V}\cdot\hat{\boldsymbol{n}})\ \mathrm{d}S = \oiint_S \left(-p\hat{\boldsymbol{n}} + \bar{\bar{\tau}}\cdot\hat{\boldsymbol{n}}\right)\ \mathrm{d}S + \iiint_\mathcal{V} \rho\boldsymbol{f}\ \mathrm{d}\mathcal{V}$	(3)
ARF	$\oiint_S \rho(\boldsymbol{V}_A\boldsymbol{V}\cdot\hat{\boldsymbol{n}})\ \mathrm{d}S = \oiint_S \left(-p_G\hat{\boldsymbol{n}} + \bar{\bar{\tau}}\cdot\hat{\boldsymbol{n}}\right)\ \mathrm{d}S + \iiint_\mathcal{V} \rho\boldsymbol{f}\ \mathrm{d}\mathcal{V}$	(4)
	Mechanical energy conservation	
RRF	$\oiint_S \rho\left(\frac{\boldsymbol{V}^2}{2}\boldsymbol{V}\right)\cdot\hat{\boldsymbol{n}}\ \mathrm{d}S = \oiint_S \left(-p\boldsymbol{V} + \bar{\bar{\tau}}\cdot\boldsymbol{V}\right)\cdot\hat{\boldsymbol{n}}\ \mathrm{d}S + \iiint_\mathcal{V}\left[p\nabla\cdot\boldsymbol{V} - \left(\bar{\bar{\tau}}\cdot\nabla\right)\cdot\boldsymbol{V} + \rho(\boldsymbol{f}\cdot\boldsymbol{V})\right]\ \mathrm{d}\mathcal{V}$	(5)
ARF	$\oiint_S \rho\left(\frac{\boldsymbol{V}_A{}^2}{2}\boldsymbol{V}\right)\cdot\hat{\boldsymbol{n}}\ \mathrm{d}S = \oiint_S \left(-p_G\boldsymbol{V}_A + \bar{\bar{\tau}}\cdot\boldsymbol{V}_A\right)\cdot\hat{\boldsymbol{n}}\ \mathrm{d}S + \iiint_\mathcal{V}\left[p_G\nabla\cdot\boldsymbol{V} - \left(\bar{\bar{\tau}}\cdot\nabla\right)\cdot\boldsymbol{V} + \rho\left(\boldsymbol{f}\cdot\boldsymbol{V}_A\right)\right]\ \mathrm{d}\mathcal{V}$	(6)
	Total energy conservation	
RRF	$\oiint_S \left[\rho\left(e + \frac{\boldsymbol{V}^2}{2}\right)\boldsymbol{V}\right]\cdot\hat{\boldsymbol{n}}\ \mathrm{d}S = \oiint_S \left(-\boldsymbol{q} - p\boldsymbol{V} + \bar{\bar{\tau}}\cdot\boldsymbol{V}\right)\cdot\hat{\boldsymbol{n}}\ \mathrm{d}S + \iiint_\mathcal{V}\rho(\dot{q} + \boldsymbol{f}\cdot\boldsymbol{V})\ \mathrm{d}\mathcal{V}$	(7)
ARF	$\oiint_S \left[\rho\left(e + \frac{\boldsymbol{V}_A{}^2}{2}\right)\boldsymbol{V}\right]\cdot\hat{\boldsymbol{n}}\ \mathrm{d}S = \oiint_S \left(-\boldsymbol{q} - p\boldsymbol{V}_A + \bar{\bar{\tau}}\cdot\boldsymbol{V}_A\right)\cdot\hat{\boldsymbol{n}}\ \mathrm{d}S + \iiint_\mathcal{V}\rho\left(\dot{q} + \boldsymbol{f}\cdot\boldsymbol{V}_A\right)\ \mathrm{d}\mathcal{V}$	(8)

from the scalar multiplication between Eqs. (3) and (4) respectively and $\boldsymbol{V}$.

It is possible to harvest the energy present in the flow in two manners, through a mechanical device or a thermal device. The former only recuperates the available mechanical energy which needs to be isolated from its total form, whereas the thermal components are related to thermal analyses whereby a heat-exchanger could be used. Therefore, Eqs. (5) and (6) complement Eqs. (7) and (8) and are further detailed with energy-based approaches in Section 2.1.3.

2.1.2. Momentum-based approaches

The Newton's second law yields the momentum conservation equations given in Eqs. (3) and (4) and describes the force that is equal to the time rate of change of momentum [52]. Those forces can be of two forms, body or surface forces and the time rate of change of momentum is a combination of the net outflow and the momentum of the fluid within its volume (in unsteady flows).

Conventional thrust-drag book-keeping

By convention, the forces on bodies are extracted [29,30] to determine the system performance and allow a drag estimation and decomposition where the perturbations in the momentum equation are substituted by forms of enthalpy and entropy [50,55–57].

In these methods, the domain is split into a drag sub-domain and a thrust sub-domain. A crude assumption is made on their definitions whereby any particle travelling through the engine contributes to the thrust (shaded region in Fig. 3) and the remainder towards penalties, or drag. The forces that act in the thrust domain, i.e. inside the streamtube, are denoted θ (not represented in Fig. 3) whereas the forces that act in the drag domain are denoted ϕ. In either domain, these terms describe the integrated pressure and friction forces on either unbounded or wall surfaces. The fluxes across the different stations (free-stream — FS, fan-face — FF, nozzle — NZ, etc.) define the gauge stream forces and help defining the intrinsic, standard and overall net thrusts, Eqs. (9a), (9c) and (9e), respectively. Nonetheless, these definitions only describe the net thrust as a result of the internal flow. To account for the forces generated outside of the thrust-domain that act as performance penalties, the net propulsive force (NPF) is considered for each net thrust definition, respectively Eqs. (9b), (9d) and (9f).

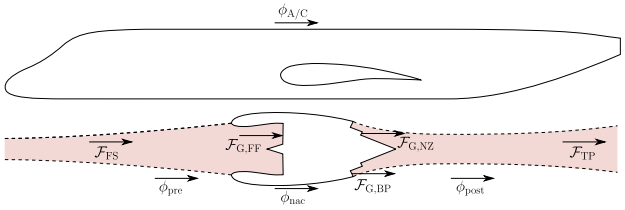


Fig. 3. Forces decomposition on stream-tubes, nacelle and airframe based on the thrust-drag accounting.

In practice, the standard definitions are the most common however, they do not consider the forces exerted on the exhaust plug and this brought forth a modified *near-field* approach [58]. In addition to the thrust and drag interactions, installation effects can also be assessed by integration of the forces over the external surfaces, e.g. wing, $\phi_{A/C}$. The magnitude of the interferences can then be assessed by comparison with an idealised configuration to create a superposition model of a clean-wing and isolated engine [58–60].

$$\mathcal{F}_{N,int} = \mathcal{F}_{G,BP} + \mathcal{F}_{G,NZ} - \mathcal{F}_{G,FF} \tag{9a}$$

$$\mathrm{NPF}_{int} = \mathcal{F}_{N,int} - \phi_{nac} \tag{9b}$$

$$\mathcal{F}_{N,std} = \mathcal{F}_{G,BP} + \mathcal{F}_{G,NZ} - \mathcal{F}_{G,FS} \tag{9c}$$

$$\mathrm{NPF}_{std} = \mathcal{F}_{N,std} - \phi_{pre} - \phi_{nac} \tag{9d}$$

$$\mathcal{F}_{N,ov} = \mathcal{F}_{G,TP} - \mathcal{F}_{G,FS} \tag{9e}$$

$$\mathrm{NPF}_{ov} = \mathcal{F}_{N,ov} - \phi_{pre} - \phi_{nac} - \phi_{post} \tag{9f}$$

Revisited thrust-drag book-keepings

Despite being applicable to podded, or pylon-mounted engines, the conventional thrust-drag book-keeping established on the decoupling of thrust and drag does not hold true in BLI. As alluded to the original drag-only contribution of the airframe is partly ingested by the BLI propulsor and should be accounted in the thrust domain. This highlights the ambiguity of considering the forces applied on the wall surfaces as ϕ or θ.

Similarly, modified *near-field* thrust-drag accountings are proposed by Matesanz-García et al. [61] and by Habermann et al. [32]. In both book-keepings, the interaction between the jet-stream and the wake is

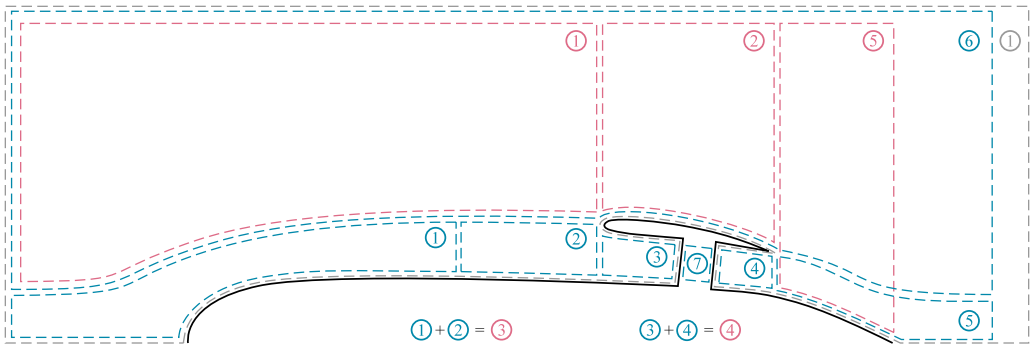


Fig. 4. Control volume divisions based on Habermann et al. [32] ① to ⑤, Sanders [31] ① to ⑦, and Gray [62] ①.

omitted and only the interferences on the pre-entry stream-tube are considered. Fig. 4 depicts a common control volume scheme for all the book-keepings presented.

Particularly, in Matesanz-García et al.'s [61] approach, the stream-tubes from ① to ③ cover all stream-lines from free-stream to the propulsor's AIP. The net vehicle force (NVF) is computed from the difference between the modified drag, D^*, and the modified thrust, $\mathcal{T}^*$:

$$\mathrm{NVF} = D^* - \mathcal{T}^* \tag{10}$$

The former results from the addition of the forces outside of the pre-entry stream-tube ③, i.e. the force on the pre-entry unbounded surface, ϕ_{pre}, and the nacelle wall, ϕ_{nac}, as given in Eq. (11). The latter is defined as the difference between the gross propulsive force at the fan-exit and the gauge force at the inlet plane of ① (Eq. (12)). The modified gross propulsive force, GPF*, is given by Eq. (13) as the sum of the gauge force at the fan-exit and the forces on the walls behind the propulsor.

$$D^* = \phi_{\mathrm{pre}} + \phi_{\mathrm{nac}} \tag{11}$$

$$\mathcal{T}^* = -\mathcal{F}_{\mathrm{FS}} + \mathrm{GPF}^* \tag{12}$$

$$\mathrm{GPF}^* = \mathcal{F}_{\mathrm{FE}} - \theta_{\mathrm{exh}} - \theta_{\mathrm{cone}} \tag{13}$$

In Ref. [61] definition, ϕ and θ refer to the conventions given in Ref. [59] and $\mathcal{F}$ denotes the sum of the axial pressure and viscous forces on fictitious survey planes.

Nonetheless, the NVF only advises on the net thrust changes from variations in the fuselage or BLI propulsor designs but does not allow any performance evaluation. In that respect, the NVF of the podded reference aircraft, $\mathrm{NVF}_{\mathrm{A/C,ref}}$, needs to be defined as the difference between the NPF generated by the main engines and the airframe drag. To isolate the thrust contribution from the BLI propulsor, based on the assumption that the force on the airframe remains unchanged between a BLI and a podded aircraft, and changes in this force are attributed to the thrust only, a relative net thrust force ($\mathcal{F}_{RN}$) is defined in Eq. (14) as the difference between the NVF of the BLI and that of the podded aircraft [31]. This metric becomes of interest when evaluating the influence of the changes in the design of the fuselage or the propulsor in the BLI aircraft performance assessment.

$$\mathcal{F}_{RN} = \mathrm{NVF} - \mathrm{NVF}_{\mathrm{A/C,ref}} \tag{14}$$

In a similar fashion and to retract any kind of ambiguity related to the thrust and the drag domains, Gray [62] considers the net axial force of the combined BLI fuselage-propulsor (① from Fig. 4) and introduces a non-dimensional force coefficient $C_{\mathcal{F}_x}$, Eq. (15). In that manner, the thrust-drag axiom that states that changes in the airframe only affect the force on the fuselage whereas those on the propulsion system only affect the propulsive force is discarded to account for the stream-wise net force. Analogous to the relative net force $\mathcal{F}_{RN}$, the comparison in $C_{\mathcal{F}_x}$ between the podded aircraft and the BLI one assesses the benefits of the configuration in net force count.

$$C_{\mathcal{F}_x} = \frac{2\mathcal{F}_x}{\rho_\infty V_\infty^2 A_{\mathrm{ref}}} \tag{15}$$

Based on the work from Seitz and Gologan [48], Habermann et al. [32] also developed a *near-field* momentum-based book-keeping whereby the net thrust of the system is defined as the sum of the fan disc force, $\mathcal{F}_{\mathrm{disc}}$, and the integrated forces over the wall surfaces. The overall CV that assesses the momentum flux at the outlet is divided into sub-domains following the notations from ① to ⑤ in Fig. 4 and the relation between the outlet momentum flux force and the *near-field* integration is given by Eq. (16). The NVF following their approach is defined in Eq. (17).

$$\begin{aligned} \dot{I}_{\mathrm{out},5} = {} & \dot{I}_{\mathrm{in},1} + \dot{I}_{\mathrm{in},3} + \mathcal{F}_{p,\mathrm{in},1} + \mathcal{F}_{p,\mathrm{in},3} \\ & + \mathcal{F}_3 + \mathcal{F}_4 + \mathcal{F}_{\mathrm{disc}} + \mathcal{F}_2 + \mathcal{F}_5 - \mathcal{F}_{p,\mathrm{out},5} \end{aligned} \tag{16}$$

$$\mathrm{NVF} = \mathcal{F}_3 + \mathcal{F}_4 + \mathcal{F}_{\mathrm{disc}} + \mathcal{F}_2 + \mathcal{F}_5 \tag{17}$$

The $\dot{I}$ terms describe the momentum fluxes at the inlet or outlet stations, *in* and *out* respectively, the $\mathcal{F}_p$ terms correspond to the sum of the axial pressure forces, $\mathcal{F}_{\mathrm{disc}}$ is the force of the fan which can be modelled in several natures, e.g. boundary conditions, body-force or fan model, and the $\mathcal{F}$ terms correspond to the sum of the forces on the unbounded and wall surfaces inside the entire domain. The numbers associated in the subscripts refer to the CV they are associated with, from ① to ⑤. The proposed method is offered as an universally applicable technique to all coupled airframe-propulsion systems and extendible from semi-empirical methods to high-fidelity CFD or wind-tunnel testing.

However, similar to Ref. [61] with Eq. (14), the comparison with the podded configuration is necessary to assess the thrust generated by the BLI propulsor. Nonetheless, these accounting systems are based on the assumption that although there is a strong interaction between the airframe, the propulsion system, and the *near-field* flow, the crude assumption that these can be somehow decoupled is taken.

As a more versatile approach, Sanders [31] offers to not only consider a single unique definition for thrust, but suggests considering several thrust-force accounting systems in combination to aid in the interpretation of the physical mechanisms underpinning BLI propulsion. It is first demonstrated by Sanders that the post-exit stream-tube cannot be omitted in BLI investigations and that therefore an additional term, ϕ_{post} - in analogy to the conventions from Refs. [29,30], needs to be accounted. Due to the interaction that exists between the jet-plume and the body wake, a difficulty arises in the position at which the transverse plane accurately calculates the axial net force of the configuration and therefore constraints the *far-field* integration to only be computed at the Trefftz plane.

Inherently, this yields another split of the overall CV whereby the pre-entry stream-tube is divided into an additional pre-diffusive zone ② accounting for the propulsor installation effects upstream. Also, rather than describing the accounting as thrust-drag, the word "force" is used to make a distinction from the "drag" definition made by Refs. [30,59], which is based upon the Prandtl's extension to D'Alembert's paradox where drag is defined as the residual force between real and potential flows. In potential flows, the resulting force over a body is

equal to zero and is referred to as a buoyancy force. This local pressure force's direct contribution to drag, acting on different locations of the airframe, may be obtained by subtracting the local buoyancy pressure force from the local pressure force from the real viscous flow. However, in conventional thrust-drag approaches, this procedure relies on the assumption that BLs are thin relative to the airframe, and that the differences between the potential and real flow stream-tubes are negligible. Additionally, to apply this thinking to a meaningful separation between thrust and drag, these conventions rely on a clear distinction between the airframe's versus propulsor's stream-tubes. This is because Prandtl's extension to D'Alembert's paradox only applies to infinite (or semi-infinite) stream-tubes such that the net buoyancy for each stream-tube is indeed zero. However, when employing BLI propulsion, these infinite stream-tubes are merged and cannot be isolated from one another. Moreover, the ingested BL is on the same scale as the propulsion system, and the differences between the potential and real flow's stream-tubes are no longer negligible, but instead are rather significant. Therefore, the well-established thrust-drag bookkeepings [29,30] become invalid as the assumptions upon which they are based no longer hold.

More rigorously, force is used in lieu of drag but does not alter the NVF definition which is equal to the summation of all the forces from *near-field* integration, or *far-field*, as given by Eq. (18) following the notations from ① to ⑦ pictured in Fig. 4.

$$\begin{aligned}\mathrm{NVF} &= \underbrace{\Psi_1 + \Psi_2 + \Psi_3 + \Psi_7 + \Psi_4 + \Psi_5 + \Psi_6}_{near\text{-}field} \\ &= \underbrace{\Omega_{\mathrm{in},1} + \Omega_{\mathrm{in},6} + \Omega_{\mathrm{out},5} + \Omega_{\mathrm{out},6} + \Omega_{\mathrm{out,SC},6}}_{far\text{-}field}\end{aligned} \tag{18}$$

In comparison to the previous accounting, Ψ is introduced in place of the ambiguous ϕ and θ and quantifies any form of force on a wall surface. The term Ω also yields the summation of both the momentum flux force and the pressure force, as well as the shear forces, omitted or neglected by Habermann et al. on permeable surfaces:

$$\Omega_i = \dot{I}_i + \mathcal{F}_{p,i} + \iint_{S_i} \bar{\bar{\tau}} \cdot \hat{n}\, \mathrm{d}S \tag{19}$$

The CV division offered in Ref. [31] enables several thrust-force definitions by encompassing different CV as well as ensuring the momentum conservation. Notably, the standard net thrust definition used by Refs. [32,61] is also defined by Sanders along the propulsive, intrinsic, pre-diffusive standard, pre-diffusive overall and overall net thrusts [31].

Alternatively, an ideally expanded momentum defect method, also referred to as isentropic expansion, is proposed [10,47,63–65]. The method consists in defining a velocity profile experienced by a free-stream ingesting propulsion system equivalent to the one seen by a BLI propulsor inlet (Fig. 5). In other words, any point in the flow-field sees its stagnation pressure expanded to free-stream. The resulting velocity, $\tilde{V}$, is called isentropic velocity and is compatible with the energy and exergy approaches reviewed in Sections 2.1.3 and 2.1.4.

$$\tilde{V} = \sqrt{\frac{2\gamma R}{\gamma - 1} T \left[1 - \left(\frac{p}{p_\infty}\right)^{-\frac{\gamma-1}{\gamma}}\right]} \tag{20}$$

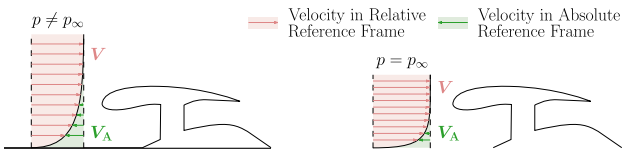


Fig. 5. Boundary layer velocity profile at the BLI propulsor's AIP (left) and its equivalent at fully-expanded isentropic conditions (right).

The integral form of the momentum conservation Eq. (3), can be re-written following Eq. (21) as the expanded momentum defect, $\tilde{P}$. The thrust of the system given in Eq. (22) is obtained from the difference of that quantity between the inlet and outlet of the propulsion system whereby a decrease in defect yields a forward force.

$$\tilde{P} = \oiint_S \rho \left(\boldsymbol{V}_\infty - \tilde{\boldsymbol{V}}\right) \boldsymbol{V} \cdot \hat{\boldsymbol{n}}\, \mathrm{d}S \tag{21}$$

$$\mathcal{T} = \tilde{P}_{\mathrm{FF}} - \tilde{P}_{\mathrm{NZ}} \tag{22}$$

A comparison of this method with energy approaches is given in Ref. [66] whose conclusion is that the isentropic expansion method is suitable at pre-design phases as long as a low interaction is observed between the airframe and propulsor, questioning its real applicability to BLI.

To conclude, the different features of the momentum-based approaches are summarised in Table 3 highlighting the relatively low computational demand required but the lack of information obtainable using energy-based methods. To relate the performance to physical phenomena, alternative approaches are considered and detailed hereafter.

2.1.3. Energy-based approaches

Considering the system holistically, one can draw a unique CV around the vehicle of interest (① from Fig. 4) and evaluate the forces, mechanical energies and powers from an energy standpoint.

Retrieving the momentum conservation equations in Eqs. (3) and (4) and forming the dot product with $\boldsymbol{V}$ yields the mechanical energy equations Eqs. (5) and (6) in integral form. Its integration over ① gives the general form of the mechanical power balance (Eq. (23)) [33] where the left-hand side terms of the equation describe the total power input and the right-hand side the power output.

$$P_S + P_V + P_K = W\dot{h} + \dot{\mathcal{E}}_u + \dot{\mathcal{E}}_v + \dot{\mathcal{E}}_p + \dot{\mathcal{E}}_w + \Phi \tag{23}$$

On the left, the power production or inflow encompasses P_S describing the net propulsor shaft power which integrates all forces on all moving body surfaces, P_V characterising the rate of volumetric pressure work provided by the fluid by expansion and P_K giving the mechanical energy inflow rate. On the right, the terms describe the total energy outflow rate that respectively correspond to the reversible power changes during ascent and descent, the stream-wise kinetic energy deposition rate, the transverse kinetic energy deposition rate, the rates of wake pressure-defect work and wave pressure work, as well as the power sinks with the rate of viscous dissipation, Φ.

In contrast to the momentum-based approaches, the mechanical power production and consumption of the aircraft are balanced in lieu of the forces — with the net vehicle force previously defined. Nonetheless, Hall et al. [36] compare the previously described ideal expansion method to the power balance method with the evaluation of the dissipation/drag. The airframe dissipation is referred to as the effective drag power that is available in the air and is compared against the effective drag; respectively the net propulsive power is compared to the effective thrust. Both methods yield similar values, in coefficient forms, for low angle of attacks only and no detail, nor explanation, are given on the discrepancies as the incidence increases.

Sato [34] extends the power balance method from Drela [33] by providing a derivation of an analytical expression of profile drag estimates. The aerodynamic performance of integrated configurations is assessed with a fuselage with an unducted and ducted actuator disc at its rear, a ducted actuator disc and two interfering aerofoils. The work is also extended to a system-level optimisation of fuel burn on a hybrid-wing body configuration [34].

To enable an improved interpretation of the causality between the power sources and sinks of the system, the ARF is considered over a RRF in Ref. [17]. An example is the power transferred from the airframe to the flow developing a BL over its surface as the aircraft moves through an initially quiescent atmosphere. From this point of view,

Table 3
Comparison of the different features offered by the reviewed approaches.

Approach family	Computational demand	Applicability/Validity	Phenomenology	Thermal effects
Momentum (near-field)	Low	✓	✗	✗
Momentum (far-field)	High	✓	✗	✗
Ideal expansion	Low	?	✗	✗
Energy	High	✓	✓	✗
Exergy	High	✓	✓	✓

Eq. (23) can be rearranged in Eq. (24) to exploit an explicit formulation of the forces imbalance over powered bodies for the evaluation of partial assemblies in isolation to the rest of the airframe (fuselage $\mathcal{F}_{\mathrm{B}}$ and propulsor $\mathcal{F}_{\mathrm{P}}$).

$$\left(\mathcal{F}_{\mathrm{B}}+\mathcal{F}_{\mathrm{P}}\right)\cdot\boldsymbol{V}_{\infty}=\overbrace{\dot{\mathcal{E}}_{u}+\dot{\mathcal{E}}_{v}+\dot{\mathcal{E}}_{p}+\dot{\mathcal{E}}_{\tau}}^{\dot{\mathcal{E}}_{m}}+W\dot{h}+\dot{\mathcal{E}}_{\mathrm{P}}+\Phi+\Theta \tag{24}$$

Analogous to the notations taken in Ref. [33], the $\dot{\mathcal{E}}_{i}$ terms relate to the $\dot{E}$ given in Ref. [33] after a change of reference frame and $\dot{\mathcal{E}}_{\tau}$ is introduced to represent the rate of viscous boundary-work. Amongst the findings made by Sato [34], his investigations on P_V led to the identification of a loss mechanism referred to as baroclinic power. Θ is therefore defined as the reciprocal of P_V to characterise the rate of volumetric pressure work from which a part is self recoverable and the other deemed more appropriately to be a sink. In addition, this term is demonstrated to not be negligible as initially expressed in Ref. [33] at either subsonic or supersonic conditions.

2.1.4. Exergy-based approaches

The exergy-based analyses extend the energy-based approaches by including the conservation of kinetic exergy, which considers the total enthalpy of a working fluid. The investigation of the total enthalpy addresses both the mechanical and thermal aspects granting a broader perspective on the amount of recoverable energy present in the flow. These two forms of energy represent the total energy of the fluid and are equivalent by virtue of the first law of thermodynamics [54]. Nonetheless, if the mechanical energy $\dot{\mathcal{E}}_{m}$ can be ideally converted into mechanical work, only a portion of the thermal energy $\dot{\mathcal{E}}_{th}$ can be ideally converted into mechanical work and this is governed by the second law of thermodynamics [54].

The approach is similar to the energy-based one whereby a unique control volume surrounding the aerodynamic body is considered. By extension of the power balance, the supply and outflow require the accounting of exergy/anergy terms. The terms exergy and anergy are employed to represent the part of energy that has an economic value, i.e. useable energy, and the part of destroyed energy, or equivalently generated anergy, by irreversible phenomena [67]. In the BL developing over the airframe, both mechanical and thermal perturbations are generated whereof a part of these perturbations dissipate (either over the surface or in the wake and contribute to the total anergy, $\dot{\mathcal{A}}_{tot}$). The available amount of energy is thus recoverable and defines the term exergy, lumping the mechanical and thermal exergy, $\dot{\mathcal{E}}_{m}$ and $\dot{\mathcal{E}}_{th}$ respectively.

In the balance between the exergy supply, and the exergy outflow and anergy generation (Eq. (25)) [68], the left-hand side terms provide the exergy supply to the system with $\dot{\mathcal{E}}_{\mathrm{P}}$ being the rate of mechanical energy/exergy by the propulsor (similarly as in Eq. (24)) and $\dot{\mathcal{E}}_{q}$ the rate of thermal energy/exergy that can be provided by heated, or cooled walls, heat exchangers etc [69]. The right-hand side terms describe the exergy outflows, $\dot{\mathcal{E}}_{m}$ and $\dot{\mathcal{E}}_{th}$, and the anergy generation, $\dot{\mathcal{A}}_{tot}$, along the rate of change in altitude, $W\dot{h}$ (as in Eq. (24)).

$$\dot{\mathcal{E}}_{\mathrm{P}}+\dot{\mathcal{E}}_{q}=W\dot{h}+\dot{\mathcal{E}}_{m}+\dot{\mathcal{E}}_{th}+\dot{\mathcal{A}}_{tot} \tag{25}$$

To demonstrate the applicability of the book-keeping and its benefits, Arntz's [35] studies focus on two-dimensional aerofoils and three-dimensional wings [70], the NASA Common Research Model (CRM) [71] and a two-dimensional BWB configuration [72] based on the exergy principles. The approach is later further developed with an harmonised formulation from Aguirre et al. [73]. An aero-thermo-propulsive vehicle performance evaluation approach is also offered by Ref. [37] who investigated the benefits of ingesting the thermal BL.

2.1.5. Comparison

The introduced accounting schemes present major differences despite all being based on the conservation principles. These differences are summarised in Table 3 and further detailed. Numerically, it appears clear that the computational demand is much more important in *far-field* approaches than *near-field* as a dense grid is required downstream of the aircraft. However, with *near-field* methods, the information extractable are rather limited. The forces are decomposable in pressure and fiction and because of the thrust and drag ambiguity, the net axial force is often preferred. As an alternative, the ideal expansion method has been vastly studied but Ref. [66] reports that the approach only stands when low interaction is observed between the airframe and propulsion systems. This comment is contradictory to BLI and the tight integration of the engine putting into question its applicability. Therefore, *far-field* methods are often considered as they provide more insights on the flow phenomena. With the momentum approach, the drag is decomposed in different fashions such as the profile, wave, lift-induced and vortex components. Nonetheless, there are limitations in the causes and effects of the different phenomena observed. Momentum approaches are Galilean invariant, as opposed to Galilean covariant, when considered in the relative reference frame. The absolute reference frame enables the covariance whereby relationships between work and energy on the flow are transferable and change by an equal amount when viewed from different reference frames yielding in the energy and exergy formulations. Physics-based and more intuitive interpretations are possible with these two approaches whereby exergy is transferred to the flow through the no-slip condition and transfers in energy forms take place in the flow, making useful work identifiable. Lastly, the difference between the two is purely thermodynamic as thermal energy aspects are considered with exergy-based analyses allowing the study of heated or cooled-down flows.

Therefore, if objectives are to evaluate the overall performance of the aircraft concept or optimise it, *near-field* are sufficient as the net axial force can be related to the power consumption and savings. For detailed analyses of the aerodynamics and propulsion, energy and exergy analyses are recommended despite their increased computation cost with denser grids in the *far-field*. These two approaches enable the flow phenomena to be studied in detail and related to the underpinning causes and effects of BLI.

2.2. Performance metrics

Stemming from the manifold of book-keepings presented, different figures of merit are hereafter discussed and critiqued. The highly integrated nature of the aerodynamic and propulsion in BLI requires different levels of assessment that can be segmented in system-, aircraft- and mission-level evaluations.

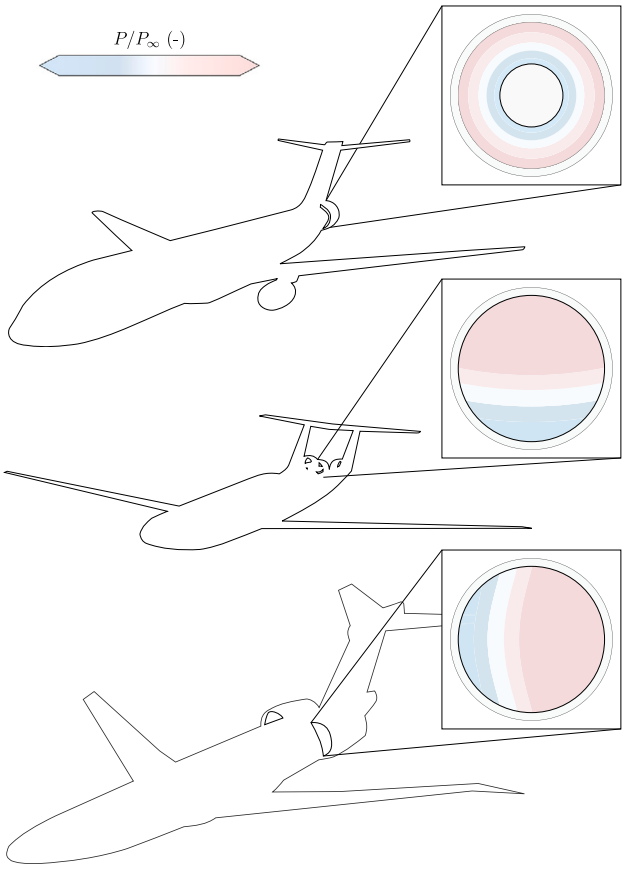


Fig. 6. Schematic of governing distortion types (normalised total pressure) for various embedded propulsion systems.

2.2.1. Intake performance

In the same vein as with an engine pod, the intake performance can be characterised but in addition to the fan-intake interaction, the propulsor integration effects can be introduced in scenarios of strong aerodynamic coupling. The position at which the propulsor is positioned plays an important role in the amount and quality of the ingested flow and thus its spillage or suction effects. For examples, the diffusion, distributions at the aerodynamic interface plane (AIP) and distortion are important characteristics to quantify the blade loading and assist designers with the constraints the fan would face [74]. In BLI, as opposed to a pod, a natural pre-diffusion takes place along the fuselage wall generating a BL which is incomparable to the flow observed ahead of under-wing turbofans. The low velocity region close to the fuselage wall is responsible for the greatest power savings (from its energy abundance observed in the ARF) but also plays an essential role in the fan operation as higher levels of distortion are experienced by the fan. Fig. 6 represents the types of distortion faced by the engines featured in the different BLI aircraft concepts.

In CFD, the grid resolution allows almost continuous data to be computed but, in experiments, data points can only be measured where probes are positioned (Fig. 7) following some installation constraints and potential flow perturbations, e.g. blockage or turbulence. A generic disposition of the probes along the rakes is illustrated in Fig. 7 where eight equi-spaced arms contain five probes each placed at the centroids of equal areas. This technique is commonly used for podded engines that face a free-stream flow nonetheless, in BLI, different aircraft configurations come with different engine integrations and therefore the positioning of the arms might differ as higher distortion is expected closer to the wall surfaces.

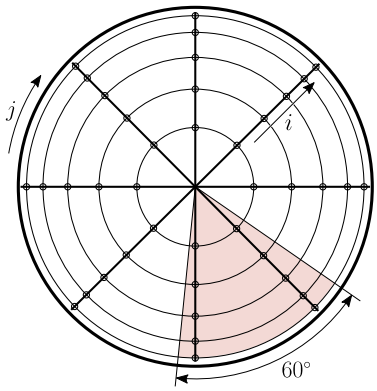


Fig. 7. Rake and pressure probes arrangement with a fictitious critical sector of 60°. *Source:* Remastered from Ref. [79].

In experimental set-ups, properties are therefore measured by multi-probe rakes [75,76] but numerically, the fineness of the grid allows for a more refined distribution. To characterise the total pressure distortion, multiple metrics can be used in tandem: the inlet, or intake, pressure recovery, IPR (Eq. (26)), the distortion coefficient measured on a specific section of the full-annulus, commonly a 60° section, $DC(60)$ (Eq. (27)) [77] and the radial and circumferential distortion indices, RDI (Eq. (28)) and CDI (Eq. (29)), respectively [78].

$$\mathrm{IPR} = \frac{\overline{P}_{\mathrm{AIP}}}{\overline{P}_{\infty}} \tag{26}$$

$$DC(60) = max\left(\frac{\overline{P}_{\mathrm{AIP}} - \overline{P}_{60,\mathrm{AIP}}}{q}\right) \tag{27}$$

$$\mathrm{RDI} = max\left(\frac{\overline{P}_{\mathrm{AIP}} - \overline{P}_{i=0}}{\overline{P}_{\mathrm{AIP}}}, \frac{\overline{P}_{\mathrm{AIP}} - \overline{P}_{i=4}}{\overline{P}_{\mathrm{AIP}}}\right) \tag{28}$$

$$\mathrm{CDI} = max_{i=0}^{n=3}\left(\frac{1}{2}\left[\frac{\overline{P}_i - P_{min_i}}{\overline{P}_{\mathrm{AIP}}} + \frac{\overline{P}_{i+1} - P_{min_{i+1}}}{\overline{P}_{\mathrm{AIP}}}\right]\right) \tag{29}$$

The IPR describes the total pressure losses between a survey plane upstream, which can be at free-stream or anywhere along the fuselage and the AIP. This makes its utilisation rather complicated as it not only describes the inlet but also the aircraft's fuselage aerodynamic performance. In highly embedded configurations, the other metrics are therefore preferred. The $DC(60)$ identifies a sectional distortion coefficient that measures the difference between the area-average total pressure $\overline{P}_{\mathrm{AIP}}$ and the lowest total pressure in a 60° section of the AIP, the RDI describes the non-uniformities in the radial direction where $\overline{P}_{i=0}$ is the total pressure of the inner ring and $\overline{P}_{i=4}$ that of the outer ring, and lastly the CDI assesses the non-uniformity of the circumferential total pressure distribution at specific radial positions where $\overline{P}_i$ is the average total pressure of the ith ring and P_{min_i} the minimum pressure along that same ring i. These metrics are favoured as they identify different portions of the flow subject to high total pressure defects, notably with a section, and the radial and circumferential distributions.

2.2.2. Propulsion systems performance

To describe the propulsion systems' performance, fan performance metrics can be equally applied from propulsors to gas-turbine engines. During the fan operation, its performance is described with isentropic and polytropic efficiencies that are related by the fan pressure ratio (FPR):

$$\eta_{isen} = \frac{\mathrm{FPR}^{\frac{\gamma-1}{\gamma}} - 1}{\mathrm{FPR}^{\frac{\gamma-1}{\gamma\eta_{poly}}} - 1} \tag{30}$$

The isentropic efficiency (Eq. (30)) describes the ratio of ideal work to the actual work done or in another terms, the energy input to achieve a given pressure rise in inviscid flow versus real viscous flow. Independent of the size of the compressor stage, the polytropic efficiency η_{poly} describes an aerodynamic performance which lumped end-to-end assesses the penalties in the stage.

The propulsive performance of an engine does not simply reduce to its amount of propulsive force it generates but rather how the amount of energy provided by the fuel is converted into motion. As such, the propulsive efficiency, η_{prop} given in Eq. (31) describes the amount of work done on the aircraft from the amount of energy provided after consideration of the thermal efficiency η_{th} which describes how efficiently the power input is converted into power output in a power-plant [80]. Nonetheless, the reduction of η_{prop} with conventional approaches is often discussed as it involves the flaws associated with its value that can be greater than 100% for BLI.

$$\eta_{prop} = \frac{\mathcal{T} \cdot V_\infty}{\dot{\mathcal{E}}_\mathrm{P}} = \frac{2\,V_\infty}{V_\mathrm{FF} + V_\mathrm{FE}} \tag{31}$$

BLI is often seen as a means of increasing the propulsive efficiency, and translates to a lower specific thrust that is obtained from a smaller deviation between the outlet and inlet velocities, or a smaller inlet velocity (Eq. (31)). Taking into considerations the specificities of BLI, another form of propulsive efficiency is derived by Plas et al. [47] accounting for the momentum and energy BL thickness in its kinetic energy shape parameter form H^* and the ratio of ingested drag to the total aircraft drag β. Nonetheless, this expression is also ill-defined as when β and H^* respectively approach 0 and 1, Eq. (32) reduces to Eq. (31) and is also bounded by 2.

$$\eta_{prop} = \frac{1+\beta}{\frac{H^*}{2} + \beta\left(1 + \frac{V_\mathrm{NZ} - V_\infty}{2V_\infty}\right)} \tag{32}$$

In search of converging towards a better definition of the propulsive efficiency, Sanders and Laskaridis [17] introduce a propulsive efficacy, κ, defined in Eq. (33). It can be noted a difference in Eqs. (31) and (33) where the numerator could be assimilated similar by taking the difference in net axial force power between the unducted baseline and the BLI configuration but the denominator differs. Whereas both are considered as the power supply, Eq. (31) considers the net mechanical energy flow rate, P_K or $\dot{\mathcal{E}}_\mathrm{P}$, whereas Eq. (33) accounts for the net propulsor shaft power P_S. In the former definition, P_K heavily depends on the position at which the inlet and outlet stations are positioned [34] and do not account for the fan's blades rotational friction losses. On the other hand, P_S quantifies the overall amount of power consumed by the fan, including all kind of losses then generated to provide the useful work.

$$\kappa = -\frac{\boldsymbol{\mathcal{F}}_{RN}}{P_S} \cdot \boldsymbol{V}_\infty \tag{33}$$

The negative sign is required by convention from CFD solvers for the computation of the relative force $\mathcal{F}_{RN}$. This metric offers a manifold of advantages: its maximum value is capped at 100% as opposed to the two previous definitions, its definition is analogous to Ref. [36] under the assumption of a uniform jet velocity, the power demand is used to account for all internal losses and therefore gets closer to a real definition of useful work divided by work input.

Nonetheless, κ still should not be mistaken with a *strict* definition of the propulsive efficiency as the numerator does not represent the exact useful work. Additionally, the denominator is not exact either but closer to the actual power input. Therefore, the metric is suggested over the others but the authors would like to draw attention to further developments. For a strict definition, the propulsive efficiency should be defined as the ratio of useful work over the power available for utilisation.

2.2.3. Aircraft-level performance

To evaluate the benefits of BLI over a conventional aircraft, it is essential to first relate the amount of propulsive force generated by the BLI propulsor to the overall requirement. As such, Valencia [81] introduces the concept of thrust-split (TS) which divides the relative net force provided by the BLI propulsors to the aircraft's overall force requirement:

$$\mathrm{TS} = \frac{\boldsymbol{\mathcal{F}}_{RN}}{\boldsymbol{\mathcal{F}}_{A/C}} \tag{34}$$

To prevent any ambiguity with the force distribution amongst the different engines, net stream-wise forces are also used by Ref. [62] with Eq. (15).

To account for the propulsive efficiencies of both BLI and underwing engines and their relative force generated, savings are evaluated from an energy standpoint with Smith [10] who introduced a power saving coefficient (PSC). The metrics contrasts the power consumption from a BLI configuration to that of a *some-sort* of equivalent podded aircraft for a given net axial force:

$$\mathrm{PSC} = 1 - \frac{\dot{\mathcal{E}}_\mathrm{P}}{\dot{\mathcal{E}}_\mathrm{P,ref}} \tag{35}$$

The PSC appears as a common point of comparison and assesses the performance of a BLI configuration albeit being subject to several challenges. Initially, Smith defines the PSC for two equivalent propulsor disc areas but intrinsically in the case of BLI, the aft-mounted propulsor presents the advantages of reducing the size of the podded engines. This questions the equivalence that one would consider for the calculation of the PSC, e.g. same fan diameter or mass-flow rate. Thus, it results that albeit having a unique definition, the saving quantification is subject to the reference aircraft and engine considered.

In addition, it is common to define the PSC using P_K or $\dot{\mathcal{E}}_\mathrm{P}$ [82,83] although it is the authors' opinion that this should not be considered and rather P_S as discussed above for κ:

$$\mathrm{PSC} = 1 - \frac{P_\mathrm{S,BLI}}{P_\mathrm{S,A/C,ref}} = 1 - \frac{\dot{m}_{fuel,\mathrm{A/C,BLI}}}{\dot{m}_{fuel,\mathrm{A/C,ref}}} \tag{36}$$

With Eq. (36), the net shaft power is used in the BLI and reference configurations to quantify the benefits of ingesting the BL. Further, the power is defined as the product between the fuel mass-flow rate $\dot{m}_{fuel}$ going through the engine's combustion chamber and the fuel heating value h_{fuel}. However, assuming the same fuel properties in both BLI and non-BLI aircraft, the PSC reduces to the form given by Eq. (36) and should be used in turbo-electric architectures (Section 5.1).

In search of alleviating the ambiguity related to the propulsion systems and the equivalence in the BLI and non-BLI scenarios, Baskaran et al. offer to substitute the power consumption from a non-ideal underwing engine by a fictitious ideal propulsor whose consumption would be equivalent to the aircraft drag power (ideal propulsive efficiency), $\mathcal{F}_\mathrm{A/C} \cdot V_\infty$. The definition of the PSC is thus traded for a strict definition yielding the minimum savings achievable by the BLI propulsor (Eq. (37)).

$$\mathrm{PSC}_\mathrm{strict} = 1 - \frac{\dot{\mathcal{E}}_\mathrm{P}}{\boldsymbol{\mathcal{F}}_\mathrm{A/C} \cdot \boldsymbol{V}_\infty} \tag{37}$$

Although Eq. (37) considers $\dot{\mathcal{E}}_\mathrm{P}$, the tentative of using the isolated body aerodynamics for reference prevents the use of low- or high-order models to derive the power consumption of the propulsion system.

Conversely, at conceptual design, the isolation of the fuselage, or airframe, allows one to evaluate the potential for energy recovery (PER) by assessing the irreversibly lost energy that manifests itself as viscous dissipation, Φ. In that scenario, the maximum power is achieved with a fictitious propulsor that fills the entire BL without generating jet loss or affecting the surrounding flow and is compared against the force power of the fuselage, $\boldsymbol{\mathcal{F}}_\mathrm{B} \cdot \boldsymbol{V}_\infty$. PER is defined by Sanders and Laskaridis [17] and also later referred as $\mathrm{PSC}_\mathrm{ideal}$ by Baskaran et al. [84].

However, accounting for the irrecoverable thermo-compressibility effects with the volumetric pressure work Θ_∞ present in the flow, PER is later improved by Lamprakis et al. [69] in Eq. (38) discarding Sanders and Laskaridis' definition for completeness and exactness. Despite the direct relation between PER and PSC, PER grants an initial potential performance metric of the airframe where the traverse plane can integrate the viscous losses at various stream-wise positions along the airframe.

$$\mathrm{PER} = 1 - \frac{\boldsymbol{\Phi}_{\mathrm{TE}} + \boldsymbol{\Theta}_\infty}{\boldsymbol{\mathcal{T}}_{\mathrm{B}} \cdot \boldsymbol{V}_\infty} \tag{38}$$

Integrating on transverse planes behind the body, in the case of wake ingesting configurations, a complement to PER is defined by Mutangara et al. in which the available, i.e. recoverable, energy is tracked at various positions within the wake [85]. This metric allows one to evaluate the potential performance of an aerodynamic shape, but yet does not necessarily imply better savings, as given by PSC, with an installed configuration.

As an extension of the previously defined performance metrics, recovery of the thermal energy rate is also assessed. For instance, in the same vein as the PSC, an exergy saving coefficient (ESC) is defined in Eq. (39a) [68] by comparing the exergy saving from the initial supply (in both BLI and podded aircraft scenarios). This metric describes the improvement from the reference configuration through the installation of the BLI propulsion system, but also accounts for pressure field interactions. Therefore, by splitting the exergy into the mechanical and thermal forms, the ESC can be directly related to the exergy waste coefficient (EWC) and exergy recovery coefficient (ERC) by Eq. (39b).

$$\mathrm{ESC} = 1 - \frac{\dot{\mathcal{E}}_{\mathrm{P}}}{\dot{\mathcal{E}}_{\mathrm{P,ref}}} \tag{39a}$$

$$= \mathrm{EWC} \cdot \mathrm{ERC} \tag{39b}$$

Arntz [68] defines the exergy waste coefficient (EWC) under three different forms (two reported here), as it depends on the position at which the exergy potential is evaluated: in the far wake, for a powered configuration at equilibrium (Eq. (40a)) and for an airframe not subject to additional exergy supply (Eq. (40b)). Analogous to the energy-based methods, EWC echoes PER^c [85] or $\mathrm{PSC}_{\mathrm{ideal}}$ [84] by accounting for the thermal management and quantifies the amount of exergy that is destroyed, or the amount of total anergy that is produced.

$$\mathrm{EWC} = \frac{\dot{\mathcal{E}}_m + \dot{\mathcal{E}}_{th}}{\dot{\mathcal{E}}_{\mathrm{P}}} \tag{40a}$$

$$= \frac{\dot{\mathcal{E}}_m + \dot{\mathcal{E}}_{th}}{\boldsymbol{\mathcal{T}}_{\mathrm{B}} \cdot \boldsymbol{V}_\infty} \tag{40b}$$

Lastly, the consideration of a device that is able to recover the exergy through its ingestion, e.g. BLI propulsor or heat exchanger, can be described by the exergy recovery coefficient (ERC) which evaluates how effectively the exergy present in the flow is recovered:

$$\mathrm{ERC} = \frac{\dot{\mathcal{E}}_{\mathrm{P,ref}} - \dot{\mathcal{E}}_{\mathrm{P}}}{\dot{\mathcal{E}}_{m,\mathrm{ref}} + \dot{\mathcal{E}}_{th,\mathrm{ref}}} \tag{41}$$

Overall, PER and EWC appear as the metrics to be used early in the design phase to evaluate the potential of the configuration. When the propulsion systems are integrated, it appears clear that the PSC quantifies the savings enabled by the configuration relative to the reference considered. However, as stated by Hall et al. [86], the PSC is not an absolute metric and is rather circumstantial. Its value can vary widely depending on the baseline selected for comparison, and likely to be dependent on other secondary or unrelated differences in airframe design.

2.2.4. Mission-level performance

In addition to the performance and savings that can be claimed at design points, the integration of those over an entire flight mission allows the benefits to be compounded and computed in terms of fuel savings or extended mission range. Particularly, with the Transport Aircraft System OPTmization (TASOPT) framework developed in Ref. [87], the aircraft's weight, and aerodynamic and propulsive performance are predicted from low-order models. The design-mission is segmented in its different phases where the thrust requirement and weight loss are tracked along the change in altitude and range. At any profile point, the climb and weight-loss gradients are computed and suitably integrated over the mission to yield the altitude and weight profiles. The trajectory equations are then integrated resulting in a form of the Breguet range equation (Eq. (42)) and allowing for the fuel burn to be interpreted from the difference in aircraft weight from take-off to landing.

$$\mathcal{R} = \frac{C_L}{C_D} \frac{V_\infty}{\mathrm{TSFC}} \ln\left(1 + \frac{W_{fuel}}{W_{\mathrm{A/C}}}\right) \tag{42}$$

The mission range is function of the lift-to-drag ratio, the flight speed in the RRF V_∞, the thrust-specific fuel consumption (TSFC) which divides the fuel-flow by the amount of thrust generated and describes the efficiency of the fuel to produce the output force, and the weights of the fuel carried W_{fuel} and aircraft $W_{A/C}$.

Subsequently, from the product between the TSFC and the flight velocity, the power-specific fuel consumption (PSFC) implements the power balance [33] into the range equation to yield the power-based Breguet equation for both non-BLI and BLI aircraft, Eqs. (43) and (44) respectively. The range comparison between the two aircraft advises on the range extension suggested by BLI, or the fuel savings granted for an equivalent range to the non-BLI aeroplane.

$$\mathcal{R}_{\mathrm{non-BLI}} = \frac{C_L}{C_{\Phi_{\mathrm{non-BLI}}} + C_{\dot{\mathcal{E}}_v}} \frac{1}{\mathrm{PSFC}_{\mathrm{non-BLI}}} \ln\left(1 + \frac{W_{fuel}}{W_{\mathrm{A/C}}}\right) \tag{43}$$

$$\mathcal{R}_{\mathrm{BLI}} = \frac{C_L}{C_{\Phi_{\mathrm{BLI}}} + C_{\dot{\mathcal{E}}_v}} \frac{1}{\mathrm{PSFC}_{\mathrm{BLI}}} \ln\left(1 + \frac{W_{fuel}}{W_{\mathrm{A/C}}}\right) \tag{44}$$

By convention, the specific fuel consumption describes a form of efficiency of the system but when BLI is involved, the metric does not yield much information. Indeed, a BLI aircraft may have a higher TSFC than a tube-and-wing aircraft but as its thrust requirement is lowered by the reduction in the aircraft's wake, the overall fuel consumption may be lower. Consequently, with the gain in popularity of the energy-based methods, the PSFC aims to alleviate these ambiguities. Nevertheless, neither the TSFC or the PSFC account for the installation effects and additional penalties associated. Although the definitions do not consider either any other form of energy that could eventually be used to power the BLI propulsion systems such as used in hybrid-electric architectures [88–90], the NPF and power supply can substitute the thrust generation and power consumption from the propulsion system to take into account these additional losses.

In this perspective, Seitz and Gologan [48] define the energy-specific air range (ESAR) which indicates the change in range per change in energy independently of the source of energy used:

$$\mathrm{ESAR} = \frac{\mathrm{d}\mathcal{R}}{\mathrm{d}\dot{\mathcal{E}}_{\mathrm{P}}} = \eta_{ov} \cdot \frac{L/D}{W_{\mathrm{A/C}}} \tag{45}$$

They demonstrate the strong sensitivity to the wing aspect ratio and Reynolds number, and conversely the weak correlation with the design Mach number, or fan efficiency. The metric quantifies how efficient is the aircraft compared to the amount of energy used $\dot{\mathcal{E}}_{\mathrm{P}}$ by the systems for a specific range $\mathcal{R}$, or alternatively by how much the range can be extended with the same supply. The ESAR is also defined as a function of the aircraft overall efficiency, lift-to-drag ratio, and aircraft weight but no explanation is retrieved on the way drag is calculated and as previously stated, that quantity is not directly extractable. Therefore, alternative means have been defined and follow.

In the same vein, for quantifying the aircraft performance along the mission, Hileman et al. [91] introduce the payload fuel energy efficiency (PFEE) which quantifies the amount of energy, contained within the fuel, that is consumed relative to the payload, in cargo or passenger aircraft. The authors also offer to use the PFEE as an environmental performance metric with the example of a carbon dioxide intensity metric that would divide the emissions of CO_2 by the product of PFEE and the fuel energy content per unit mass. The concept is further investigated by Sato who redefined the PFEE as the payload fuel energy intensity (PFEI) in Eq. (46) that can also be re-written as a function of the aircraft aerodynamic and propulsive performance using a modified Breguet range equation in its thrust or power balance terms.

$$\mathrm{PFEI} = \frac{W_{fuel}\, h_{fuel}}{W_{payload}\, R} \tag{46}$$

From an exergy standpoint, Arntz et al. [35] define a range equation $\mathcal{R}_{\mathcal{E}}$, alike with the energy-based formulation, with the exergy specific fuel consumption (ESFC), the lift, the anergy generation coefficients and the weights of the empty aircraft and the fuel carried:

$$\mathcal{R}_{\mathcal{E}} = \frac{C_L}{C^*_{\dot{\mathcal{A}}}} \frac{1}{\mathrm{ESFC}} \ln\left(1 + \frac{W_{fuel}}{W_{\mathrm{A/C}}}\right) \tag{47}$$

It is opined that Eq. (47) is akin to Eqs. (43) and (44) with the substitutions of the energy terms for exergy terms, thus considering the thermal energy aspects. Whereas increasing the thrust-, power-, or exergy-specific fuel consumption would exhibit a larger range, in the energy- and exergy-based book-keeping schemes, the objective is rather to reduce the losses associated, either in the form of Φ or $\dot{\mathcal{A}}^*$, respectively in Eqs. (44) and (47).

At a mission level, the range equation to consider is circumstantial as it depends on the approach considered for the study. As such, all range equations are considered equivalent but for the reasons previously exposed, Eqs. (42) and (45) are ambiguous as they depend upon the lift-to-drag ratio whereof drag is not extractable. Whether the energy or exergy analyses are followed, viscous dissipation or total anergy generations appear as more pragmatic and the difference in ranges quantify a form of mission savings.

2.2.5. Discussion on figures of merit

The numerous metrics retrieved from the literature appear to present different levels of implementation or practicality. In their work, Ref. [32] rates their reviewed metrics by degrees of universality and applicability at conceptual design phases based on weighed sub-criteria. As summarised in Table 3, the energy/exergy-based approaches feature higher degrees of universality but lower applicability to conceptual design phases due to their high computational demand. However, at refined design phases, these methods aid in the interpretation of the physical mechanisms underpinning BLI propulsion.

At any given point along the flight envelope, the PSC appears as the most versatile figure of merit to quantify the savings enabled by BLI relative to the considered reference. However, as mentioned, this presents several challenges from which a common reference aircraft is necessary to compare different novel aircraft as well as the means of quantifying the amount of power required in both scenarios. Eq. (36) is thought to best describe the power savings considering the shaft power of the BLI propulsion system due to the caveat related to $\dot{\mathcal{E}}_{\mathrm{P}}$. In concert with the PSC, the TS should act as a trade-off metric between the propulsive force share from the thruster and the savings claimed (in thrust-splitting architectures).

Extending from the PSC for considering the entire flight envelope, the difference between the novel aircraft and its reference can either be calculated in terms of extended range (for the same fuel/power carried) or fuel block savings (for the same design range). As such, either Eqs. (43) and (44) or Eq. (47) can be used but the ESAR allows to combine both changes (Eq. (45)). However, the authors only retrieved Ref. [48] discussing the metric and it seems that no other reference applied it.

3. Numerical methods and models

3.1. Numerical methods

To evaluate a vehicle's performance, it can either be performed from a scaled-down wind-tunnel model or a numerical geometry based on aerodynamic and propulsive models. Inherently for the latter, the performance is subject to the modelling fidelity and the time allocated to perform those assessments. A trade-off between the degree of fidelity and computational cost of the investigations must be found giving rise to the development of more robust and developed low-order models. This section therefore introduces several methods that are commonly used in the evaluation of BLI aircraft, notably with the breakdown of the drag components as well as the different flow features present in the flow-field.

3.1.1. Drag decomposition

In the analysis of the aerodynamic forces, their decompositions allows one to capture the phenomenology into different components Drela. compares different breakdown methods and categorises them into different attributes: exactness, consistency, and uniqueness [92]. The treatment of the *near-* and *far-field* integrations is achieved by different methods considering tightly integrated engine-airframe configurations.

Near-field forces

The *near-field* examination of forces on physical surfaces consists in attributing local forces to either the pressure or friction components:

$$\mathcal{F} = \underbrace{\oiint_{S_{\mathrm{B}}} -p\hat{n}\,\mathrm{d}S}_{\mathcal{F}_{\mathrm{pressure}}} + \underbrace{\oiint_{S_{\mathrm{B}}} \bar{\bar{\tau}}\cdot\hat{n}\,\mathrm{d}S}_{\mathcal{F}_{\mathrm{friction}}} \tag{48}$$

Alternatively, a recasting of the *near-field* investigation with the actual forces on the bodies, into a flux definition enables a further component to be included in the breakdown:

$$\mathcal{F} = \underbrace{\oiint_{S} -p_{\mathrm{G}}\hat{n}\,\mathrm{d}S}_{\mathcal{F}_{\mathrm{pressure}}} + \underbrace{\oiint_{S} \bar{\bar{\tau}}\cdot\hat{n}\,\mathrm{d}S}_{\mathcal{F}_{\mathrm{friction}}} - \underbrace{\oiint_{S} \rho(\boldsymbol{V}\boldsymbol{V}\hat{n})\,\mathrm{d}S}_{\mathcal{F}_{\mathrm{flux}}} \tag{49}$$

This integration is performed on permeable inlet and outlet stations defining a control volume surrounding a body. Conventionally, this form emanates from the momentum conservation whereby the stream-wise $\mathcal{F}_{\mathrm{flux}}$ is often unjustly characterised "thrust". In addition to the previous reasons given on the debatable designation of thrust, the reference pressure used to define the gauge pressure p_{G} brings another ambiguity in BLI scenarios as to how should the reference pressure be defined (free-stream, integrated at a given location along the airframe...).

To enable a refined interpretation of the experienced force by the body, a novel *near-field* decomposition method is proposed [93] which separates the pressure field into a constitutive dissipative (viscous, $\mathcal{F}_{p,\mu}$) and non-dissipative (Euler, $\mathcal{F}_{p,E}$) contribution. Eq. (50) decomposes the viscous and Euler components along the body's surface. The universality of the partial pressure field (PPF) analysis [93–95] allows one to couple it to momentum- and energy-based analyses, similar to the velocity decomposition proposed in Refs. [73,96]. With a more robust decomposition of force terms, Mutangara et al. [97] improves the velocity decomposition approach by coupling it with PPF and demonstrates its applicability with an assessment, understanding and tracing of the phenomenological sources of aerodynamic drag on sub- to transonic flow regimes over a NACA 0012 aerofoil.

$$\mathcal{F}_{\mathrm{pressure}} = \underbrace{\oiint_{S_{\mathrm{B}}} -p_{\mathrm{E}}\hat{n}\,\mathrm{d}S}_{\mathcal{F}_{p,E}} + \underbrace{\oiint_{S_{\mathrm{B}}} -p_{\mu}\hat{n}\,\mathrm{d}S}_{\mathcal{F}_{p,\mu}} \tag{50}$$

"Ingested drag"

Several Refs. [47,48,64,98] refer to an "ingested drag" quantity $\mathcal{D}_{ing}$ that is computed at the inlet station of the BLI fans using Eq. (49). They all agree on defining the quantity as the amount of drag captured inside the internal stream-tube that crosses the fan, as the perturbations emanate from the development of the BL around the airframe. Following that reasoning, the profile drag ingested appears as a positive thrust contribution and can be interpreted as a reduction in ram drag. Here, the authors disagree as an effect from BLI is the attenuation of the aircraft's wake and not its drag. Inherently, depending on the size of the BLI fans integrated, the portion of $\mathcal{D}_{ing}$ can be outweighed by the penalties caused by the nacelle.

Far-field forces

An extension of the control volume defined in Eq. (49) recasts the *near-field* force expression into a *far-field* definition. Whereas the previous definition can be applied to ④ from Fig. 4, the *far-field* integration is performed on ① but yields the same information as juxtaposing several smaller CV to form ①.

From this point of view, the forces can be subdivided in more fashions with the profile (skin-friction, or lift-independent), wave, and induced (lift-dependent, or vortex) force components.

In the wake, surface integrals can be extracted by identifying the change in total energy, through enthalpy terms, as the thrust, and the generation of chaos and losses, with entropy terms, as the profile, wave, lift-induced and interference drag [51,99]. From this decomposition, Gauss' theorem transforms the surface integrals in volume integrals which can be related back to the local physical mechanisms within the flow-field. Nonetheless, this process requires the separation of the shear layer, shock, vortex and jet regions from the entire flow-field (Section 3.1.2) that respectively correspond to the profile, wave and lift-induced drags and thrust [55].

More specifically for the profile drag prediction of an isolated fuselage, Nicolosi et al. [100] investigated slender fuselage geometries in CFD. They divided up the fuselages into three sections — nose, cabin and tail, isolating fuselage drag coefficients. This method proves its importance at a conceptual stage where estimates must be made on the fuselage shape.

Additionally, other volume integral approaches [50,56] use surface integrals to approximate the lift-induced drag. Nonetheless, the complexity in the extraction is detailed by Spalart [101] who calls into question the rigour to which lift-induced drag can be defined. Méheut et al. [57] compare different profile and induced-drag definitions that despite providing an accurate phenomenological breakdown do not apply to all configurations and therefore suggest and test theirs both numerically and experimentally.

An energetic/exergetic decomposition discards the artificial concepts like ingested drag and enables a physical interpretation of the contributions by investigating the power sources and sinks. However, these methods only treat the stream-wise component and Lamb vector methods can be employed to approach the lift forces [51]. Notably, the viscous component present in shear layers is isolated (and can be combined to the wave component to characterise the profile force). A drag breakdown of an aerofoil and a wing is offered by Aguirre and Duplaa [103] along with exergetic drag curves and a complement with a *far-field* wave anergy extraction suitable for wind-tunnel applications. However, the formulation of the exergy method [35] does not allow for drag prediction and decomposition in wind-tunnel testing and a velocity decomposition technique is proposed to suit an exergy analysis [96].

3.1.2. Flow features extraction

To attribute the benefits and penalties to particular mechanisms in the flow, their identification in numerical studies is achieved by different formulations. First, in BLI, it is vital to qualify the BL and quantify its quantities before its (partial) ingestion. In parallel, the different flight conditions and aircraft geometries affect the flow that develops around the airframe. As such, it is also possible to identify and extract regions of the flow where major accelerations are experienced and generate shocks, produce a propulsive force or form vortices. Fig. 8 depicts the flow features extractable in CFD by different means discussed hereafter.

(Quasi-)1D boundary layer

At conceptual-level, to prevent the resolution of the Navier–Stokes equations in CFD, Goldberg et al. [104] propose a method to evaluate the performance of a propulsion system by using BL theory and one-dimensional gas dynamics. On their BWB aircraft, the power law [105] that defines the BL velocity profile and thickness over a flat-plate is used to approximate the airframe upper surface. After a validation procedure to assess the exactness of the developed method when compared to CFD, a 0.2% difference in total pressure losses is reported and 3.8% in the captured height of the incoming flow on the NASA N3-X [104]. Nevertheless, it should be stressed that the model, despite being able to capture relatively well the inlet flow conditions at a lower cost, is based on flat-plate theory and is only suitable for BWB-like configurations not subject to strong pressure gradients on curved surfaces and whereof installation effects must be accounted for [106,107].

Alternatively, still in the scope of reducing the computational cost, Ref. [108] proposes a coupled method which makes interactions between an aircraft sizing tool and an engine cycle model. The aircraft model is fed into a potential flow solver that filters out the viscous region of the flow and defines the edge of the BL. The streamlines exported from that initial run help define the BL properties such as the thickness and momentum defects to describe the inlet properties. The engine cycle model then computes the reduced ram drag and inlet pressure losses to assess the performance of the propulsion system. For validation, the results are compared with experimental data of the MIT D8 [109] and give a 4.9% discrepancy, at the centreline, in BL thickness and 2.3% in kinetic energy defect.

In a similar vein, following a layered strategy, Kaiser et al. [110] developed a quasi-analytical method based on the application of several theories to account for the pressure gradients and installation effects. To start with, potential theory, alike Ref. [108], provides the pressure gradient along the body. Then, boundary layer theory is used and feeds the actuator disc and blade element theories to consider installation effects, from which the former advises on the effects upstream and downstream of the fan, and the latter provides a radial work distribution across the fan stage.

Shear layers

As an alternative to using inviscid, or potential flow solvers, one can identify the shear layer regions from viscous compressible CFD. Ultimately, when relating to the shear layer, the δ_{99} definition arises as to the first method which identifies any point normal to the surface that reaches 99% of the free-stream velocity — or, of the temperature for the thermal layer. Nevertheless, besides flat-plate theory, this method is argued when changes in curvature and adverse pressure gradients are experienced and δ_{99} rather takes the definition of any point normal to the surface that reaches 99% of the edge velocity. This, on the other hand, implies the BL edge to be identified and its velocity to be extracted.

Lovely [111] examines vorticity to calculate the BL momentum thickness from CFD but despite being powerful on simple bi- and three-dimensional geometries, it proves to be impractical for complex geometries and unsteady simulations [112]. Consequently, rather than considering integral methods, scalar expressions are also employed by Lovely [111] with entropy and vorticity but present the drawback of also capturing regions like shock waves. Baskett and Haimes [112] developed an approach which iteratively calculates a conservation equation yielding a shear layer identification in both laminar and

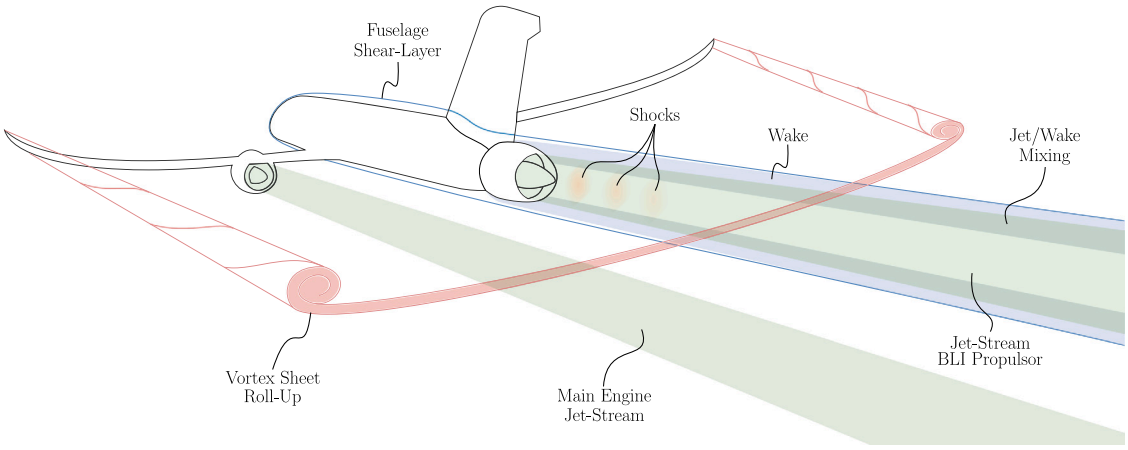


Fig. 8. Flow features around a propulsive fuselage aircraft.

viscous flows and successfully omitting shocks despite the relatively high computational demand from the iterative process.

From an energy point of view, Sanders and Laskaridis normalised the viscous dissipation Φ by the absolute volumetric pressure work and coupled it to the normalised turbulent viscosity factor which metric can capture the laminar and viscous zones as well as filter the shocks without an iterative procedure [17]. Despite identifying correctly the viscous layer, some deviations appear with complex geometries (powered aircraft):

$$\xi = \left(\frac{\mu + \mu_t}{\mu}\right) \frac{\overbrace{\left(\nabla \cdot \bar{\bar{\tau}}\right) \cdot \boldsymbol{V}}^{\Phi}}{|p\nabla \cdot \boldsymbol{V}|} \tag{51}$$

Shock wave

The shock waves identification in CFD is not as trivial as locating flow regions whereby the local Mach number rises to unity. The discontinuity and mesh definition make difficult the identification of the region which thus requires the consideration of the gradient. For that matter, Lovely and Hairnes [113] developed an algorithm capable of identifying shocks in steady and transient conditions from one- to three-dimensional models. The implementation of a filter prevents the identification of falsely located shocks which result from numerical discrepancies. A first algorithm treats the flow-field by identifying regions whereby a shock test scalar is unity and rejects a subset of surrounding grids that make-up that surface. Alternatively, another algorithm filters out grid elements that fall below a particular pressure gradient magnitude threshold but requires an appropriate definition of that threshold. The last technique enquires jumps in density and temperature around the shocks. After comparing the three different techniques, Lovely and Hairnes conclude that additional filtering is not as effective as a sole pressure gradient magnitude threshold of 0.95 on ζ [17,71]:

$$\zeta = \frac{\boldsymbol{V} \cdot \nabla p}{a\,|\nabla p|} \tag{52}$$

Recently, Saetta and Tognaccini [114] implemented an unsupervised algorithm to identify the viscous and wave regions of the flow-field by use of machine learning. Unlike the deterministic methods reviewed above, the regions are identified in their work without input thresholds. These efforts tested on aerofoils and wings on subsonic and transonic regimes enable the flow regions to be isolated without visual inspection from the user [114].

Vortex

To evaluate the influence of the lift-induced drag, source of noise and energy loss, that results from the difference in pressure between the pressure- and suction-surface of any lifting body, it becomes necessary to identify the structures formed from the shed vorticity at the wingtips. Soto-Valle et al. [115] compare different vortex identification methods and differentiation schemes, notably with the experimental work of Graftieaux et al. [116] using particle image velocimetry (PIV) and Hunt et al. [117] whose method is based on vorticity magnitude.

Velocity gradient-based vortex identification methods are notably the most well-known, with popular examples such as the Q- and λ_2-criterion. To concisely elaborate further on these, the Q-criterion [117] defines a vortex as a connected fluid region which pressure is lower than the ambient and which second invariant is positive, i.e. greater vorticity than strain-rate magnitude ($Q > 0$) [118]. On the other hand, the λ_2-criterion defines a vortex as a region whereof the value of λ_2 is negative; which is achieved by identifying a region of minimum local pressure which entrains the vortex [119]. Both methods do carry their own inherent limitations in particular scenarios discussed in Ref. [118] which should be considered during application. A more detailed description of other types of identification methods can be found in Refs. [51,115,120].

Jet-stream

Whereas the preceding methods identify the mechanisms responsible for *drag* with its profile, wave and lift-induced components, enthalpy aids determining the region responsible for *thrust*. Most Refs. [55,56,99] favour a force decomposition rather than the identification of the whole jet-plume however, in configurations not subject to heat addition from the airframe, the propulsor is the only source of stagnation enthalpy raise therefore it appears logical to build an identifier on this metric. Sanders and Laskaridis [17] isolate the jet-plume volume from a large deviation in total enthalpy when compared to the free-stream condition. Nevertheless, they report the importance of the threshold as shear stresses can cause a redistribution of the free-stream enthalpy outside of the jet region, particularly when the wake of the BLI aircraft merges with the jet. A 10% deviation in total enthalpy is found to be insensible to changes in jet-stream viscous dissipation rate, Φ, and volumetric pressure work, Θ and thus defines the identifier, Υ:

$$\Upsilon = \frac{\Delta H}{H_\infty} > 0.1 \tag{53}$$

3.2. Aero-propulsive numerical modelling

In numerical simulations and more importantly with regards to BLI, fully coupled multidisciplinary modellings are essential [42,62]. The tight integration of the propulsion system within the airframe entails the use of a coupled aerodynamic and propulsive model to study the aero-propulsive benefits of BLI. Formerly, uncoupled analyses were performed in which the aerodynamic performance was assessed without any propulsion model [26,121,122], or the propulsion system was

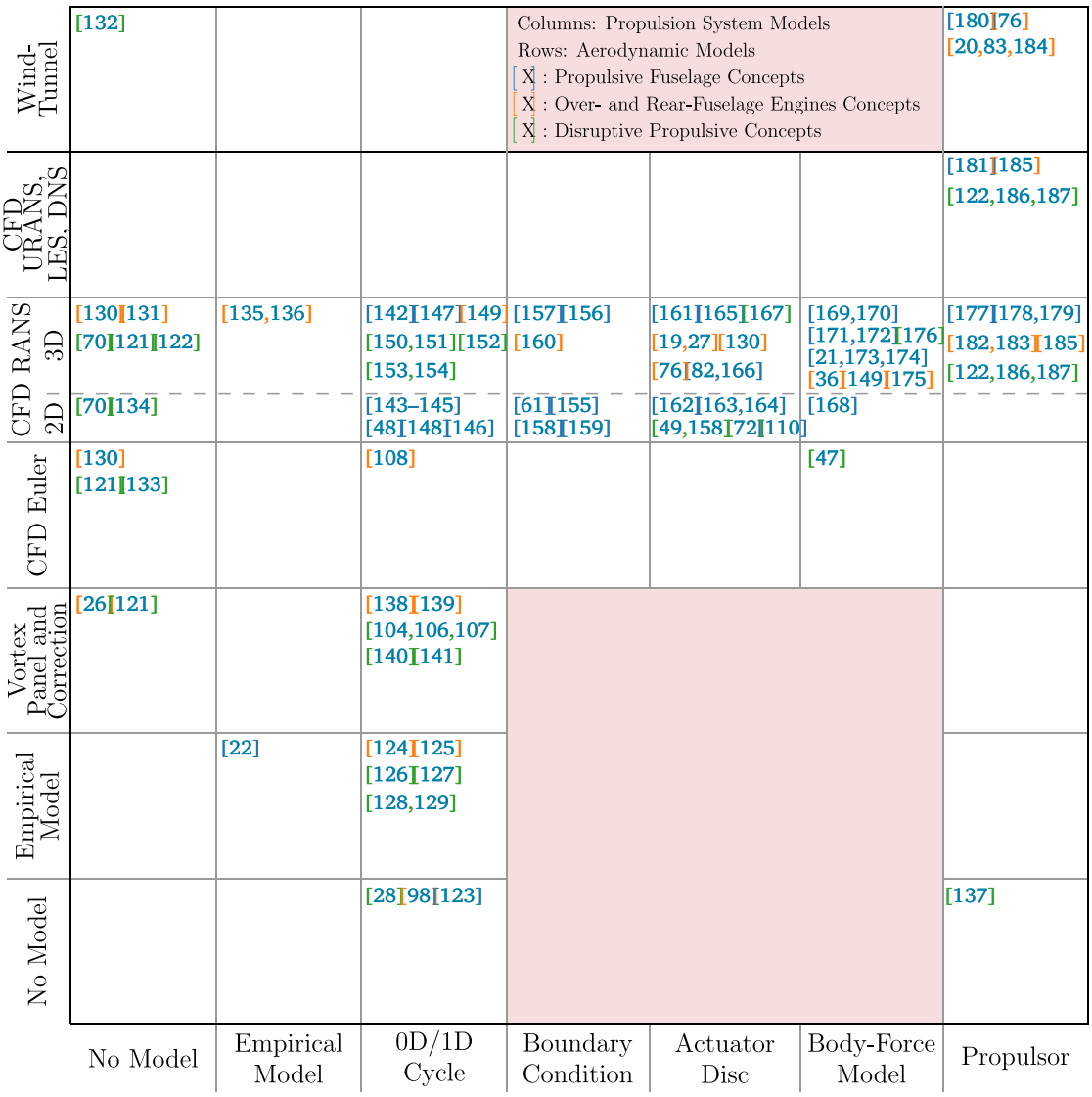


Fig. 9. References mapped out with their respective aerodynamic models (y-axis) and propulsive models (x-axis).

evaluated without the aerodynamic performance [28,98,123]. With the never-ceasing development of numerical solvers, the aerodynamic and the propulsion are weakly- or strongly-coupled [42] and the propulsion model can either be a 0D/1D thermodynamic cycle that iteratively communicates with the solver or with boundary conditions (BC), actuator discs (AD) or body-force models (BFM), if not modelling the full rotating fan.

To numerically model the different BLI concepts, one needs to design the airframe, whether it be in two or three dimensions, generate its structured or unstructured mesh, to model the aerodynamic of the flow and BC, AD, BFM, or single passage or full annulus fan to model the propulsion system. Different CFD software allow for externally communicating with thermodynamic cycles which can interact and iteratively update the propulsion system model back to the CFD. The numerous aero-propulsive modellings from the references reviewed in this work are categorised in Fig. 9 for different fidelities. Additionally, a review from Menegozzo and Benini [43] focuses on the numerical modelling approaches along with their methods. They collate the studies and characterise the geometric, aerodynamic and propulsion models.

First, in the modelling of the airframe, different numerical degrees of fidelity can be designed. For two-dimensional axi-symmetric studies, a common practice relies on the extraction of a reference aircraft contour that accommodates a rear-mounted propulsor [143–145]. Alternatively, the fuselage can be approximated with an elliptical nose, cylindrical centre body, S-shaped curve leading to the propulsor and aft-cone downstream of it such as in Refs. [61,155,159]. Habermann et al. [155] approximate an A330-300 in such a way that it prevents shocks on the outer contour from previous work by Seitz and Gologan [48] and Bijewitz et al. [163,164]. In a similar vein, Battiston et al. [159] and Matesanz-García et al. [61] approximate the fuselage using either circular arc and Bell–Mehta curves [188] for the former or iCST curves [189] for the latter to define the propulsor region. It is opined that only BLI concepts based on a tube-and-wing aircraft baseline can be approximated with models in axi-symmetric two dimensions and all other conceptual designs require three dimensions bringing additional challenges in the modelling, or 2D planar investigation for particular cut-through planes.

The 3D modelling of the NASA STARC-ABL aircraft [22] relies on openVSP [190] which is a 3D modular modelling software to generate and optimise geometries [21,169,170,173,174] that are meshed volumetrically via mesh morphing [191]. Nonetheless, although being acknowledged for accurately predicting the physics, structured meshes are computationally expensive and rather complicated to generate. Instead, over-set meshes are often preferred for their *simple* implementation which allow the model to be split down into several sub-domains individually meshed such as with the ONERA NOVA [19] using Pointwise [192], Refs. [131,146,156] with STAC-CCM+ [193], Refs. [194] with ANSYS ICEM [195,196] or using Cart3D [197,198], AutoGrid [199] or GSMH [200].

The choice made in the meshing structure is critical as it impacts the accuracy of the results obtained in CFD. For instance, structured meshes are favoured for refined grids to capture the different aerodynamics effects close to the surfaces like viscous dissipation. The choice in turbulent modelling is also vital as it drives the mesh quality requirements notably with the y^+ to solve the viscous layers or decompose the pressure field. To overcome these potential issues, it is recommended to perform grid and domain sensitivity studies following procedures such as suggested by Celik et al. [201].

As per the numerical simulations, a variety of commercial software and in-house codes are used. To cite a few, ANSYS Fluent [202], openFOAM [203] and ONERA elsA [204] are common but DLR Tau [205] or ANSYS CFX [206] can also be named. Based on differentiated adjoints, ADflow [207] is extensively used on the NASA STARC-ABL [21,62,161,169,170,173,174]. Although most work is based on steady computations, motivations are found in the unsteady resolutions [181,186,187].

On the propulsion side, BC's are common practice whereby the fan-face is accounted as a pressure outlet whereas the fan-exit ensures mass continuity through the propulsor stage with a balanced mass-flow inlet [61,143,144,155,159]. With BC, the propulsion system can incorporate a thermodynamic cycle, which most widespread models are called GasTurb [208] used in Refs. [48,49,140,148,158,163,164,167] or OpenMDAO with pyCycle[4] [21,62,173,174] which is based on NASA's software NPSS [209]. The outflow from the fan-face is fed into the 1D cycle and iteratively calculates the engine properties communicated back to the CFD solver at the fan-exit. To virtually take into account the effects of the blades that are not captured by the BC, immersed boundary conditions have been developed and implemented by the ONERA [160,210,211].

Alternatively, and increasing the fidelity of the solutions, actuator discs [35,161–164,212] or body-force models [21,149,168,169,172,173,176] with source terms can be used to simulate the fan effects.

The most computationally demanding representation of the propulsor is the full-annulus blade model of the fan which requires a fine meshing of each blade passage [137,177,179,183,213] but allows an accurate representation of flow blockage and swirl with RANS or unsteady RANS.

3.3. Direction of numerical analyses

As given by Fig. 9, a multitude of numerical studies have been conducted in the past two decades. It appears clear that high fidelity is often sought, and more with years, with RANS modelling and actuator discs or body force models. Nonetheless, *simple* propulsive modelling as provided with the boundary conditions often suffices to focus on aerodynamic behaviours and flow mechanisms. There is however a distinct progress towards higher modelling with 3D RANS and BFM as preliminaries have matured. The choice of models is rather circumstantial and highly depends on the objectives of the studies. For example, BC satisfy most propulsive conditions and enable a simple representation whilst still studying aerodynamics effects. On the other hand, BFM are likely chosen to study the flow through the fan stage with the transport of the distortion to the exhaust and jet plume.

[4] https://github.com/OpenMDAO/pyCycle.

4. Experimental apparatuses and practices

Whilst computational fluid dynamics constantly evolved to accurately represent the flow phenomena, numerous experimental studies have been performed on sub-scale models, and have been subject to the following challenges:

- the similitude between the full- and sub-scale models is not ensured [214];
- the propulsor emulation and operability cannot be directly scaled;
- the instrumentation requires calibration and sometimes correction;
- the utilisation of sparse measurement might require coupling with CFD (data fusion).

4.1. Aircraft models

A major difficulty in wind-tunnel experiments is the scaling effects [215,216]. Not only geometric, but also kinematic and dynamic similarities need to be ensured for similitude which require the model to be identically scaled, non-dimensional numbers such as Mach, Reynolds and Prandtl, to be equivalent and flow-field properties like pressure or drag coefficients to be the same [217–219]. Even though the free-stream Mach number and geometry scaling are often possible, it is common to note a Reynolds mismatch which prevents similitude [83,220,221]. Notably, a review on sub-scaled models and similitude theory on structural and vibratory components is provided by Coutinho et al. [222] but also applies to aerospace. With regards to the scaling of aerospace models, a reasonable state-of-the-art scaling for subsonic flows on small Reynolds numbers is findable but degrades as testing approaches transonic conditions and higher Reynolds numbers [215].

In addition to the testing conditions, the wind-tunnel facility and model support also play a detrimental role in the accuracy of the results obtained. The influence of the walls on the surrounding needs be accounted with for example different cross sections to prevent the pressure field to be affected or transpiration to attenuate the development of the walls' boundary layers. Also, the mounting supports need to be cautiously selected depending on the BLI aircraft architecture to not capture losses or disturb the flow around and behind the model (Appendix A.1).

When conventional aircraft are experimentally tested, the development of the boundary layer around the airframe and inside the podded engines' intakes is of minor importance whereas it is the essence of BLI. If the aircraft is linearly scaled and equivalent flight conditions are replicated, the Reynolds number will mismatch as well as the BL development impacting the flow properties at the AIP. When similitude is not respected, mainly from Reynolds mismatch [223,224], corrections on scaling are necessary [215,225,226]. To reduce those corrections, the NASA N2A-ExTE [132], MIT–Aurora–Pratt & Whitney D8 [20,76,83,109,184] and also propulsive fuselages [180,221,227] attempted to mitigate this mismatch by reducing the free-stream velocity of the testing to match the Reynolds number albeit producing a Mach number difference. This unavoidably impacts the compressibility effects and affects the flow that is ingested by the propulsor.

Inherently, all this affects the operability of the BLI propulsor and an additional challenge lies in its own scaling. Indeed, if comparison is performed between CFD and experiments and both between an aircraft flying at flight conditions and its sub-scaled version at wind-tunnel conditions, the amount of mass-flow ingested needs to be compared [46]. As mentioned, if similitude is not ensured, the amount of energy imparted into the flow (from an ARF standpoint) is different and the mass-flow needs to be scaled accordingly to the cost of the fan operation (distortion) and its emulation with the potential savings stemming out. Whilst commonly a fan is used within a nacelle, additional concerns might be brought to the discussion if the fan faces high amount of distortion [76] and the blades are not designed to sustain

it [228]. Instead, the fan can be substituted with an ejector-powered engine simulator from which high-pressure gas pumps the ingested flow [229,230]. Despite its effectiveness in podded engines to generate thrust, no experimental data have been found on BLI in the literature despite an on-going project [231]. Nevertheless, additional challenges emerge with the importance of designing the assembly to minimise losses. The addition of mass-flow in the system also necessitates the control volume calculations to consider these extra source terms in the wake and requires the book-keeping schemes (e.g. power balance) to be adapted.

4.2. Measurement techniques and instruments

4.2.1. Force

Through the years, the set-ups and instrumentation never ceased to evolve and led to more practical performance evaluations. To prepare for future research campaigns, Atinault et al. [165] at ONERA conducted a synergistic experimental and numerical study of a movable electric ducted fan ingesting the wake from a body of revolution at low-speed conditions. The aerodynamic forces experienced by the body are measured from a floor balance whereas the thrust generated is monitored from a six-component balance mounted on the engine. Blunt bodies of different sizes are modelled to ensure a constant BL area that corresponds to that of the engine's fan face. As for the engine, it can be positioned axially from the body's trailing-edge to 500 mm behind it, and radially to ingest different mass-flow rate — radial offset from the fuselage's centreline (Appendix A.2). Similarly, Sabo and Drela [232] tested another body of revolution with an equivalent approach and came to the same conclusions that maximum power savings are achieved for a propulsor positioned at the trailing-edge of the fuselage with a PSC of 22% for Atinault et al. and 25% for Sabo and Drela. In both scenarios, the further away axially and radially, the lower the BLI benefits as energy dissipates and more free-stream air is ingested. Unlike the main balance used by Refs. [20,83,165], forces on the model were measured by a load cell that can only evaluate the axial component. Nonetheless, the objectives of Ref. [232] were to obtain a net-zero stream-wise force and evaluate the benefits of BLI and the load cell fitted that purpose.

4.2.2. Pressure

With regards to the pressure measurements, they are of high importance to quantify the amount of mass-flow that is ingested by the BLI propulsor, the total pressure distortion at the AIP, the total pressure at the nozzle and within the wake, and the pressure distributions to validate *near-field* forces along surfaces. A simple arrangement of pressure rakes is its fix mounting on the model where guidelines are provided in Ref. [75] on military intake — BLI was not considered at the time of writing. The rake disposition agrees with the one discussed in Section 2.2.1 and illustrated in Fig. 7. Nonetheless, the fixed position of the arms and probes provides relatively sparse data which needs to be interpolated and therefore reduces the accuracy of the measurements. As a solution, rotating rakes have been developed [233] in which the arms move altogether to sweep the AIP plane and obtain a more populated data coverage (Fig. 10) [20,76,83,109,184]. The drawbacks from this practice nonetheless is the time required to measure all data in the wind-tunnel and the potential flow perturbations (Appendix A.2).

Although these techniques are popular for engine's inlet and outlet planes measurements, in the wake, other methods are favoured, e.g. traversing wake rakes [180,220]. The measurements in the mid-to-far-field become essential to apply energy-based methods from which the energy-flux transfer is described and the power balance ensured [180]. Notably, previous experiments yield power consumption reductions of respectively 10 and 18% for the wake ingesting and BLI configurations but additional testing are required to predict in-flight savings.

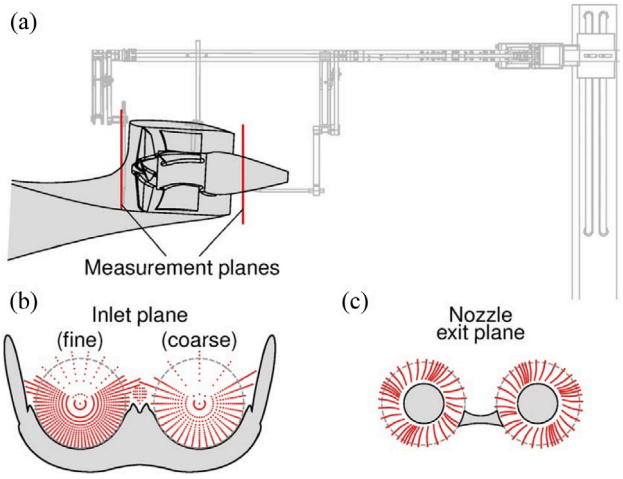


Fig. 10. Experimental (a) model-mounted survey systems and measurement plane locations, (b) measurement grids for BLI inlet and (c) nozzle exit surveys, from Ref. [76].



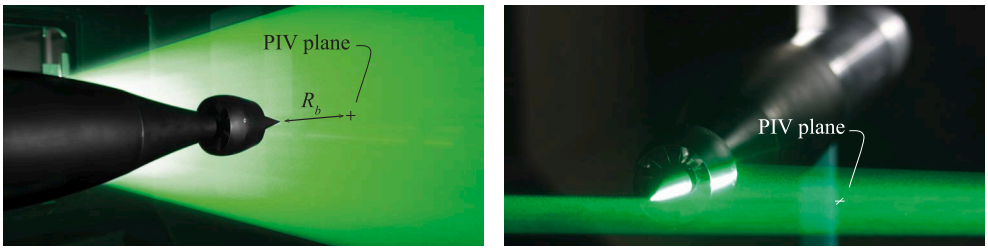
Fig. 11. Photograph of an oil flow visualisation around the tail of a novel aircraft wind-tunnel model, courtesy of ARA.

Along wall surfaces, pressure can also be measured by means of pressure taps [221] or pressure-sensitive paint [234,235] nonetheless, the latter technique is more fastidious despite providing CFD-like pressure distributions on surfaces. To enable the paint to react to the pressure, the model needs to be thoroughly cleaned and get an epoxy base layer before being baked. The pressure-sensitive paint is then applied adding some surface roughness and drag up to 10 drag counts or 1% of the lift coefficient [234]. Through a lighting excitation and a camera set-up (Appendix A.3), oxygen molecules react with pressure and luminescent probes enable the painting to be seen.

4.2.3. Velocity

A flow visualisation technique that does not capture the flow velocity but its path along surfaces consists in tracking oil particles left on the model surfaces. As the air travels along the wind-tunnel model, the thin oil droplets follow the path showcasing streaklines. Fig. 11 depicts an example on a BLI aircraft tested in Aircraft Research Association (ARA) transonic wind-tunnel as part of the SUBLIME project (Supporting Understanding of Boundary Layer Ingestion Model Experiment) [231].

An optical measurement lies in the particle image velocimetry (PIV) technique [236] which relies on the displacement of small particles entrained by the flow around an aerodynamic body. A pulsed light-sheet (Fig. 12) generated by a laser and a lens illuminates a field of view where a synchronised camera records images of the light pulsations. Examples of laser and camera set-ups are discussed in Appendix A.3. Although the cost and precautions to be taken for such set up are onerous, they gained popularity for large wind-tunnel facilities. The challenges for such measurement techniques are first the manipulation of the laser which are delicate pieces of equipment that can only be mounted outside of the wind-tunnel section to avoid sensitivity to changes in temperature and pressure. Moreover, the inherent vibrations in large facilities require complex alignment methods to prevent blurry



(a) Wake-plane field of view (b) Symmetry-plane field of view

Fig. 12. Stereoscopic particle image velocimetry measurement set-up, from Ref. [180].

photographic captures as well as oscillations from the model itself entering transient conditions and from which unsteady measurements are more complex.

Nonetheless, PIV is a non-intrusive technique for obtaining velocities without disturbing the flow [180]. For BLI, its applications can be upstream of the propulsor to characterise the mass-flow capture ratio, the BL momentum and energy profiles (Fig. 12(a)) and therefore the distortion, as well as downstream where the jet-plume mixes with the wake (Fig. 12(b)).

Lv et al. [220] use PIV to compare BL and wake ingestion configurations on an axi-symmetric body. To capture sheets of velocity fields, particle seeds populate a region for which lasers extract their velocities and map out the entire flow-field — BL included. Nonetheless, the light reflection close to the wall surface prevents the sub-viscous layer to be well captured and information lacks to characterise the flow ingested by the propulsor [227]. Further, Della Corte et al. [180] extended the work by investigated the aerodynamics to characterise the BL (Fig. 12(a)) and wake flow (Fig. 12(b)) which set-up is further detailed in Appendix A.3.

4.3. Performance evaluation

Another difficulty related to wind-tunnel testing is the data collection process and the data usability. Although sparse data can often be interpolated following different methods (Appendix A.2), the uncertainty associated increase as well as its propagation when determining other metrics — i.e. uncertainty in indirect measurements [237].

In most experiments, a balance is used on the model to determine the different forces and momenta experienced [20,220,227] but mid-/far-field approaches also enable the calculation of the body force with notably an exergy-based approach [73] through a decomposition of the flow-field in an isentropic and non-isentropic regions [96]. As the isentropic region is akin to a potential flow, no losses occur and the viscous losses, or drag, are captured by the non-isentropic part of the flow. Nonetheless, depending on the mounting system used, the rake instrumentation cannot be positioned far away downstream and a close installation to the body's trailing-edge requires a correction of the data [73]. Equally, the propulsive power can be determined by a mid-field wake investigation using an energy approach, as intended in Ref. [180]. A major drawback from these approaches is to use a fine wake rake spacing to map out the distributions and reduce the uncertainty propagation. Nonetheless, it appears to be as an effective means of determining the axial force, or power, without any balance.

As the axial net body force is determined, it can be related to the power consumption from the propulsive device. With a power measure on the shaft, savings can be computed and compared to the reference aircraft to report savings, if any [20]. However, there is a caveat in the emulation of the propulsion system whereby it should ingest an equivalent non-dimensional mass-flow rate as the full-scale aircraft at flight conditions, or be represented with the same size, linearly scaled-down. Indeed, the performance of the tested BLI mock-up is related to the wind-tunnel conditions and not the flight conditions where similitude needs to be ensured to translate the data. As similitude is not respected, either the kinematic or dynamic similarity alters the performance.



(a) NASA STARC-ABL [144] (b) MIT-Aurora-P&W D8 [238]

(c) ONERA NOVA [27] (d) NASA N3-X [239]

Fig. 13. BLI aircraft designs.

5. Aircraft conceptual designs

New conceptual designs arose with the consideration of BLI propulsion systems. Whilst some concepts adapt long-established tube-and-wing aircraft, others endorse more unconventional shapes like lifting or blended-wing bodies. Therefore, to highlight their differences, these configurations are distinguished into three categories:

- Propulsive fuselage concepts (PFC): based on a conventional tube-and-wing configuration, a circumferential BLI fan is mounted around the aircraft's tail ingesting the boundary layer developed, e.g. NASA STARC-ABL (Fig. 13(a));
- Over- and rear-fuselage engines concepts (ORFEC): traded-off the under-wing turbofans for over- or rear-side-mounted engines on a lifting-fuselage, e.g. MIT–Aurora–P&W D8 (Fig. 13(b)) and ONERA NOVA (Fig. 13(c));
- Disruptive propulsive concepts (DPC): revisited entirely the conventional airframe to incorporate hybrid- or blended-wing bodies with a distributed array of fans, e.g. NASA N3-X (Fig. 13(d)).

To perceive at a glance the abundance of publications available in the literature, Fig. 14 maps out the different references by distinguishing the aircraft's concepts by their colours (blue for PFC, orange for ORFEC and green for DPC). The inner region relates to the different book-keeping, methods and models previously reviewed. Moving outside the schematic, parametric studies, design of experiments and design space explorations are reported whereby the different references are connected by solid and dashed arrows to highlight the research efforts and more refined studies (from aircraft- to system-level). Follows the optimisation studies as well as the experimental work on the outer ring. At first glance, it is noted important efforts in the PFC studies which aim to appear as an alternative to conventional aircraft in a nearer future. Long-term objectives aimed by the ORFEC and DPC lack optimisation studies which are expected to be performed after a down-selection of the aircraft architecture and systems.

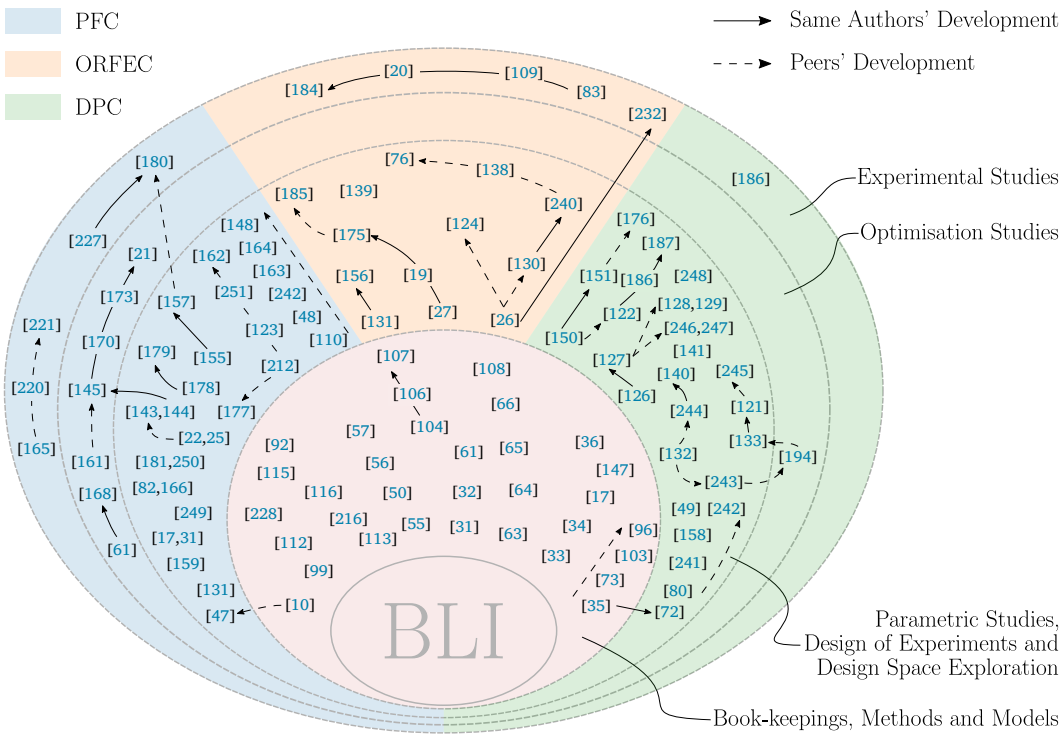


Fig. 14. Map of BLI studies in the literature.

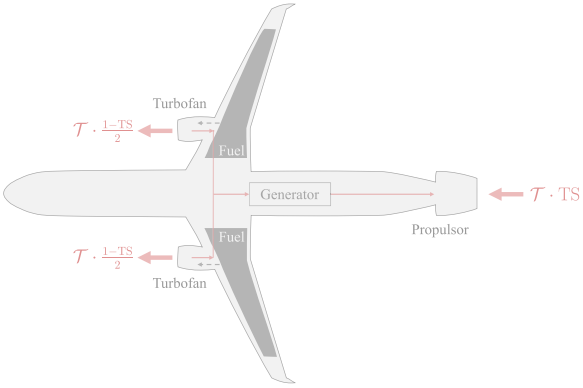


Fig. 15. Propulsive fuselage and thrust-split concepts.

5.1. Propulsive fuselage concepts

The propulsive fuselage concept (PFC) refers to configurations with an aft-mounted propulsor encircling the rear fuselage section of the aircraft. This resembles an early project, the FMA IA 36 Cóndor [252], with five engines positioned circumferentially ingesting the fuselage boundary layer of a short-range aircraft featuring a regional aircraft capacity. In more recent concepts, the airframe structure is comparable to a conventional tube-and-wing aircraft partly powered by two under-wing turbofans and also providing electrically or mechanically the power necessary to drive the BLI propulsor and propel the aeroplane through a thrust-split (TS, Eq. (34)) configuration (Fig. 15).

In the case of a TS of 100%, power is extracted from the under-wing engines and fed into the aft-propulsor which provides the entire aircraft's propulsive force requirement. The turbofans therefore either incorporate a free turbine to supply the power demand from the rear propulsor, or the energy, respectively torque, is extracted from the low-pressure shaft, and the configuration is described as fully turbo-electric, respectively turbo-mechanical.

Amongst the conceptual designs based on the PFC, the NASA STARC-ABL [25], the European Union projects CENTRELINE [212] and DisPURSAL [49] can be named. The former targets short-to-medium missions using the Boeing 737–800 as reference whereas the CENTRELINE and DisPURSAL accommodate wider bodies for long-haul based upon the Airbus A330-300. A specificity of the latter is its propulsion system which does not account for a *simple* propulsor but for a gas-turbine engine at the tail. Appendix B compares these different designs in terms of aircraft operating conditions at design point (steady-level cruise flight) as well as the under-wing engines and propulsor characteristics.

5.1.1. NASA STARC-ABL

The NASA STARC-ABL (Single-aisle Turboelectric AiRCraft with Aft Boundary Layer) has been introduced in 2016 by Welstead and Felder [25] and is based on a turbo-electric distributed propulsion (TeDP) architecture (Fig. 13(a)). The fuel coming from the wings is fed into the main under-wing turbofans and mixed with the compressed air to drive the turbine. The engines partly propel the aircraft and generate power through a generator, directly related to the aft-propulsor ingesting the boundary layer coming from the fuselage to generate the remaining force requirement. The architecture leads to an overall efficiency increase albeit losses due to the power conversion from mechanical to electrical, the transmission of the electrical power to the aft-propulsor and the conversion back to mechanical power needs to be addressed.

Welstead and Felder initiated the STARC-ABL design using OpenVSP [190] and performed analytical studies to obtain estimates on fuel reduction along a whole flight mission using FLOPS [253]. Inspired by the Refined SUGAR concept [254–257] for the technology assumptions and flight mission of the baseline configuration (N3CC), the study aimed at determining if any potential benefit exists in using turbo-electric architectures. Nonetheless, no high-order tools have been used and a generic BL from a Boeing fuselage was used at both on- and off-designs. It is thus opined that the results from Welstead and Felder rely heavily upon the Boeing CFD solution and do not represent a realistic fuel consumption from the high angle-of-attack and potential flow separation not considered. In addition, the BLI propulsor was run

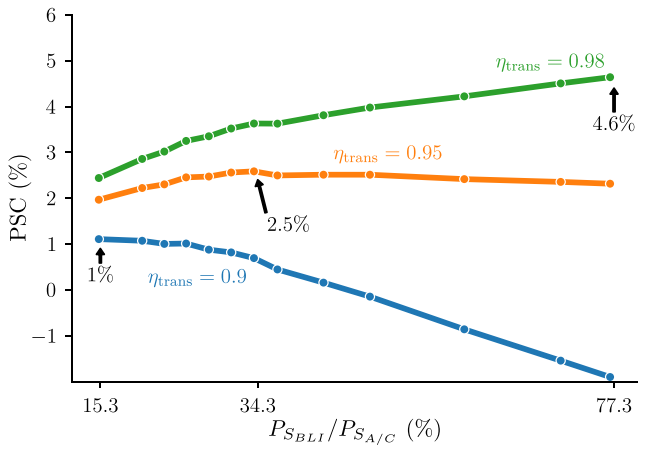


Fig. 16. Overall aircraft PSC at cruise versus the fraction of shaft power used for BLI under different transmission efficiencies, η_{trans}.
Source: Adapted from Ref. [145].

at fixed power input, regardless of the flight condition showing a 12% fuel burn reduction for a full mission in comparison to a conventional podded variant. However, because it operates at constant power, a smaller and lighter electrical power system was installed, reducing the aircraft weight and hence its consumption. The assumptions are very optimistic as more power is needed during the ascent phase of the mission however, for a BLI fan ingesting only a portion of the fuselage's BL, the propulsion system efficiency was increased, and the gain in size and weight of the twin under-wing turbofans allowed the weight of the additional electrical system components to be offset. Overall, the conceptual design exploration study showed that the STARC-ABL concept was a good first candidate for turbo-electric systems and subsequently, numerous studies followed from Gray et al. [143–145,169] and Yildirim et al. [21,173,174] which contributed to the development and optimisation of the design.

From this work, Gray et al. [143,144,169] developed an aero-propulsive analysis model for fully-coupled airframe propulsion, using a 1D thermodynamic cycle. A study on the effects of the fan pressure ratio (FPR) on the propulsor performance was conducted which results showed a growth of the BL thickness for reduced FPR — at fixed shaft power, resulting in the BLI-installed propulsion system outperforming the conventional podded engines. Also found, was that a larger nacelle (lower FPR) leads to slower flow ahead of the fan, causing the static pressure effects to propagate much farther forward than the change in velocity profiles suggested. This discovery emphasises the fact that a strong interaction exists between the airframe aerodynamics and the propulsor. However, the inferences gained from the study may provide a premature conclusion and it can be argued that the FPR is not entirely responsible for that strong interaction but it is believed that the propulsor's size plays a larger role in the integration effects.

Later, Gray and Martins [145] showed that small BLI propulsors offer a better power saving coefficient (PSC). However, it is essential to note that the transmission efficiency between the under-wing podded engines and BLI propulsors plays a crucial role as suggested by Fig. 16. Considering a transmission efficiency of 90% results in a PSC of only 1% which could call to question the usefulness and benefits of BLI propulsors but an increase to more realistic targets for the next decade, 95% or even 98%, could lead to a PSC increase to almost 5%.

To ensure the fan operability, maintaining a low level of distortion is vital. Ordaz et al. [142] developed an adjoint-based design capability to improve the fan efficiency. Whereas the distortion metric therein investigated is the DCθ, it is opined that this metric cannot solely assess the distortion performance. However, it is a first step in the demonstration of a consistent adjoint-based sensitivity analysis for gradient-based optimisations. The mesh adaptation capability is able to reduce the distortion error associated as well as to enable the design optimisation under free-stream and BLI conditions. Nevertheless, it is emphasised that the study only applies under particular circumstances, i.e. steady cruise conditions at a different altitude than the design one, of a bare fuselage without wings. Kenway and Kiris [161] demonstrated that the wing down-wash has a significant impact on the fan-face distortion by investigating a three-dimensional tube-and-wing model. Fig. 17 depicts a comparison between a ducted body (tube only) and a tube-and-wing ducted body, where the authors report that the distortion metric doubles when mounting the wings. The shape sensitivities at all design conditions point in the same direction, and modifications made at the design point improve all other conditions — showcasing the distortion independence between the tube-and-wing baseline and its optimised geometry. As the wing down-wash was the main driver, and since the optimiser had no control over it, the fuselage and nacelle shapes are nearly independent of the design condition to mitigate this effect.

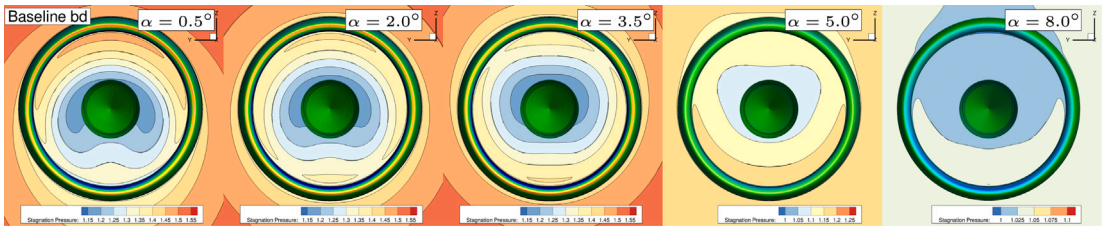
Following on the design optimisation but more particularly on the nacelle and plug-cone shapes, Lee et al. [171,172] emphasised their research on a quasi-2D through flow model. The method accounts for the incoming BL radial effects from a 1D mass-flow rate BC that is corrected and constructed with a quasi-2D model. In order to optimise the wake recovery, the exhaust cone and nacelle shapes follow a set of optimisations yielding a reduction in entropy rise all along the plug as the jet flow accelerates, and a wake loss reduction with the less cambered nacelles.

The first-of-its-kind optimisation study on coupled aero-propulsive design variables is performed by Gray et al. [170]. The propulsor size varies with respect to the FPR totalling 25 shape parameters to take into consideration on a 3D aircraft model, along with the angle of attack and a body force representing the propulsor behaviour, hence amounting to 27 design variables. To strategically reduce the computational demand, three different BLI designs were down-selected. They are designed to contribute to different stream-wise forces where the highest value corresponds to the smallest propulsor matching the shaft power used in Ref. [25]. When subject to distortion, the largest BLI propulsor requires 1.2% more shaft power than the non constrained configuration to obtain the same output. Through the design optimisation of the aft-fuselage and inlet region, distortion could be mitigated albeit not falling below 0.03. Bigger flexibility in the design variables could allow reducing the distortion metric even more however, it is stressed that this study lies as the first fully-coupled aero-propulsive optimisation study accounting for both aerodynamic and propulsion design variables.

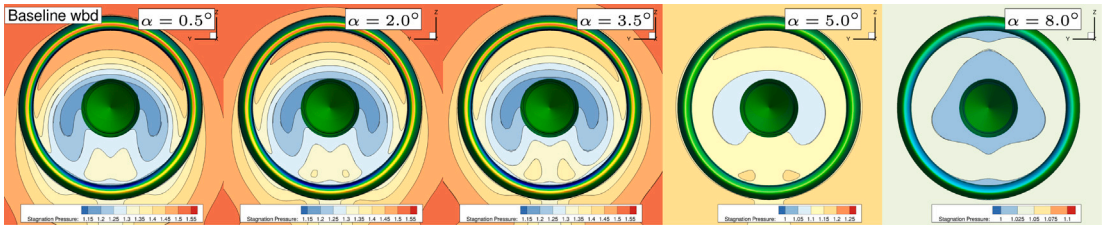
Additional efforts from Yildirim et al. contributed to the design optimisation of the propulsion system with the use of the coupled aero-propulsive approach developed by Gray [62]. Optimisation studies at cruise condition were initiated for different net force and FPR [173] yielding 9 optimised geometries. The study is further extended with the PSC as an objective function yielding 18 designs [174]. Using these 18 optimised geometries for cruise, off-design was investigated to cover the entire mission profile [21]. Starting with cruise and take-off conditions as the study bounds, the approach and hold stages complete the mission profile. It is noteworthy that the previous work performed at cruise does not imply an optimal behaviour of these designs at low velocity and altitude therefore the PSC is also tracked at off-design - for different altitudes, Mach numbers, lift coefficients and FPRs. The results suggest that although the PSC is insensitive to changes in the altitude at low flight velocity, the power requirement from the podded fan is more sensitive to FPR than the BLI fan [258].

5.1.2. EU CENTRELINE

Towards the European efforts, the CENTRELINE project (ConcEpt validatioN sTudy foR fusElage wake-filLIng propulsioN intEgration) extends the work initiated in DisPURSAL (detailed in Section 5.1.3). This concept considers the Airbus A330-300 as a state-of-the-art baseline whereby an equivalent design is derived based on the potential



(a) Baseline body and duct



(b) Baseline body-and-wing and duct

Fig. 17. Computed total pressure contours at AIP for different angles of attack highlighting the down-wash effects, Ref. [161].

technologies available in 2035. The project targets the proof of concept and its experimental validation whilst aiming at reducing the aero-structural complexity and the intake distortion and losses.

CENTRELINE, alike STARC-ABL, is composed of two turbofans mounted under-wing that electrically drive the aft-mounted propulsor as well as partially propelling the aircraft. Introduced by Seitz et al. [212], this EU-funded project aims at addressing several challenges. Notably, a thorough understanding of the aerodynamic effects of the fuselage wake-filling propulsion system, the coupled aero-structural design as well as the layout and design of the fuselage fan drive train and the multidisciplinary systems design integration and optimisation.

Setting off with aero-structural studies from Goraj et al., the aircraft 3D model was parametrised and generated and the robustness of the configuration evaluated [259]. The models parametrisation allows for numerous studies to be performed even if numerous components is not considered, reducing the practicality of this tool and giving profits to only series of products and manifold simulations. To contrast this lack at the early stage, the authors informed on the continuing development of these tools along the project.

In tandem, Bijewitz et al. designed the under-wing turbofans from parametric studies accounting for significant power off-takes as well as its aft-mounted propulsor model [123]. They highlight the difference in power extraction from a single low-pressure spool to a coupled low- and high-pressure spool. The high demand in power from the propulsor necessitates to extract a portion from the high-pressure spool. These constraints identified at off-design were shown to be alleviated with the latter configuration thus, rising the need for further investigations in the optimal power off-take strategies.

In the review publication from Habermann et al. [32], figures of merit are discussed with their limitations. Regarding these limitations, Seitz et al. [162] provided a rigorous approach to the PSC evaluation of PFC. Although it is expected that improving the transmission systems efficiency results in higher achievable power savings, it can be mitigated if the effective propulsive device efficiency of the reference increases, emphasising on the importance of the baseline definition. A comparison of the mechanically- and electrically-driven transmission systems highlights that the former option features higher potentials in fuel savings.

A series of trade studies from Troeltsch et al. [251] provide guidance on the design refinements and gauge potential optimisations. The study justifies the plausibility of such configuration providing improvements compared to their reference aircraft. On the propulsive performance, the turbine cooling highly impacts the potential reductions in block fuel and additional parametric studies need to be performed. On the fan design, a greater blade height tends to reduce the fuel consumption overcoming the longer and heavier undercarriage penalties. However, this is suggested to be further assessed with higher fidelity studies. To follow on, Castillo Pardo and Hall carried out an experimental campaign compared to CFD computations on the BLI fan [178] and later focused their work on the fan design assisted by CFD [179]. The numerical modelling of the free-vortex fan tested experimentally is run using RANS CFD which results on the axial velocity, swirl angle, stagnation and static pressures reinforce the confidence in the approach developed [178]. This allows a fan design optimisation to handle better the non-uniformities restoring the work input and increasing the operating range. Further developments led to a final optimised design that increases the forward force by 1.2% and the stability margin by 4%–10% relative to its datum design [179]. Petit et al. [177] pushed forward the blade design optimisation, albeit taking the perspective from a propeller. The tool is coupled to CFD and aims at comparing two configurations: a free-stream ingesting configuration and its BLI form. It is opined that the study performed is not entirely representative of the PFC design-point as the cruise Mach number herein studied is 0.47 and the altitude 20,000 ft. Although it is noted that this work relies upon as an introductory work for future improvement and wider applications.

At a larger scale, a systematic design space exploration is applied to a 2D axi-symmetric model using surrogate models [155]. The study intends to characterise the effects of geometrical parameters on aircraft performance. The approach starts with independent parameters' variations (parametric studies) to then be varied in combinations. Whilst the procedure permits an understanding of the mechanisms at an early stage, several key points need to be highlighted. Indeed, the model parametrisation presents important drawbacks such as a variation in either the fan axial position or its radius alters the body slenderness as well as the nacelle shape. This strong interdependence notably affects the amount of BL ingested as well as the BL profile and the integration effects. Another important point is the accuracy of the results obtained as it is reported an over-prediction of 10 to 30% of the absolute drag that one can question the paper's conclusions. Nonetheless, the tools developed in this study could lead to further optimisations of 2D axi-symmetric models later extendible to 3D.

More recently, Habermann et al. [157] demonstrated the fuselage tail upsweep effects on the PFC by investigating the inlet distortion caused by the 3D flow behaviour and its impact on the aero-propulsive performance. Needless to mention the significant 3D effects on the propulsion system performance due to the highly distorted incoming flow, a non-negligible consequence of this detrimental effect is the increase in shaft power which is correlated to the upsweep angle.

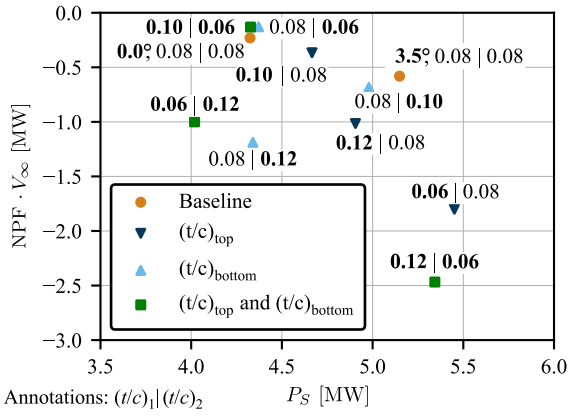


Fig. 18. Comparison of the aero-propulsive performance between the baseline and geometries with variations in thickness-to-chord ratios (t/c), from Ref. [157].

Notwithstanding this drawback, the penalties are alleviated with a nacelle design adjustment. When variations in the thickness-to-chord (t/c) ratio are made on the nacelle upper and lower regions, the PFC performance is restored to the axi-symmetric baseline geometry (Fig. 18) despite the fact that no interaction with the other aircraft components, i.e. wings and tail plane, has been considered.

The final investigation performed on the CENTRELINE project is an experimental low-speed wind-tunnel campaign using a power balance analysis. Della Corte et al. [180] scaled down a wing-less axi-symmetric fuselage version of the PFC. The net axial force of the body and PIV allow for momentum- and energy-based analyses to be conducted. At axial equilibrium, the propulsor installation implies a flow acceleration through the fan which increases the mass-flow flux and is represented by a BL thinning upstream. This observation goes against Ref. [144] who reported that the nacelle integration thickens the BL upstream however, the flight conditions differ as Gray et al.'s study was at transonic conditions and Della Corte et al.'s testing between M0.04 and M0.12 omitting compressibility effects. Nevertheless, one drawback from the testing campaign is that when outlet guide vanes are omitted, the nozzle rotates coincidently with the fan generating a local strong hub vortex in the wake caught by a low total pressure in the wake which increases the wake losses and biased the performance of the system. The fan installation highlights the BLI benefits with an axial momentum flux and kinetic energy deposition rate increase upstream, and a wake attenuation downstream in the wake (Fig. 19). At different thrust levels nonetheless, the power balance analysis suggests that performance decays from the ideal wake-filling conditions with an increase in dissipated mechanical energy within the wake. This work represents a ground-breaking experimental power balance analysis of an axi-symmetrical BLI propulsive fuselage albeit being performed at low subsonic condition. Additionally, the authors claim an application of the power balance where neither the shaft power or viscous dissipation rate are reported preventing the balance or PSC to be calculated.

5.1.3. EU DisPURSAL

As alluded, the CENTRELINE project resulted from an initiative started in 2013 from another EU-funded project called DisPURSAL (Distributed Propulsive and Ultra-high by-pass Rotor Study at Aircraft Level). Although DisPURSAL initially focused on distributed propulsion systems with a hybrid-wing body (Section 5.3.1), they also considered a PFC slightly different from the ones detailed above. In place of a propulsor fan installed at the rear-fuselage, the propulsion system pictured in Fig. 20 is preferred. The fan is driven by a gear system mounted on a drive-shaft thereto connected to the core engine that is alimented from the incoming air passing through a S-duct.

A multidisciplinary pre-concept design is initiated by Isikveren et al. [158] where the preliminary aircraft sizing is defined from CFD-based results on a 2D axi-symmetric model powered by an actuator disc. Following, Kaiser et al. compared the previous results with their quasi-analytical method for investigating the power savings under different disc loadings [110]. The relative difference in terms of BL, momentum and energy thicknesses between their model and the CFD results are respectively of −5.1%, 5.7% and 8.0% making the approximates fast and reasonable compared to computational simulations. Also early in the project, Seitz and Gologan [48] developed a book-keeping based on thrust and drag with common metrics such as the PSC as well as the estimated specific air range (ESAR) based upon the specific air range (SAR). Although it is reminded that the results pertain to an arguable thrust-drag split on BLI configurations. An outcome from their parametric studies are the small sensitivity of propulsive efficiency to speed changes whereas it is more significant on specific thrust in comparison with podded engines.

A comparative efficiency analysis on both powered fuselage and distributed propulsors concepts is performed by Mirzoyan et al. [242]. Focusing on the PFC, two reference configurations are used: an entry-into-service (EIS) year 2000 represented by the Airbus A330-300 powered by the Rolls–Royce Trent 700 and a conventional tube-wing configuration equipped with advanced geared turbofans targeting an EIS year 2035. Their investigations predict a fuel burn reduction of 32% between the two references, from which 9.2% can be added when the BLI technology is implemented, compounding to 38.3% with respect to the state-of-the-art 2000 configuration.

The fuel burn prediction is confirmed by a multi-disciplinary design investigation on various FPR for given duct heights using actuator discs modelling [163]. The performance is investigated with the use of an integration factor, f_{int} which not only captures the drag spillage from the nacelle but also covers the additional effects from the fan and nacelle integration to the fuselage. It is found that f_{int} primarily depends on the propulsor intake size where a decreased duct height implies more spillage and a stronger interaction between the nacelle stagnation point and the main stream going through the fan whereas the dependence on FPR has a suction effect which reduces the spillage for greater FPR's. The integrated performance assessment from Ref. [163] proves to confirm the semi-empirical methods from Ref. [48].

Whilst recommendations would have been on extending the design space to different thrust-split configurations as well as flight conditions, these trade studies are conducted in Ref. [164]. It is shown that the greatest impact on block fuel occurred for changes in the intake pressure ratio which depends on the flight conditions. Varying the Mach number and sizing the aircraft according to their optimum cruise speeds, savings in terms of block fuel could be reduced to 14% but when compared at identical speeds, the benefits fall down to 11% [164]. Extending the trade study to different specific thrusts, a fuel-burn reduction of 12.1% is expected whereas adjusting the thrust-split ratio could lead to an additional 1.3% benefit [148] as highlighted by the two designs (A and B) from Fig. 21. The results from these studies are promising and it is also emphasised that cycle settings such as overall pressure ratio, turbine entry temperature or specific thrust would potentially lead to bigger fuel burn reductions.

5.1.4. Other significant PFC studies

In addition to the three PFC designs, other studies have contributed towards the development of methods or tools.

To complete NASA's efforts on the STARC-ABL, Refs. [82,166] examined the potential aero-propulsive benefits of using a BLI configuration on the NASA CRM aircraft using the power balance method. One of the main objectives from applying this method is to evaluate the dissipation reduction, i.e. irrecoverable mechanical energy, through changes in the stream-wise velocity from the BL development. The study demonstrates the use of different tools, e.g. NASA's VGRID [261] for meshing, NPSS [209] for the engine cycle, USM3D [262] for the CFD solver and CDISC [263] for the *on-the-fly* geometry re-design.

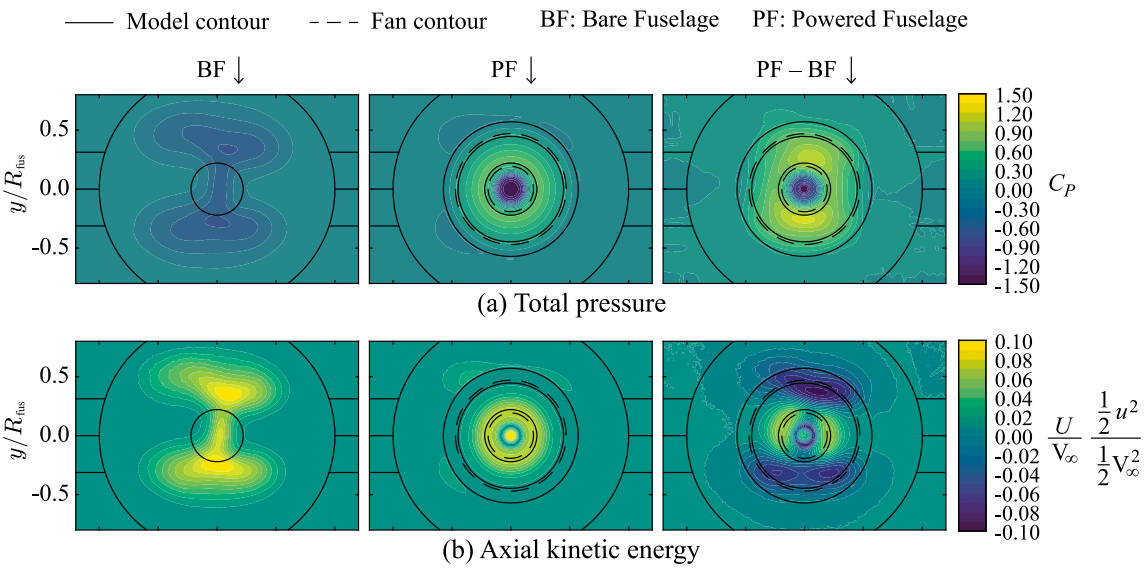


Fig. 19. Measured total pressure and axial kinetic energy in the wake-plane field of view for the bare fuselage, powered fuselage and their difference, from Ref. [180].

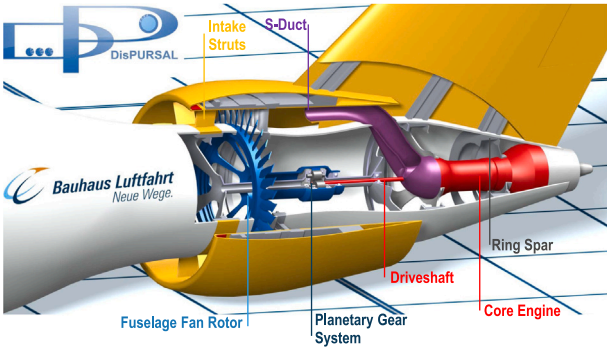


Fig. 20. Cutaway view of the rear-mounted DisPURSAL propulsion system, from Ref. [260].

Whether with or without the iterative surface curvature alterations from CDISC, an actuator disc modelling the fan at the rear of the aircraft offers a reduction of power of around 15% which mainly comes from the reduction in velocity of the propulsor incoming flow. Although, the estimates are relatively optimistic as detrimental interactions from the nacelle and engine integration are not implemented, the work done is a good starting point for designing and evaluating the potential BLI benefits.

Giannakakis et al. also used the power balance method for the fuel burn evaluation of such configuration and challenged the previous efforts made by NASA and MIT on the mass evaluation of those configurations [147]. They highlight that although the under-wing turbofans can be scaled down as their contribution diminishes, a fuel burn penalty of around 3% is expected due to a 31% mass increase in the turbo-electric system installation compared to the baseline. On the other hand, Hall et al. predicted a 5.4% increase in mission fuel burn for the non-optimised geometries [125]. Both studies agree on the penalty of mounting a BLI propulsor in terms of fuel consumption but when optimisation is performed on the design and the uncertainty in the results is quantified, the authors suggest opposite results with a 0.7% penalty in the best scenario for Ref. [147] and a 4.8% benefit for Ref. [125]. Another study analytically estimates the BLI benefits at aircraft-level enabling a quick and cost-effective design space exploration [249]. They emphasise the importance of the assumptions made on the under-wing turbofans and BLI propulsor as their size and mass largely contribute to the fuel burn estimation. The assumptions on the transmission system efficiency, engine efficiencies as well as the mission range also play an important role and in that respect, the authors compared several candidates and assessed their expected performance.

Continuing with the application of the power balance method, the aerodynamics of a different design from Tse and Hall is investigated [181]. Unlike the previous concepts presented, an array of multiple circumferentially distributed aft-fuselage BLI propulsors are electrically driven by the under-wing turbofans as illustrated in Fig. 22. Although this concept deviates slightly from the PFC, it could be discussed that it belongs to a distributed PFC category along with a similar design by NASA [250]. Both concepts seem to originate from the FMA IA 36 Cóndor [252] that featured 5 engines in a likely manner, as opposed to the propulsors herein considered. A major strength of this device is the possibility to independently control the propulsors allowing some degree of thrust vectoring despite not ingesting as much BL as the other PFC. The concept expects to fare better benefits in weight, power system integration and noise. notably, Tse and Hall offer the first-of-its-kind URANS CFD assessment on a three-dimensional model with a full annulus fan modelling (rotating blades/mesh) and the application of the power balance method [181].

A preliminary design space exploration has also been performed by Battiston et al. [159] on a scaled wind-tunnel BLI aircraft model as part of the SUBLIME project. Following some wind-tunnel constraints, they investigate the influence of the nacelle intake, height and length on the propulsion system performance of a 2D axi-symmetric model. It is concluded that tightly embedded short intakes are more promising in terms of shaft power requirements for a given net assembly force. Although it is noteworthy that this applies to a particular design that has not been optimised in any way and a different parametrisation of the model could lead to other conclusions. Similarly, Matesanz-García et al. [61] explore a thorough design space on a medium haul reference aircraft where they assess the system performance with the thrust-split, thrust-specific power consumption, fan-face distortion–radial distortion index, and intake pressure recovery. The exploration of 16 design variables allows them to conclude that less aggressive intake slopes are favoured to reduce the distortion levels and enable a narrow-down of the design space for multi-objective optimisation. They follow with a design optimisation on the exhaust design for a 2D axi-symmetric PFC with the implementation of a BFM [168]. A benefit of 0.32% is achieved on the aircraft's required force with a compact exhaust and they stress

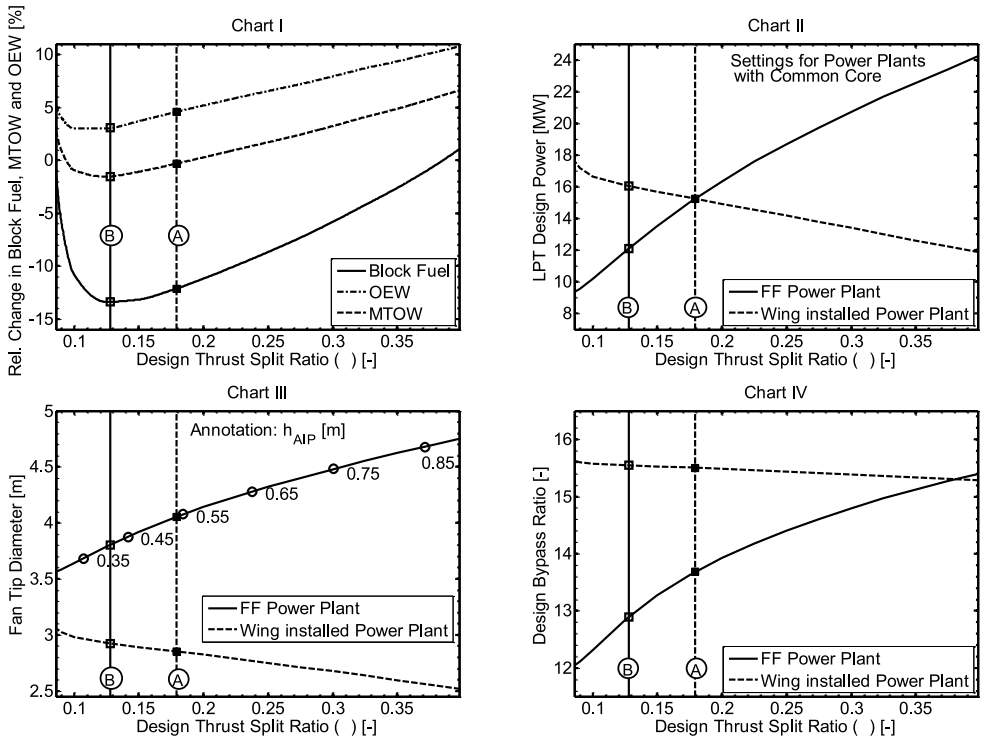


Fig. 21. Characteristics of thrust-split optimality study for two designs (A and B), FF denoting fuselage-fan, i.e. BLI propulsor, coupled to two under-wing engines for a design range of 4800 nmi carrying 340 PAX with a cruise segment flown at M0.82 and FL350.
Source: Retrieved from Ref. [148].

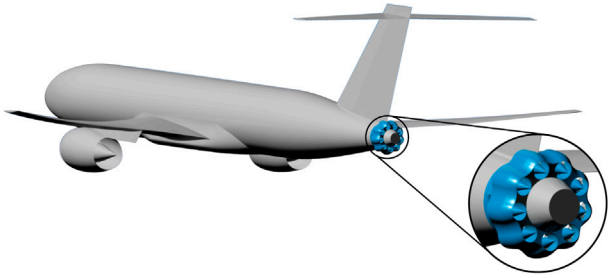


Fig. 22. Distributed propulsive aft-fuselage aircraft concept.
Source: Modified from Ref. [181] with the authors' permission.

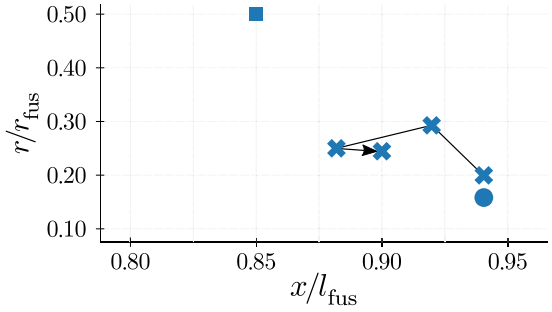


Fig. 23. Positions of the STARC-ABL (●), CENTRELINE (✖) with its evolution (➛) and DisPURSAL (■) relative to their fuselage dimensions.

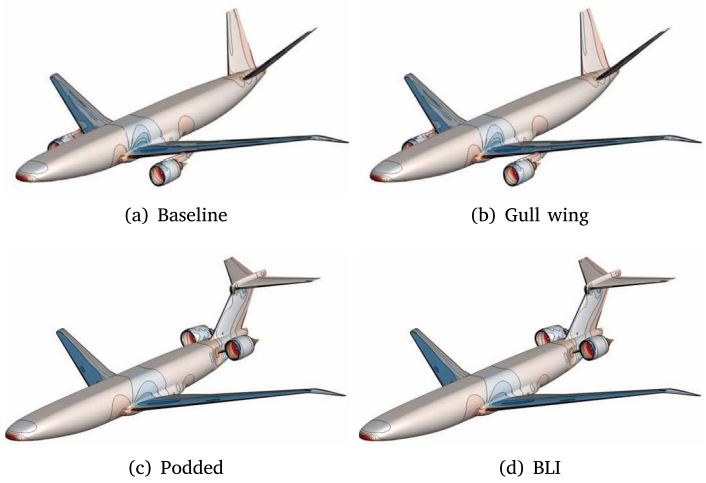
that the exhaust and nacelle after-body have a considerable impact on the aerodynamic performance.

Because the majority of studies chose to study the flow-field impacts on the propulsion system rather than the opposite, Gray et al. [144] demonstrated the importance of coupling the two with the use of CFD. However, this coupling has a computational cost that Pokhrel et al. [146] offer to reduce through a novel approach that assesses the effect of the propulsion system on the flow-field. To follow this study, Ahuja and Mavris [156] investigate the BLI effects caused by changes in fan annulus and mass-flow demand assessing both the on- and off-design impacts. Although the metrics used for the performance assessment could be criticised, it is agreed that both the propulsor size and mass-flow demand play an important role in the performance as different amounts of energy are ingested by the fan and hence contribute to the system's effectiveness.

Lastly, the different PFC are mapped out in Fig. 23 with their propulsors various axial and radius positions along the tail. Ref. [156] notes different degrees of integration and influence whereas here the authors offer to segment these effects in three manners: the primary, secondary and tertiary effects. In the former, the position and size of the BLI propulsor can be named as their integration differ. More refined design aspects such as the pre-diffusive slope, the cowl definition or the plug-cone shape belong to the second category whereas the exhaust shape, droop angle or weighed-curve parametrisation would have more minimal effects but still contribute to greater performance levels after optimisation.

5.2. Over- and rear-fuselage engines concepts

Unlike the PFC associated to a typical tube-and-wing airframe, the over- and rear-fuselage engines concept (ORFEC) widens its fuselage for a lifting-body and trades its under-wing turbofans for flush-mounted or semi-buried turbofans at the rear of the fuselage. The popular concepts based on this configuration are the ONERA NOVA [27], wherefrom the Airbus Nautilius concept was born [175], and the MIT–Aurora–Pratt & Whitney D8 [26] which aircraft and turbofans characteristics are summarised in Appendix B.



(a) Baseline (b) Gull wing

(c) Podded (d) BLI

Fig. 24. Development of the different NOVA configurations.
Source: Adapted from Ref. [19]

5.2.1. ONERA NOVA and Airbus Nautilius

Introduced in 2015 by the ONERA, the French Aerospace Lab, the NOVA (Nextgen ONERA Versatile Aircraft) concept is a medium-haul twin-aisle configuration laying seven seats per row. Its wide-body lift-generating fuselage allows for its length to be shrank by 14% compared to a narrow-body aircraft of same capacity. The high aspect-ratio wings also feature downward with swept winglets, and at the rear of the fuselage a vertical tail plane accommodates two semi-buried turbofans on either side. This configuration is observable in Fig. 13(c).

Wiart et al. are at the origin of this conceptual design whereof after sizing the preliminary fuselage, they investigated its aerodynamics using CFD [19,27]. During its development, four configurations were considered namely (a) the baseline with under-wing turbofans and V-tail planes, (b) the gull-wing design and, (c) the rear podded-equivalent of (d) the BLI configuration which has aft-mounted turbofans around the T-tail plane as given in Fig. 24. They compare two actuator disc models and conclude on the robustness of the results obtained with one yielding a 5% PSC at cruise — the other model does not replicate the expected physical behaviour and represents a bias in fan power prediction. Also, in the non-BLI scenario, thanks to the investigation of the multiple designs, it appears that higher by-pass ratios (BPR) could be considered if mounted under gull-wing concepts but other innovative architectures such as strut-braced- or box-wing configurations should be taken into consideration.

Few publications are available on the NOVA for several reasons. Its tightly-embedded engines on either side of the tail favour separation and distortion within the intakes whilst the flight Mach number of 0.82 fosters shocks on the cowls. Also, little benefits arose from the preliminary studies despite noting encouraging noise reductions which would meet the EU environmental targets. Whereas it seems that its development has been ceased — from the available literature, Airbus joined their efforts with the development of another ORFEC, the Airbus Nautilius which intends to maximise the ingestion of the BL whilst limiting the amount of distortion at the fan-face.

To ease the development of the Airbus Nautilius, the pre-existing NOVA podded reference (Fig. 24(c)) was used whereof the rear-end of the aircraft was modified to accommodate two ultra-high by-pass ratio engines on two distinct parts of a split-fuselage. This design compares with the PFC previously detailed permitting the ingestion of the entire BL whilst taking all the advantages of ultra-high BPR (Fig. 25).

Wiart and Negulescu [175] studied the aerodynamics of a simplified axi-symmetric engine using AD and BFM to represent the fan. A more uniform pressure distribution was input to the AD fan-face to prevent flow separation and another AD was used at the fan-exit to mimic the swirl from the fan blades. As for the BFM, it was used to prove confidence in the results shown by the AD models. Nevertheless, axi-symmetric studies are not suitable for the Nautilius concept and therefore an introductory study on the 3D design is performed to showcase the strong three-dimensional effects at the rear-end of the fuselage. To highlight the separation, two designs iterations are compared whereby the lateral distance gap is adjusted. It is noted that the farther apart the nacelles, the stronger the separation but the lower the nacelle interaction drag [175].

A further step to the engine integration is studied by Godard and Negulescu [185] with both steady and unsteady RANS computations using elsA [204]. The former is used to estimate the power savings without considering the fan performance whereas the latter isolates the fan stage using the steady computation for the inlet BC. A comparative assessment of different URANS codes on the fan/airframe aerodynamic is performed in Ref. [102] using an isolated ultra-high BPR turbofan which can be installed on the ONERA NOVA gull-wing configuration. The results obtained by Godard and Negulescu suggest a PSC greater than 10% although the distortion is not considered — resulting in fan performance loss. After completing a fan design optimisation on an isolated engine, half of the initial performance loss was restored albeit the authors emphasise that the fan stage design must be coupled to the airframe to accurately represent the integrated losses.

5.2.2. MIT–Aurora–Pratt & Whitney D8

In a different fashion, MIT, Aurora and Pratt & Whitney joined efforts in the design of the D8, also referred as the “double-bubble” aircraft, or simply D8, in reference to its shape. Initially designed with three engines at its back, the revised version dropped one to comply with the operational and economic drivers of 2011 [26]. D8’s uniqueness lies in its layout: a wide twin-aisle lifting body — producing 19% of the aircraft’s total lift, upturned nose, shrinked, smaller, lighter and nearly unswept wings and two flush-mounted BLI turbofans embedded within a π-tail (Fig. 13(b)).

Drela outlines the considerations in the aerodynamic development of the D8 through a preliminary vehicle multidisciplinary optimisation (TASOPT [87]) [26]. The motivation for using TASOPT over other codes is that it uses structural theory, variable wing aerofoils and CFD for drag prediction, full engine flow-path simulations and variable flight trajectory, in lieu of historical correlations, wetted-area methods, tables/decks and correlations, and fixed cruise profile, respectively. Although TASOPT acts as the main evaluation tool for the configuration, the different components were developed using *traditional* methods

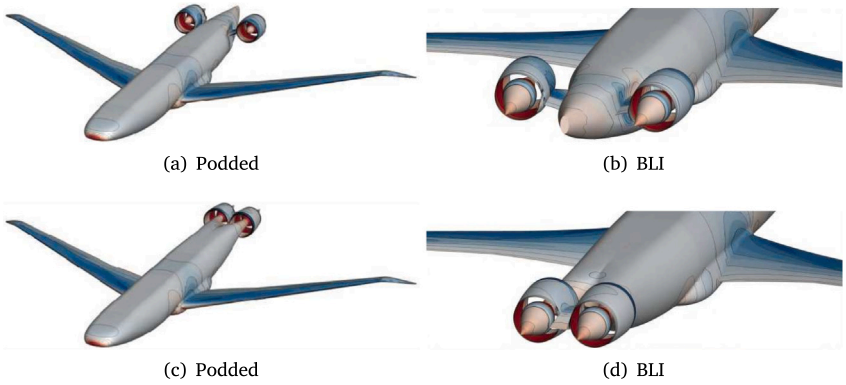


Fig. 25. Representation of the (a) podded configuration from the NOVA (Fig. 24(c) without tailplane), and (b) the Airbus Nautilius derivative.
Source: Adapted from Ref. [175].

[26]. In addition, as a means of validating the aerodynamic performance and stability characteristics, experiments on a 1:20 scale model in a wind-tunnel were performed. Results suggest a close correlation between the experiments and TASOPT with the latter under-predicting the lift-to-drag ratio by about 10%. When compared to a Boeing 737-800, the author claims a fuel-burn reduction of up to 33% which provides a launchpad for further investigations. However, it is difficult to decipher what proportion of these benefits may be directly attributed to BLI as a mechanism, versus all of the other drastic airframe configuration changes.

To complement that work, the benefits are assessed from a CFD standpoint whereby the mechanical power is predicted to be reduced by 9% when the axial net force of the D8 and reference aircraft match [130,240]. A groundwork is established on a clean aircraft with the CFD validation of wind-tunnel conditions at different angle of attacks [130]. Good agreements with the experimental data are obtained enabling future studies with a BLI-mounted propulsor [240]. Additional examinations indicate that a reduction of around 6% of the overall dissipation is obtained with the integrated engines compared to their podded form.

Later, Uranga et al. [20,83] completed these studies with additional experimental investigations in the NASA Langley 14 × 22ft subsonic wind-tunnel on two 1:11 scale models of the D8 (podded and integrated configurations). A 6% electrical power saving was observed, a surrogate of fuel burn, with a 95% confidence interval of 2.3% in power. Nevertheless, those benefits only contribute at system-level and wind-tunnel scale. At full-size, the D8 fuel savings estimates amount to 15% when secondary drag and weight reductions are considered. Notwithstanding the fuel burn benefits claimed, those results are shown to be rather conservative when compared to the N+3 Phase 1 that predicted a reduction of 36% [264]. To associate the savings to their benefits sources, Ref. [184] investigated the same pair of configurations with constant nozzle areas between the podded and BLI layouts and assessed the reduction in mechanical power as shown in Fig. 26.

It is reported a reduction of 57%–69% of jet dissipation, 23%–38% of surface dissipation and 5%–8% in wake dissipation between the configurations leading to an equivalent increase of 3% in propulsive efficiency or a cruise power requirement reduction of between 7.6 and 8.5% by ingesting between 9 and 14% of the airframe dissipation. In practice, if the BLI configuration flies at the same power demand as the podded configuration, the BLI propulsors would be about 40% smaller in size, thus lighter.

Taking into account incidence angles, a synergistic numerical-experimental performance assessment is carried out by Hall et al. [76] on a 1:11 scale model for various propulsive power settings. In the wind-tunnel, the fan inlet distortion is investigated and the numerical set-up allows for the entire flow-field to be examined which assists

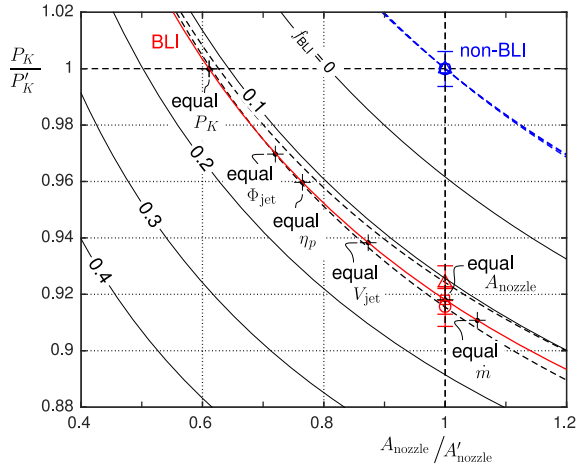


Fig. 26. Range of potential BLI propulsors with their cruise power reduction at different nozzle areas. Prime indicates non-BLI quantities and non-primed quantities relates to BLI.
Source: Retrieved from Ref. [184].

in interpreting the underlying mechanisms. Three mechanisms are observed: a reduced stagnation pressure in the BL and stream-wise vorticity through the rolling up over the fuselage are consequences of the aircraft's angle of attack, and fan distortion interaction that results from the combination of near- and far-field effects.

From the D8 design initiated in 2011, the various studies performed confirmed the feasibility of the figures claimed as part of the N+3 Phase 1 program. Thus, Yutko et al. present a thorough conceptual design by assessing the aircraft weight, balance and airline operations as well as the aircraft and BLI propulsor aerodynamic performance through CFD studies [138]. The analysis is performed on an EIS of 2016 and 2035 using foreseeable improvements in technologies. Through the use of a in-house code, higher fidelity estimates are given on a full design cycle with a 26% block fuel improvement, compared to a B737-800, which compares well with the 27% estimated by TASOPT.

Whereas the double-bubble conceptual aircraft seems promising from its potential benefits claimed, a question arises as regards the reference aircraft one should consider, i.e. a D8 unpowered equivalent design or a conventional A320/B737 aircraft. Whether one or the other, PSC or fuel block benefits can differ. It is also noteworthy that the D8 is designed to fly at M0.72 which highly contributes towards advantageous reductions when compared to the ONERA NOVA flying at M0.82.

5.2.3. Other significant ORFEC studies

At ONERA, aeroacoustics studies have been performed on the different NOVA configurations. Mincu et al. developed ghost immersed BC to non-negligibly reduce the computational demand whilst preserving the quality of the results [210]. They firstly validated their code on generic shapes to then applied it to full aircraft configurations, e.g. Airbus A320-like and NOVA, for the evaluation of noise shielding. Later, Lorteau et al. extended the work with over-wing nacelle configurations that are compared to under-wing engines mounted on a NOVA-derived airframe using the immersed BC for fan noise installation assessments at take-off [160]. They highlight that over-wing engines could reduce the perceived noise by 12 decibels (dB) when compared to their reference.

On the ONERA NOVA BLI configuration, Delft University of Technology with Romani et al. [182,183] investigated the fan noise and its turbulent flow effects developing. For that numerical study, a high-order modelling coupled with a CFD/CAA analysis was performed on the whole aircraft with a fan/OGV stage model. The highly distorted flow going through the S-duct-like intake and propulsor provokes unsteadiness at the fan stage that is represented by haystack peaks. Nonetheless, the BLI configuration, compared to an isolated engine, suggests a 5 to 10 dB reduction on the ground arc encouraging the use of the ONERA-designed aircraft for noise reduction targets.

Similarly to the ONERA NOVA, DLR, the German Aerospace Centre, derived a BLI concept from the Airbus A320 family. Implementing the foreseen technologies of 2035, a baseline aircraft is designed to assist with the BLI performance benefits. Silberhorn et al. [139] designed two intermediary designs to isolate the impact of the BLI propulsion system's integration and its benefits. They reported that major benefits arise from the tailplane whose conventional shape has been substituted by a T-tail, reducing the wetted area. The semi-buried turbofans on either side of the rear-end fuselage yield a 1.1% fuel benefit which questions the benefits of such configuration when considering the existing uncertainties.

At the conceptual level, an emphasis is given to the sensitivity of the BLI effects to the ORFEC airframe designs in Ref. [131]. They perform numerous CFD investigations on different key design variables in the scope of identifying and classifying the critical parameters. With the use of the power balance method, they highlight that the axial and circumferential position of the BLI propulsor plays a key role — especially as the wings have a great impact. The macro parameters such as the length, aspect ratio or angles play a more important role than the detailed parameters, e.g. radii, camber angles, nose shape, for the reason that shock or separation is more likely to happen with *important* design changes.

In the same vein as the joint MIT-Aurora–P&W D8, NASA contributed towards the understanding and development of the same aircraft layout but adapted its flight mission from a range of 3000 nmi at a cruise altitude of 37,000 ft and flying 180 passengers at M0.72 originally, to the same mission but a flight Mach number of 0.785. For differentiation, the next studies described will refer to the NASA D8 (ND8). Marien et al. [124] assessed the fuel consumption impact of the ND8 BLI configuration whereby the BLI effects were considered in terms of wake dissipation reduction and propulsive efficiency increase, and penalties with the inlet pressure loss increase, propulsor efficiency reduction and weight increase. Several references have been considered to benchmark the BLI benefits: a 2.8% block fuel increase is noted when analytically disabling the BLI impact. When taking into reference the ND8 underwing-podded version, the fuel block decreases by 5.6%. Regardless of the reference configuration considered, Marien et al. notably showed that the D8 aircraft flying at their flight mission outperforms any kind of non-BLI aircraft in terms of fuel block reduction but presents lower benefits than the original D8 mission. To complement that work at NASA, Clark et al. assessed the aircraft system noise of the ND8 [265,266], and that of the ND8 and single-aisle tube-and-wing concepts [267] to comply with the NASA N+3 goals.

5.3. Disruptive propulsive concepts

Despite the previous concepts' differences from the customary aircraft, one could argue that they are still relatively close to a conventional airframe. Therefore, this last category gathers disruptive propulsive concepts (DPC) which utterly revisit the design of an aeroplane.

They appear in the form of hybrid-wing or blended-wing bodies (HWB and BWB, respectively) prevailing in the most synergistic and seamless embedded propulsion systems integration [154]. Because these designs differ from one another, they cannot be introduced and described as a unique one. Nevertheless, amongst those concepts, the ONERA DRAGON, the EU DisPURSAL, the CMI SAX-40 or the NASA N2 and N3-X can be named wherefrom the majority arranges an array of propulsors electrically driven by another propulsion system. A comparative summary of the aircraft and propulsion systems' characteristics is given in Appendix B.

Such configurations bring additional technological challenges that must be understood up-front despite being of interest for more than two decades [153]. Laskaridis et al. provide a top-level assessment of distributed propulsion concepts applied to different aircraft architectures and mission specifications demonstrating the possibility of novel synergistic technologies [248]. These technologies and concepts based on distributed electric propulsion are also reviewed by Kim et al. [41] and particular attention is given to the evolving trends in BWB aircraft designs by Okonkwo and Smith [40].

5.3.1. EU DisPURSAL

Previously, the EU-funded project DisPURSAL was discussed with its PFC but initially, a DPC was investigated featuring a HWB whence an array of propulsors is mounted on the upper side of the airframe. Within the array, four BLI propulsors are powered by two gas-turbine engines laid as two groups of three propulsion systems (Fig. 27).

Alike the PFC, the DisPURSAL DPC is conceived to perform a 4800 nmi mission accommodating 340 passengers using an Airbus A330-300 for benchmarking the performance benefits. Isikveren et al. [49,158] provide a down-selection of the aircraft characteristics amongst 20 identified candidates taking inspiration from Steiner et al. [80]. In this previous work, a qualitative evaluation of the integrated and distributed propulsion system configurations is given based on the power system integration, its efficiency, operability, weight and noise. After rating all the configurations based on six categories and twenty-nine criteria following a procedure akin to Steiner et al., the retained layout by Ref. [49] is composed of two pairs of propulsion systems which are themselves composed of a core gas-turbine and two mechanically-driven fans on either sides, amounting to six propulsive modules. A preliminary 2D set of computations suggests that efforts should be given during the project on the design parameters as they inherently affect the Mach distribution and lift: higher FPR accelerate the flow upstream reducing the BL thickness, and high incidence favours shocks along the aircraft's upper surface thickening the BL ingested. The initial results indicate a 9% reduction in fuel burn compared to an EIS 2035 A330-like aircraft, albeit based on low-fidelity results (2D with a span-wise cut at the engine axis).

Despite showing promising BLI benefits, the DPC bring new architectural challenges. Amongst fully-mechanical, turbo-electric and fully-electric distributive systems, Isyanov et al. conclude that the former is the most feasible in the near future thanks to its minimal technical risk however it might not be the most efficient system [241]. When super-conductive technologies becomes available, alongside electrical components improvements, fully-electric transmission systems appear as the best performing architectures regardless of the positions of the core engines and driven fans. Yet, this remains assumptions and experimental or numerical campaigns are necessary to approve the configurations' performance and efficiencies.

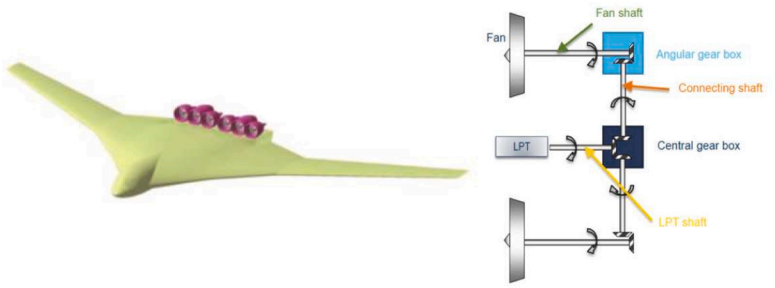


Fig. 27. Schematic of the DisPURSAL architecture and power transmission.
Source: Modified from Ref. [49].

To follow with a more thorough comparative efficiency analysis, Mirzoyan et al. [242] oppose their potential DPC with their PFC and two reference aeroplanes, namely an Airbus A330-300 reflecting an EIS year 2000 and 2035. For comparable missions, the DPC aircraft reduces the block fuel by 38% compared to its EIS 2000 reference and by just below 8% compared to the 2035 reference, just like the PFC. With regards to the environmental challenges, both concepts should meet the noise requirements with the DPC outperforming the PFC thanks to its shielding. NOx and CO_2 levels are predicted to be up to the same standards and comply with the ACARE targets with a reduction of 40%–42% compared to the 2000-reference aircraft.

5.3.2. CMI SAX-40

With the aim of designing an aircraft whose noise would be almost imperceptible around an airport, the Silent Aircraft Initiative was born from the partnership between Cambridge University, U.K., and MIT, USA, with their Cambridge-MIT Institute (CMI). Their concept aircraft, the Silent Aircraft eXperimental, is a result of an iterative design process (from SAX-01 to SAX-40) to achieve low noise and improved fuel burn. The observation made on current aircraft is that the engines are the main sources of noise generation with the rotating fan and high-speed jet. On approach, the noise induced by the airframe contributes as much as the engines with the flaps, slats and undercarriage. To mitigate this perceived noise, a greater integration of the engine and aeroplane is necessary and a potential solution is to use the airframe to shield the engines' noise by installing them above the fuselage. Therefore, the SAX-40's layout is based on a BWB which installs three buried engines at its rear upper surface.

Based on Liebeck's work [132], merged fuselage and wing airframes suggest higher lift-to-drag ratios and significantly lower empty weight than conventional tube-and-wing aircraft. This observation motivated the CMI to investigate the engine installation on these layouts [244]. Following some constraints on the structure behaviour, payload, fuel tanks and doors, the most feasible location is judged to be above, or within, the centre-body, and behind the cabin, to benefit from the ingestion of the BL. The wings also aid with their large surface area allowing to accommodate the embedded engines at the back of the aircraft following an array architecture. The investigation of different configurations draws several conclusions on the future endeavour. A large exhaust area would contribute towards lower noise emissions, and embedding the engines will mitigate the drag and allow for boundary layer ingestion. Nonetheless, a trade-off needs to be made with regards to the engines count as a greater number will lower the weight and drag generated but also lower the thermal efficiency.

First, from the airframe side, multiple studies contributed towards its development for low-noise and low-emissions. From the SAX-10, slight modifications in the aircraft design led to the SAX-12 [194]. The configuration is derived from multidisciplinary designs models and optimisation which final version, i.e. SAX-12, is assessed in terms of performance. The combination of the different modules, namely the propulsion, the aerodynamic and mission profile, allowed for the weight and noise evaluation. Although suggesting promising behaviours, the figures still do not meet the aggressive targets of the "silent aircraft". Dowling and Hynes [243] took over with a major revised version of the aircraft and its SAX-20 derivative. The disruptive configuration contributes towards shielding noise but to further reduce the perceived noise close to the airports, large and low speed jets from the engines are necessary. The SAX-20 using UHBR engines with variable nozzle exhausts still could not meet the target but the investigators were confident that further design iterations will allow it.

From the understanding gained on the engine installation, Hall and Crichton [140] and Crichton et al. [137] emphasised their work on the engine design and fan design, respectively. In the former study, a gearbox and other shaft speed reduction devices (multi-spool) — coupled with a low-speed fan and high gap-chord spacing turbine, are proposed to further reduce the turbomachinery source noise on a three-engine architecture. The latter study, takes back the initial configuration with four engines and focus on the fan design that will efficiently propel the aircraft at both take-off and cruise conditions whilst keeping low the noise emissions. Further designs iterations led to the most-known layout of the "silent aircraft", the SAX-40. The joint efforts from the different partners resulted in parallel developments on the airframe design [133], engine design [268], BLI performance [47] and off-design noise performance — take-off [245] and approach [269].

It has been mentioned that the SAX airframe has seen several aerodynamic and aeroacoustic improvements which led to the changes in design observable in Fig. 28. The SAX-12 was designed to minimised the take-off weight accommodating four semi-buried engines consuming 88 passenger-miles per gallon and generating 80 and 83 dBA (A-weighed correction on decibels) of noise at the airport perimeter at take-off and approach, respectively. Moving towards higher numerical fidelities, the second generation of SAX was aimed at reducing stall speed. Therefore, the centre-body leading-edge design became critical resulting in revisions from SAX-15 to SAX-29. In that configuration, three engines were favoured and 3D RANS calculations were computed. The methodology developed therein was validated such that the centre-body shape of the SAX-29 could be used in the subsequent designs. Hence, the third generation was obtained using optimisation capabilities for reducing noise and fuel burn. The final version, the SAX-40, incorporates three BLI gas generators driving nine fans reducing the fuel burn from 88 passenger-miles per gallon with the SAX-12 to 124 and the noise emissions to 63 dBA corresponding to the background noise of a well-populated area. In conclusion, the SAX-40 conceptual aircraft achieved the objectives set despite integrating a number of technical challenges that could yield considerable risks that need to be overcome [121,133].

Although the "silent aircraft" main aim was to design an aeroplane acoustically unnoticeable around the airports, other challenges in terms of fuel consumption and mechanical reliability needed to be accounted for. As an answer to these aspects, a BLI multi-fan embedded turbofan is proposed integrating a variable area nozzle, a low-pressure turbine, an axial-radial high-pressure compressor, and a low-speed fan optimised for cruise and take-off conditions and advanced acoustic liners



Fig. 28. Main conceptual aircraft designs generations: SAX-12, SAX-20, SAX-40.
Source: Retrieved from Ref. [133].

[268]. The assessment of the BLI propulsion system performance was conducted by Plas et al. [47] introducing the power saving coefficient (PSC), the ratio of ingested drag to the total aircraft drag, distortion and efficiencies. Its application to the SAX-40 resulted in a 3 to 4% decrease in power input and a PSC of 10%–40% depending on the fidelity of the fan model chosen.

5.3.3. NASA N2 to N3-X

With regards to NASA's efforts to meet their environmental goals [5,6], a campaign had been initiated with their N + 1, N + 2 and N + 3 programs. Their aircraft concepts belong to each aircraft's architecture herein reviewed with the STARC-ABL as PFC, the D8 for the ORFEC and the N3-X for this latter category (DPC). Hendricks [42] reviewed NASA's in-house BLI modelling efforts and methodologies, weighing the strengths and weaknesses of each. More specifically on the HWB and BWB concepts, Okonkwo and Smith [40] reviewed the evolving trends of those concepts whilst Liou et al. [270] reported the challenges and progress of HWB aircraft with a focus on the embedded propulsion systems of the NASA N2-B and N3-X.

Initially, the NASA N2-A concept originated in the 2000s with two pylon-mounted turbofan engines at the top-back of the wing-body. In 2006, NASA funded a one-year project to evaluate the synergistic benefits of distributed propulsion and airframe integration on the CESTOL configuration (Cruise Efficient Short Take-Off and Landing) propelled by twelve high BPR turbofans [271,272]. In 2011, Boeing concluded that the N + 2 goals could be reached with a revised version of the N2-A called the N2A-ExTE. In contrast, the N2-B concept embeds three BLI propulsion systems on the upper surface of the wing-body, each composed of three side-by-side propulsors driven by a common turbine [273]. The N3-X was a direct answer to N+3 goals and can accommodate 300 passengers in its HWB form where two wing-tip mounted turboshafts power an array of propulsors embedded in a mail-slot-like nacelle on the body's upper-surface at its trailing-edge. This architecture echoes the TeDP using superconducting generators and electrical transmission systems where the specifications are discussed in Ref. [28]. A complementary study on the effects of BLI on TeDP systems recommended a narrowed-down range of additional, detailed, studies to be conducted at higher fidelity [150,151].

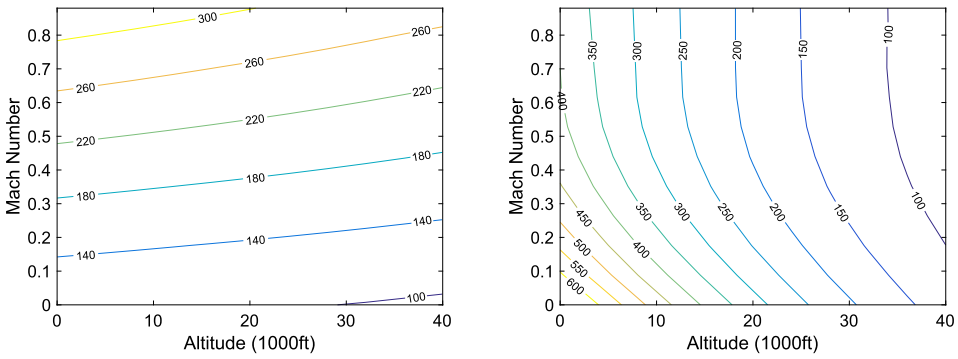
In that respect, a couple of studies from Florea et al. [122,187] contributed towards the development of the N2A-ExTE's propulsion system. First, to demonstrate the feasibility of a low-distortion BLI propulsor, coupled inlet/fan design optimisations are performed. To target a minimum total pressure loss and distortion, and a preliminary assessment on the fan performance impact, 3D CFD on different intake designs were introduced. This study led to an optimal design whose intake length is reduced by five times relative to the initial design yielding a 3%–5% fuel burn benefit relative to a pylon-mounted configuration. Additionally, shrinking the inlet allowed a reduction in pressure loss (maintained below 0.4%) and distortion harmonic amplitudes by 30%–50%. To carry on with a distortion-tolerant fan design, Florea et al. [186] analysed the aerodynamics of a coupled inlet/fan stage. Also, an experimental wind-tunnel inlet/fan configuration was designed and run for the preparation of an experimental campaign. These investigations are completed by Bakhle et al. with their aeromechanic analyses of a BLI fan [274]. In parallel to these system-level studies, the aircraft-level investigation of its aerodynamics is conducted by Hardin et al. [152]. The propulsive efficiency is assessed by Ochs et al. [64] and the benefits resulting from BLI are identified. These benefits amount to around 4% for a fan that has been primarily designed for aerodynamic performance without additional nacelle drag. Hardin et al. [152] reported a reduction of drag from 2 to 3% from the lack of pylon and reduction in nacelle wetted surface area, thus Ochs et al. expect benefits of up to 7% with these losses.

From the Friedman's [275] 3D CFD, the BL, Mach number and pressure profiles were extracted for Felder et al. [150] to design the N3-X concept. With the use of FLOPS [253] and NPSS [209], for the mission range and propulsion system assessments, the actual TeDP concept is derived from the Boeing 777-200LR. The N2A-ExTE therefore predicts to reduce the fuel burn by 70%–72% compared to the B777 reference aircraft, depending on the technology used, i.e. cryo-cooled and LH_2-cooled, respectively. The strategic position of the propulsors' array at 85% of the aircraft chord also plays an important role in its propulsion and noise shielding. A noise and emissions assessment is conducted by Berton and Haller [239] on two derived N3-X versions, one with thrust-vectoring, and the other with relocated turboshafts to reduce noise propagation. The latter version exceeds the N + 3 objectives by 12EPNdB with a noise emission of 64EPNdB (Effective Perceived Noise in decibels).

A multi-fidelity methodology is proposed by Kim and Liou [176] based on a BFM. The model is implemented on a 3D CFD model of the N3-X and is validated against the R4 fan rotor designed by General Electric Aircraft Engines and tested at the NASA Research Glenn Center. At M0.84, FL350 and for an angle of attack of 2°, sectional side views of the propulsors array are presented where a strong shock is observed at the centreline. Additionally, the difference in BL thickness is noted due to the chord length travelled.

Complementary to those efforts, a NASA grant was awarded to Cranfield University in 2013, following the work from Liu et al. [126] on distributed propulsion systems, including TeDP. They built low-order models for assessing the BLI at different inlet conditions, and the weight estimates of the propulsion system and the thermal cycle at both on- and off-design conditions. The effects of BLI on the propulsion models are also examined predicting a fuel burn reduction of 10% considering cryo-cooling and superconductors with the generators' efficiency above 99% and where recommendations on the FPR and equivalent BPR (eBPR) are given to maximise those benefits. Notably, they highlight that the benefits are highly affected by the intake losses, as noticed by Florea et al. [122,187], and the evaluation of the inlet flow distortion needs to be further assessed at it strongly ties to the fidelity of the modelling. Thus, to improve the inlet distortion evaluation fidelity, Liu et al. [127] provide a modelling approach which examines both radial and circumferential distortion by separating their various impacts. Compared to other methods, lower benefits are expected with notably a 0.5–1.5% drop in PSC. Nonetheless, those studies are independent of blade shape and only suitable in the preliminary stages. It is believed that the consideration of new blade designs could curb fan pressure losses and efficiency drops.

To provide insights into the potential benefits of distributed propulsion and BLI, Kirner et al. developed a tool on conventional tube-and-wing configurations [246], and followed up with BWB configurations [247]. The latter assessed stability, mass estimation, drag prediction and simplified distortion analysis based on 2D power-law profiles. The



(a) Specific power consumption. (b) Net propulsive force.

Fig. 29. Propulsor array performance in terms of (a) specific power consumption and (b) net propulsive force as a function of altitude and Mach number, retrieved from [107][5].

figures give a 5.3% benefit in fuel burn for a 2% total pressure loss and a 7% benefit if the losses are reduced to 1%. Kirner [276] also demonstrated that altering the mass-flow and thrust fraction produced by the fans can mitigate these duct losses and hence, offer more benefits.

Merging technologies, Valencia [81] presented a preliminary design evaluation of different propulsion system architectures involving synergies from distributed propulsion, BLI and electrical pieces of equipment for hybrid-electric propulsion. Despite the potential benefits that can arise from the technologies' implementation, the main challenges originated from the high level of integration, leading to mechanical design complexities, intake pressure losses and BLI induced distortion.

At a system level, Valencia et al. [129] assessed the performance of TeDP using a 1D approach to model the effects of distortion on propulsor performance. To maximise the benefits available with current technologies, the thrust-split concept was introduced and showed a reduction in thrust-specific fuel consumption with an optimum obtained at a TS of 65%. A step further in the propulsion system modelling led to a comparative study between parametric 1D and parallel compressor methods [128]. Despite offering comparable benefits, the 1D approach tends to show optima at lower FPR compared to the parallel compressor method. The reason stands in the high sensitivity to intake losses captured by the latter. Additionally, for low thrust-splits, turbofans with higher BPR were more favourable but minimal thrust-specific fuel consumption was obtained for thrust-splits above 60%.

In a rapid preliminary analysis of BLI propulsor performance, Goldberg et al. [104] reported the influence of local flow behaviours on both individual propulsors as well as the entire array. The span-wise flow variation resulted in an increase in power demand due to the BL thinning and the higher Mach number at the AIP [106]. The work is further extended with the method application to off-design conditions [107]. For comparison, the propulsors at the centreline showcase better performance at off-design due to the difference in flow condition than at the edge of it. The on- and off-design performance in specific-power and -propulsive force is illustrated in Fig. 29. Importantly, it is stressed that the map is obtained for 100% rotational speed, not representative of the full flight envelope. A full mission is thus investigated [141] and recommendations are given on the optimal thrust-split to reduce the fuel consumption by a mere 1.5%.

An exergy management formulation proposed by Arntz et al. [70] was introduced for predicting the aerodynamic performance of unpowered configurations. The validation of the code is achieved through various 2D and 3D test cases and compared against a momentum near-field approach. The authors highlight that approximations in the velocity gradients could lead to discrepancies on coarser meshes and recommend a fine grid to be used to mitigate those penalties. Therefore, an application on a N3-X 2D representation led to the conclusion that an exergy-based approach is to favour aero-thermo-propulsive performance as the decoupling between the internal and external flow is unnecessary [72]. BLI improvements of up to 50% are reported and little exergy is wasted in the jet and wake exhibiting an exergy-waste coefficient (EWC) lower than 3%. Additionally, the implementation of heat transfer upstream of the propulsion system yields a further 1.5% fuel burn benefit. Similarly Sato [34] introduced liquefied natural gas along with proper thermal management techniques which allowed for cooling the outer wing delaying laminar to turbulent transition and promoting favourable laminar flow on the wing surfaces. This yielded an additional 2% in fuel burn reduction when compared to conventional jet fuels amounting to a total reduction of 57% relative to a Boeing 777-200LR reference. The propulsion system performance was estimated from cycle performance tools and coupled to an aerodynamic assessment of the airframe based on 3D CFD using an energy analysis. The BL properties as well as the wake, shock and vortex- induced dissipation sources were identified in this method.

With the introduction of synergistic technology combinations by Sato [34] with liquefied natural gas and Arntz and Atinault [72] with heated walls, Smith and Laskaridis [277,278] offered an airframe integration for LH_2 hybrid-electric propulsion system. Despite the challenges associated with BWB, one advantage offered is the implementation of liquid hydrogen tanks. A preliminary design is suggested highlighting a number of specific issues and their potential solutions. On a wider range, accounting for short-, medium- and long-range mission aircraft, Rompokos et al. review synergistic technology combinations by short-listing two potential candidates based on thirty-four criteria [279].

5.3.4. ONERA DRAGON

In another fashion, ONERA developed the DRAGON (Distributed fans Research Aircraft with electric Generators by ONERA) that is not based on HWB or BWB but incorporates distributed propulsors located along the wings' pressure sides that are powered by two turboshafts installed on either side of the rear-fuselage, as illustrated in Fig. 30 (left). It is known that lowering the FPR whilst increasing the BPR contributes to higher efficiencies however, it is jeopardised by operability, integration, size and weight challenges. Dividing the main turbofan into an array of fans allows to maintain a low FPR whilst maintaining full operability using a hybrid-electric distributed propulsion solution [134].

[5] Reproduced from Goldberg et al. Method for Simulating the Performance of a Boundary Layer Ingesting Propulsion System at Design and Off-Design. Aerospace Science and Technology 2018, 78: 312-319. Copyright © 2018 Elsevier Masson SAS. All rights reserved.



Fig. 30. ONERA DRAGON [167], ESAero ECO-150 [136][6] and NASA CHEETA [280][7].

ONERA's expertise started in 2013 with the AMPERE project whereby distributed electric propulsion was studied on a high-wing concept plane incorporating 40 electric-ducted fans located along the wing-span leading-edge of a small business aircraft [281]. To better understand the mechanisms associated with such configurations, numerical simulations were carried out along a wind-tunnel campaign for providing data validation. A collaboration with ISAE-Supaero, France, allowed the design space exploration of a large passenger aircraft [282]. From these campaigns, they extended further their understanding of aero-propulsive layout by investigating a high-speed distributed propulsive concept [134].

To comply with today's aeroplanes, the DRAGON is investigated for a mission of 1200 nmi at a cruise Mach number of 0.8 accommodating 150 passengers [134]. A 2D study assessed the interactions between the aerofoil and a fan installed at its rear-lower surface. A design is selected to provide a clean supersonic flow over the wing whilst preventing separation on the pressure side but nonetheless requires further investigation on 3D models to confirm the design on a flap-wing integration. Moreover, an initial mission assessment advised to reduce the range from 1200 nmi to 800 nmi for comparison with short-to-medium range aircraft. With these top-level aircraft requirements, the DRAGON reduces the fuel burn by 8.5% when compared to an EIS 2035 podded aircraft. Extending that investigation, it is suggested that the DRAGON performs better than its reference as long as the range remains below 1100 nmi and that uncountable improvements at disciplinary- and system-levels could be obtained as the aircraft did not undergo any optimisation.

From the understanding gained in Ref. [134], 3D RANS computations were performed [167]. Aware of the unrealistic 2D modelling, a step-by-step approach is followed to move to 3D computations. Still, numerous challenges arise from this switch: periodicity between the fans must be ensured, inlet and nozzle sections must be well-defined, the 2D aerofoil needs to be represented with a cylindrical section before the inlet and the FPR needs to be incrementally increased to ensure convergence. A comparison of the models highlights good agreement despite operating at different FPR. In spite of concluding that the DRAGON performs better for a mission range under 1100 nmi [134], Freeman and Schiltgen report that turbo-electric distributed propulsion aircraft prove most benefits on a 3500 nmi design mission, such as performed by an Airbus A320 [136]. Consequently, ONERA's efforts focused at a 2750 nmi range to size their fully-distributive electric propulsion aircraft. For this design mission, 26 ducted fans powered by two turbo-shafts offer a reduction of 7% in fuel burn, against an EIS 2035.

Notwithstanding the long-term goals envisaged by the DPC, the concept appears as the most widespread architecture and it is the authors' decision to present only the ones above. Numerous other studies have been done by fellow researchers and are of interest. Amongst those, can be named the TU Delft Flying-V, [8] which reduced model flying campaign already started despite lacking the BLI technology, the ESAero ECO-150 [135,136,283,284] and NASA CHEETA [280] which

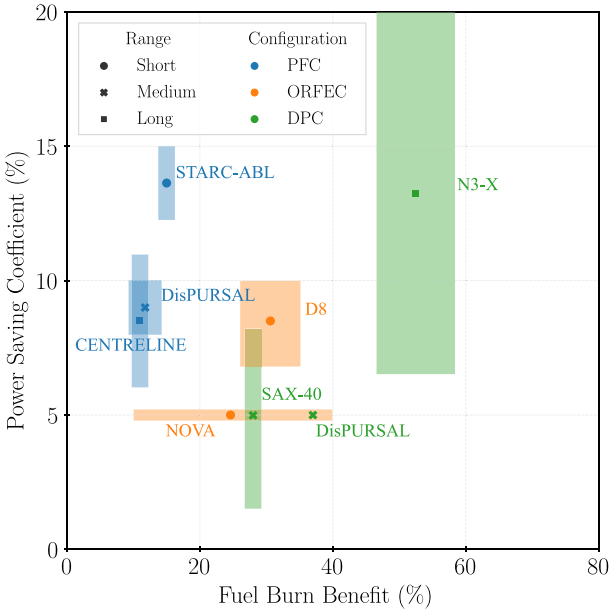


Fig. 31. Boundary layer ingestion benefits in power savings coefficient, relative to the concepts' podded equivalent, and technology and synergistic benefits in fuel burn, relative to their tube-and-wing reference.

designs can be compared with the ONERA DRAGON (Fig. 30), and the Airbus projects MAVERIC[9] whose scaled flying demonstrator already performed a flight or the ZEROe concepts with their BWB[10] based on a hydrogen propelling system.

5.4. Foreseeable benefits

Numerous studies, led by institutions and universities, contribute towards the understanding of BLI through their various aircraft concepts. Whether they focus more on the noise or fuel burn reductions, all studies intend to comply with the challenging targets set by the EU and NASA.

The various architectures give rise to promising environmental-friendly contributions that are partly summarised in Fig. 31. Although they are compared in terms of fuel burn benefits and power savings, they consider their own references to highlight the BLI benefits and a fair comparison is only possible if they share a common conventional reference aircraft at similar mission. Yet, Fig. 31 indicates a qualitative comparison between the concepts for their respective references given in Appendix B. The power savings are reported against their podded equivalent to demonstrate the benefits of BLI only whereas the fuel savings are given against a reference aircraft showcasing synergistic benefits.

It is opined that the PFC, based on tube-and-wing configurations, suggest less fuel burn benefits as only the BLI benefits are assessed

[6] Reproduced from J. L. Freeman and B. T. Schiltgen, ECO-150-300 Design and Performance: A Tube-and-Wing Distributed Electric Propulsion Airliner; reprinted by permission of the American Institute of Aeronautics and Astronautics, Inc.

[7] Courtesy of D. Chandel et al. and NASA's CHEETA program.

[8] https://www.tudelft.nl/en/ae/flying-v/.

[9] https://www.airbus.com/newsroom/press-releases/en/2020/02/airbus-reveals-its-blended-wing-aircraft-demonstrator.html.

[10] https://www.airbus.com/innovation/zero-emission/hydrogen/zeroe.html.

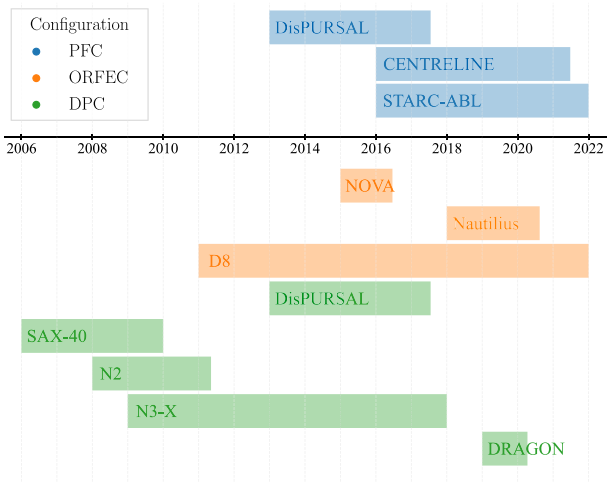


Fig. 32. Timeline of aircraft concepts featuring boundary layer ingestion based on the literature retrieved.

whereas the new propulsion architectures implemented in the ORFEC and DPC yield higher fuel burn reductions as benefits arise from other sources — e.g. airframe and propulsion architectures.

Particularly for the N3-X, very high benefits are claimed, but put into perspective, when compared to a pylon-mounted reference aircraft, the fuel consumption is reduced by *only* 18% from the sole BLI benefits as majority of the reductions result from the aircraft configuration and its transmission architecture [150]. Specifically, between the N3-X and SAX-40, a large difference is observed in power savings and fuel burn reduction but it is reminded that efforts were mainly given to acoustic performance and noise reduction for the latter.

6. Conclusions

In this review, the literature on boundary layer ingestion propulsion concepts was scrutinised to identify and collate the different approaches employed to evaluate the performance as well as the numerical and experimental models and set-ups (Fig. 9), and the design exploration and optimisation of prospective civil aircraft. The diverse challenges and their present achievements were presented in accordance with a classification of the different aircraft concepts (Fig. 14). A time-line of these concepts and progress, amongst others, is depicted in Fig. 32 for the retrieved literature.

As regards the different performance evaluation approaches, energy- and exergy-based analyses yield the most information (Table 3). The introduction of the absolute reference frame with these book-keeping schemes enhances the interpretations one might perform on the aero-dynamics with causal work-energy pathways and the underpinning boundary layer ingestion mechanisms. Nonetheless, momentum-based approaches are useable if the net axial force suffice, e.g. optimisation studies. Ideally, these approaches should be used in synergy, unlike suggested by Hendricks [42] who sees the approaches serving different purposes. Although initial work attempts to unify all approaches, efforts should keep going into that direction and eventually lead to a unique and universal book-keeping scheme for highly integrated aircraft. Additionally, the numerical modelling plays an important role in the aero-propulsive performance reported. As an example, boundary conditions to mimic the propulsor's fan ideally fill the defects in the flow and do not transport the total pressure distortion through the stage which would reduce the potential savings.

To maximise the overall performance of these aircraft, strongly-coupled approaches need to be developed between the aircraft's aerodynamics and the propulsion system. This innately requires the development of multidisciplinary frameworks that allow inter-communications between the aerodynamic and propulsion solvers. Despite seeing current numerical efforts going into that direction, this requires the use of high-order fidelity tools which necessitates experimental validations. In spite of the progress in experimental instrumentations, set-ups and techniques that are reviewed, many challenges arise with respect to the similitude, i.e. geometric, kinematic and dynamic similarities, and current state-of-the-art work conducted at low-speed testing is preferred, often omitting the compressibility effects related to boundary layer ingestion.

Notwithstanding the different aircraft concepts to meet the environmental targets, rather *small* benefits arise from boundary layer ingestion. However, the majority of the concepts enable the use of other technologies, e.g. lighter materials, liquid hydrogen (LH_2), turbo-electric distributed propulsion, enabling synergistic and larger benefits.

- The propulsive fuselage concept (PFC) offers the opportunity to partially meet the aims in the short-term, particularly because of the lack of aero-acoustics analyses. A main advantage of this arrangement nonetheless is the *easy* inclusion of the aft-mounted propulsor from an engineering point of view but operability and safety investigations need to ensure its further development and use;
- The over- and rear-fuselage engine concept (ORFEC) still presents a premature development even if it demonstrates promising savings and intensive efforts in experimental techniques. The wide-body lifting-fuselage enables a reduction of the aircraft's length and an increase of the wing's aspect ratio both contributing to synergistic improvements that the PFC cannot offer. Nonetheless, as the engines provide the entirety of the thrust requirement, safety studies needs to also be performed to ensure safe flights in case of an inoperable engine;
- The disruptive propulsive concept (DPC) promises the greatest benefits in the long-term, including noise reduction from the body's shielding and facilitates the integration of liquid-hydrogen tank. However, multi-disciplinary challenges need to be overcome and a lack of optimisation and experimental studies prevents the full exploitation of the configuration's benefits.

It is emphasised that for only assessing the benefits from boundary layer ingestion, concerns should be given to the choice in reference aircraft. The difference between the boundary layer ingestion aircraft and its reference should only be on the propulsion systems installation, i.e. embedded against podded, otherwise synergistic benefits are captured, e.g. transmission, architecture, aerodynamics. Nevertheless, the comparison between the engines yields another challenge, should it compare size, mass-flow rate, or output force, encouraging the use of idealised scenarios to claim minimal achievable benefits. These observations raise several key points, an alteration in traditional performance accounting approaches must be considered, particularly taking note of the recent new energy- and exergy-based approaches to help discover absolute metrics that can quantify and characterise boundary layer ingestion performance, without having to resort to a comparison against a podded equivalent.

Lastly, recent efforts are observed in the field of experiments and aircraft scaling but numerous challenges are still present as regards the similitude between the full- and wind-tunnel-scale models. Despite the constant development of numerical solvers and the wide knowledge of the researchers in the field, experimental data are vital to ensure that the models used numerically accurately represent the reality. Nonetheless to compare, or validate, the data, efforts should not stop in the cutting-edge data acquisition techniques and uncertainty calculations to couple experiments with numerical investigations.

CRediT authorship contribution statement

Nicolas G.M. Moirou: Conceptualisation, Data Curation, Investigation, Visualisation, Writing – original draft, Writing – review & editing. **Drewan S. Sanders:** Writing – review & editing. **Panagiotis Laskaridis:** Writing – review & editing.

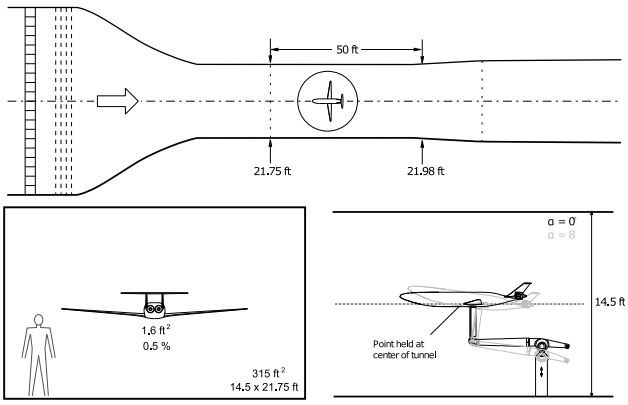


Fig. A.1. Schematic of the top, rear and side views of the MIT D8 aircraft in the NASA Langley's 14 × 22 wind-tunnel.
Source: Retrieved from Ref. [83].

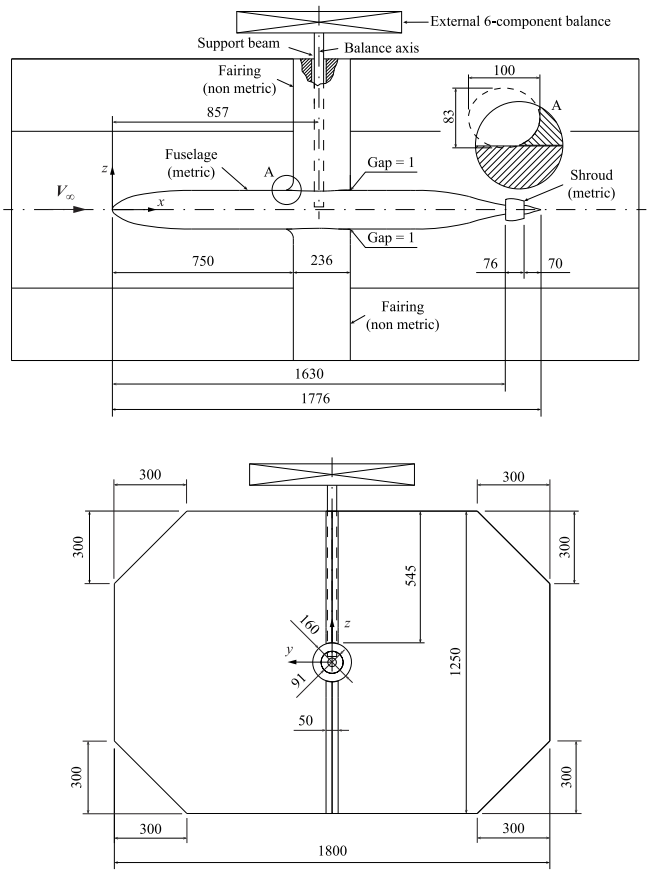


Fig. A.2. Schematic of the side and rear views of the CENTRELINE aircraft in the Low Turbulence Tunnel of Delft University of Technology.
Source: Retrieved from Ref. [180].

Declaration of competing interest

The authors declare that they have no known competing financial interests or personal relationships that could have appeared to influence the work reported in this paper.

Data availability

No data was used for the research described in the article.

Acknowledgements

This publication is funded by the European Union's Horizon 2020 research and innovation program under Grant Agreement No. 864803. The authors express their gratitude to Ioannis Lamprakis and Ngonidzashe E. Mutangara for the fruitful discussions and suggestions.

Appendix A. Experimental apparatuses description

A.1. Wind-tunnel and model installation

Wind-tunnels can be of different cross sections where the aircraft model is mounted in. Large subsonic wind-tunnels such as the NASA Langley 14- by 22-foot represented in Fig. A.1 accommodates the D8 concept that is tested at low-speed conditions. The model is attached from the wing root with a pitch head and trunnion mounting system controlling the height and angle of attack, itself connected to the wind-tunnel floor.

In a different manner, the Delft Low Turbulence Tunnel has an octagonal cross section with a height of 1.25 m and a width of 1.8 m. Unlike the D8 which features wings and a π-tail, the aircraft model of the CENTRELINE project only presents an axi-symmetric fuselage connected to the floor and roof by fairings containing a support beam to measure the forces applied on the structure (Fig. A.2).

As regards the model support, it should allow the model to cover the range of motion desired, e.g. yaw, pitch and roll, without obstructing any data acquisition from the instrumentation. The support must also respond to various needs: to be discrete from an aerodynamics standpoint, to allow supply and eventually return of energy or flow, and more importantly to insure mechanical hold with limited oscillations and deformations.

For rear-powered BLI architectures, sting and strut supports are depicted in Fig. A.3. A single straight sting attachment (Fig. A.3(b)) from the downstream end of the model can be used on PFC but prevents the measurement of any data in the wake. In place, Z-sting or fin sting supports (Figs. A.3(a) and A.3(c)) allow an important clearance behind the model for wake measurements but prevent skidding. With a strut, full mobility is provided whilst also freeing the wake from any instrumentation. A combination of the Z-sting and strut supports is favoured for the MIT D8 [20,83] (Fig. A.1) whereas the CENTRELINE project used two struts at the top and bottom of the model (Fig. A.2) mounted on the roof and floor of the wind-tunnel, respectively, but data correction is necessary to filter the perturbations caused by the struts [180]. Lastly, models can be supported at the tip of truncated wings (Fig. A.3(f)) or from the under-wing engines (Fig. A.3(e)) also allowing full mobility of the system as well as the instrumentation to be installed in the wake — to some extent. Nonetheless, data correction might also be necessary to remove the vortices generated around the booms.

A.2. Apparatuses

Measuring balance

Further to the six-component balance as used by Ref. [165] and depicted in Fig. A.4, Ref. [285] designed and developed a six-component balance with a floating frame to mount models on. The forces and moments acting on the model are measured by the six rods installed perpendicular to each other to obtain all components.

In essence, balances are a transducer that converts a load into an analogue output proportional to the force applied. Several balances exist which are more or less adapted to the different supports. The six-component balance is the most spread apparatus for sting-mounted models but prevents any wake measurements. For the strut fixture, the balance can equally be used as the rear-region of the fuselage is *live* and comes to the form of a small or large flanged device. Rotating shaft

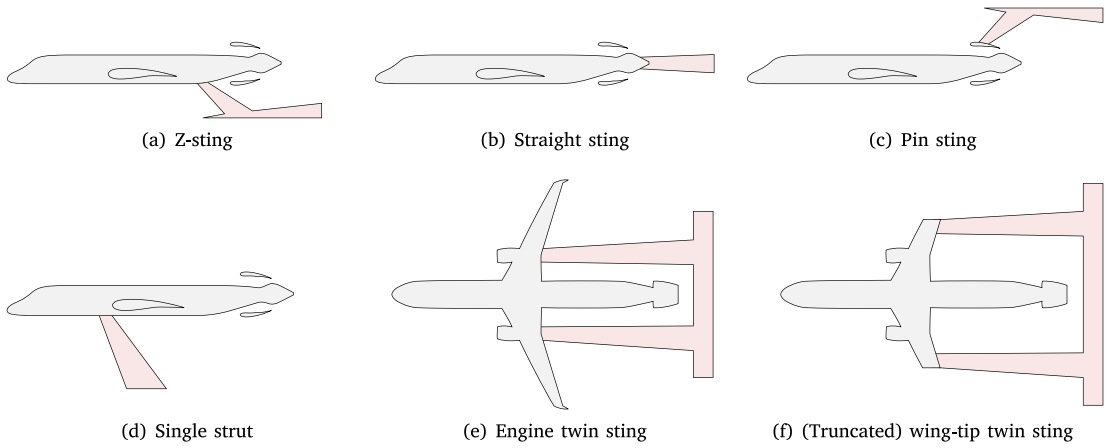


Fig. A.3. Schematics of wind-tunnel model supports applicable for powered boundary layer ingesting aircraft.

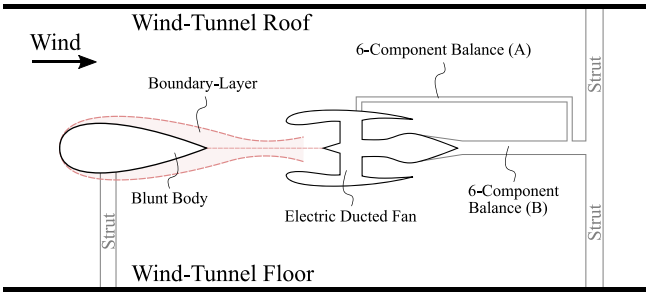


Fig. A.4. Schematic of the experimental set-up with measurements of (A) the nacelle drag and other forces and momentums, and (B) thrust, torque and other forces and momentums.
Source: Remastered from Ref. [165].

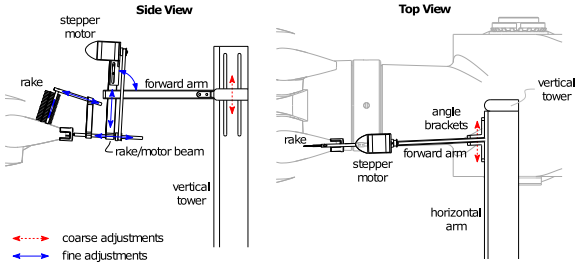


Fig. A.5. Rotating rake of pressure measurements n the NASA Langley's 14 × 22 wind-tunnel [109].

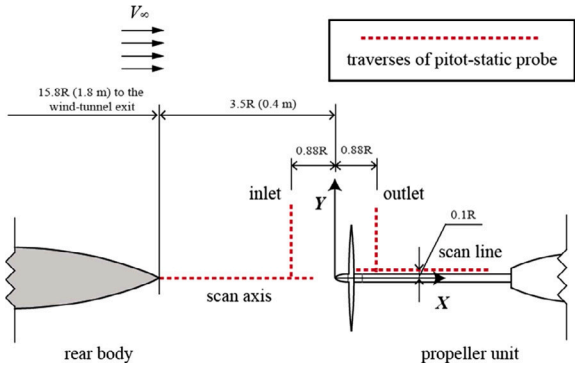


Fig. A.6. Traverse rake of pressure measurements in the Delft University of Technology's OJF wind-tunnel [220].

balances are also designed to measured the torque during powered tests but the range of the forces and moments are significantly lower than the flanged balances.

As an alternative to balances, load cells can also be employed to measure the axial force on a system. The cells measure both compression and tension and are referred as pancake, S-beam — with higher accuracy, or in-line — more compact and with a larger force range possibility.

Wake rake

For pressure measurements, fixed rakes are often used in conventional propulsion systems to characterise the flow distortion at the AIP or the total pressure distribution at the nozzle plane. Equally, the method can be followed for BLI configurations but the ingestion of the BL necessitates a different distribution of the arms to accurately map the flow distribution. As such, rotating rakes (Fig. A.5) have been introduced [233] and vastly used in the D8 project [20,76,109]. The arm(s) rotate(s) and data is either acquired continuously or intermittently with different degrees of revolution (Fig. 10).

In the wake, uneven distributions of probes can be coupled to a traversing rake which covers different axial and lateral positions in the wake (Fig. A.6). Alike the rotating rake, the traverse rake can continuously or intermittently sweep over the survey plane and take measures.

In either method, interpolation might be necessary to solve the relatively sparse distribution of points. To that extent, methods such as the followings can be used for radial and circumferential distributions:

- bi-linear: standard linear interpolation for both radial and circumferential directions [75];
- linear and cubic spline: standard linear interpolation in the radial direction and cubic spline in the circumferential direction;
- bi-cubic spline: cubic spline in both directions;
- guided: guided interpolation uses a template to enhance the current distribution in both directions.

A.3. Optical measurements

Pressure-sensitive paint

To obtain a detailed field of pressure distribution, a pressure-sensitive paint system uses multiple cameras and lamp illuminating the surfaces of interest priorly covered to react to changes in temperature and pressure. In the case of the Aircraft Research Association (ARA), UK, their system is composed of 12 cameras and 16 UV lamps to obtain a full coverage (Fig. A.7). To enable this capture, the model is painted

Table B.1
Aircraft and propulsion systems characteristics of the different boundary layer ingestion aircraft.

	Characteristic	Unit	Propulsive fuselage concepts			Over- and rear-fuselage engine concepts		Disruptive propulsive concepts			
			STARC-ABL	CENTRELINE	DisPURSAL	NOVA	D8	DisPURSAL	SAX-40	N3-X	DRAGON
Aircraft	Reference aircraft	–	B737–800	A330–300	A330–300	A321-200/B767–200	B737–800	A330–300	B777–200	B777-200LR	A320-B737
	Range	nmi - km	3500–6500	6500–12,000	4800–9000	3000–5500	3000–5500	4800–9000	4000–7400	7500–13,900	2750–5000
	Fuel block	kg	9680	39,300	38,380	19,700	15,700	38,960	–	38,550	5120
	Passengers	–	154	340	340	180	180	340	215	300	150
	Cruise altitude	ft	37,000	35,000	35,000	37,000	37,500	35,000	40,000	30,000	–
	Cruise Mach	–	0.785	0.82	0.8	0.82	0.72	0.8	0.8	0.84	0.78
Airframe	Airframe length	m	42.1*	70.5	69	38.3	37.9	37	42.1	40.6	–
	Cabin diameter/Height	m	3.96	6.09	6.07	3.9	7.62	–	3.96	–	–
	Cabin width	m	–	–	–	4.9	5.4	–	–	–	–
	Wing span	m	36	64.6	65	43.1	35.8	65	36	66	36
Main engine	Fan diameter	m	1.32	2.85	2.77	2.16	1.85	1.88	2.16	–	–
	Nacelle diameter	m	1.48	3.05	–	2.5	–	–	–	–	–
	By-pass ratio	–	6.4	15.5	18.1	16	10	20	12.3	–	0
	Fan pressure ratio	–	–	–	–	1.4	1.45	–	–	–	–
	Overall pressure ratio	–	58	60	–	42	40	51	49	–	37
	Boundary layer ratio	%	–	–	–	40	40	–	–	–	–
	Power	MW	–	–	–	–	13	–	–	–	–
BLI power-plant	Fan diameter	m	2.06	2.34	4.13	–	–	–	1.2	1.1	–
	Nacelle diameter	m	2.29	–	–	–	–	–	–	–	–
	By-pass ratio	–	∞	∞	17.9	–	–	∞	12.3	∞	∞
	Fan pressure ratio	–	1.25	1.4	1.39	–	–	–	1.5	1.3	1.25
	Inlet pressure recovery	–	–	0.99	0.86	–	–	–	–	–	–
	Boundary layer ratio	%	45	19–36	29	–	–	–	16.6	–	–
	Thrust-split	%	44	6	13	–	–	–	100	100	100
	Power	MW	2.6	8	12	–	–	–	–	30	–
	Power saving coefficient	%	12–14 [21]	6–11 [162]	8–10 [48]	5 [19]	7–10 [20]	5 [80]	2–10 [47]	10–20 [104]	–
	Fuel burn benefits	%	15 [22]	11 [212]	13 [148]	–	36 [20]	37 [242]	28 [121]	55 [34]–70 [270]	–

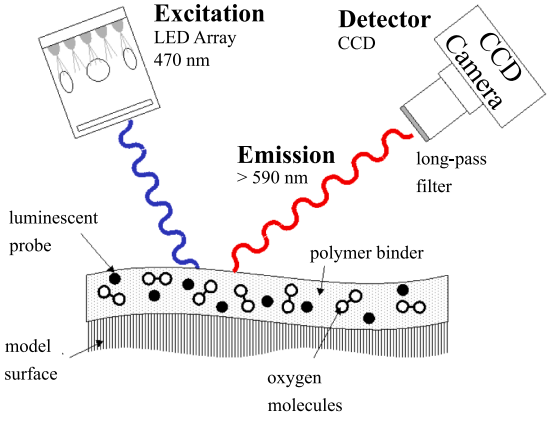


Fig. A.7. Pressure-sensitive paint, light and camera system in the ARA 9 × 8 Transonic Wind-Tunnel [234].

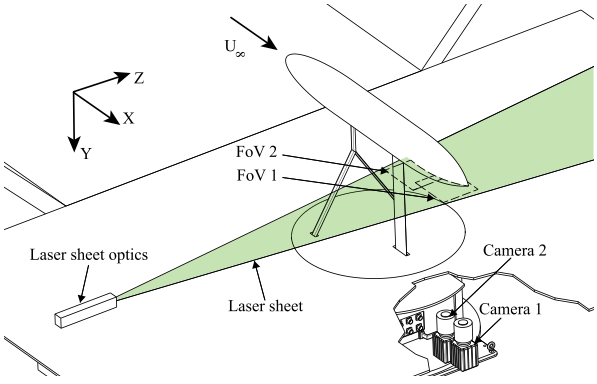


Fig. A.8. Updated stereoscopic particle image velocimetry set-up in the Delft University of Technology's OJF wind-tunnel [227].

following a particular procedure. A white epoxy base layer is applied on clean surface before baking the model at 65° for up to 24 h. This process provides a better surface roughness to adhere to, isolates the active layer from internal changes in temperature and improves the signal by reflecting more light outwards.

The paint used contains particular molecules (PtTFPP) that absorb photons for wavelengths around 400 nm and emit light around 690 nm. The emission process (Fig. A.7) is quenched by the presence of oxygen and highlights a range of different intensities of red sensitive to the local pressure — low pressure means less oxygen and a brighter red. The data acquisition can take up to eight minutes as comparison is needed between wind-on and -off images. The obtained data field is then calibrated to a CAD mesh from which markers are identified against pressure taps to reduce the temperature effects.

Particle image velocimetry

A second optical measurement technique is related to the velocity field acquisition by use of particle image velocimetry (PIV). The flow travelling around the model is seeded with tracer particles small enough that they faithfully follow the flow. A set-up of laser(s) (Fig. A.8) illuminate a slice, or a sheet, by subsequent pulsations in the region of interest where cameras capture images. The displacement of the particles over the span of the two photographic taken defines the velocity of the particle and thus the local velocity of the flow. Afterwards, from a data acquisition software, the region of the flow illuminated is mapped alike obtained with CFD.

PIV is a non-intrusive measurement technique from which data can be simultaneously acquired over a wide 2D or 3D area, depending on the camera set-up. For instance, stereoscopic PIV utilises two cameras to extract the displacement in a particular plane whereas dual plane stereoscopic PIV would cover two planes of laser light. The size of the seeds is chosen to be sufficiently small to not affect the stream-flow and represent the testing when seeds are not included. Nonetheless, the materials chosen for the model are also of importance as they can absorb or reflect part of the laser light with different levels. As such, an anodisation on aluminium increases the corrosion resistance but also prevents the reflection of the light sheet very close to the surface such that the sub-viscous layer velocity can be captured — unlike in Ref. [180]. Other techniques are reviewed in Ref. [236].

Appendix B. Novel aircraft characteristics

The different novel aircraft characteristics are summarised in Table B.1 and categorised following the paper structure to highlight the different concept features. Notably, for the PFC, the under-wing engines describe the main engines as an additional propulsor is aft-mounted (BLI power-plant) whereas main turbofans are aft-mounted on the fuselage for the ORFEC. As for the DPC, different distributed architectures are selected.

References

[1] A.H. Epstein, Aeropropulsion for commercial aviation in the twenty-first century and research directions needed, 52 (2013) 901–911.
[2] European Commission, European Aeronautics: A Vision for 2020, 2001.
[3] European Commission, Flightpath 2050 Europe's Vision for Aviation, 2011, http://dx.doi.org/10.2777/50266.
[4] ACARE (Advisory Council for Aviation Research and Innovation in Europe), Strategic Research & Innovation Agenda 2017 Update Volume 1, 2017.
[5] K.L. Suder, Overview of the NASA environmentally responsible aviation project's propulsion technology portfolio, in: 48th AIAA/ASME/SAE/ASEE Joint Propulsion Conference and Exhibit, Atlanta, Georgia, USA, 2012, http://dx.doi.org/10.2514/6.2012-4038.
[6] NASA (National Aeronautics and Space Administration), NASA Aeronautics: Strategic Implementation Plan 2019 Update, 2019.
[7] EASA (European Union Aviation Safety Agency), European Aviation Environmental Report 2019, 2019, http://dx.doi.org/10.2822/309946.
[8] G.F. Wislicenus, Hydrodynamics and propulsion of submerged bodies, Am. Rocket Soc. J. 30 (12) (1960) 1140–1148.
[9] W.S. Gearhart, R.E. Henderson, Selection of a propulsor for a submersible system, J. Aircr. 3 (1) (1966) 84–90.
[10] L.H. Smith Jr., Wake ingestion propulsion benefit, J. Propuls. Power 9 (1) (1993) 74–82.
[11] M. Gad-el Hak, Modern developments in flow control, Appl. Mech. Rev. 49 (7) (1996) 365–379.
[12] D.M. Bushnell, M.H. Tuttle, Survey and Bibliography on Attainment of Laminar Flow Control in Air using Pressure Gradient and Suction, NASA, 1979.
[13] W. Pfeminger, Laminar Flow Control Laminarization, Technical Report, 1977.
[14] S.P. Wilkinson, Investigation of an oscillating surface plasma for turbulent drag reduction, in: 41st Aerospace Sciences Meeting and Exhibit, American Institute of Aeronautics and Astronautics, Reno, Nevada, USA, 2003.
[15] T.N. Jukes, K.-S. Choi, G.A. Johnson, S.J. Scott, Turbulent drag reduction by surface plasma through spanwise flow oscillation, in: 3rd AIAA Flow Control Conference, American Institute of Aeronautics and Astronautics, San Francisco, California, USA, 2006, http://dx.doi.org/10.2514/6.2006-3693.
[16] D.M. Bushnell, I. Wygnanski, Flow Control Applications, Technical Report January, NASA, 2020.
[17] D.S. Sanders, P. Laskaridis, Full-aircraft energy-based force decomposition applied to boundary-layer ingestion, AIAA J. 58 (10) (2020) 4357–4373.
[18] I. Lamprakis, D.S. Sanders, P. Laskaridis, Fundamental concepts of boundary layer ingestion propulsion, 2023, (Unpublished).
[19] L. Wiart, O. Atinault, J.-C. Boniface, R. Barrier, Aeropropulsive performance analysis of the NOVA configurations, in: 30th Congress of the International Council of the Aeronautical Sciences, 2016.
[20] A. Uranga, M. Drela, E.M. Greitzer, D.K. Hall, N.A. Titchener, M.K. Lieu, N.M. Siu, C. Casses, A.C. Huang, G.M. Gatlin, J.A. Hannon, Boundary layer ingestion benefit of the D8 transport aircraft, AIAA J. 55 (11) (2017) 3693–3708.
[21] A. Yildirim, J.S. Gray, C.A. Mader, J.R.R.A. Martins, Performance analysis of optimized STARC-ABL designs across the entire mission profile, in: AIAA SciTech 2021 Forum, American Institute of Aeronautics and Astronautics, 2021, http://dx.doi.org/10.2514/6.2021-0891.
[22] J.R. Welstead, J. Felder, Overview of the NASA STARC-ABL (Rev. B) advanced concept, 2017, p. 14.
[23] P. Laskaridis, V. Pachidis, P. Pilidis, Opportunities and challenges for distributed propulsion and boundary layer ingestion, Aircr. Eng. Aerosp. Technol. J. 86 (6) (2014) 451–458.
[24] P.D. Bravo-Mosquera, F.M. Catalano, D.W. Zingg, Unconventional aircraft for civil aviation: A review of concepts and design methodologies, Prog. Aerosp. Sci. 131 (2022).
[25] J.R. Welstead, J.L. Felder, Conceptual design of a single-aisle turboelectric commercial transport with fuselage boundary layer ingestion, in: 54th AIAA Aerospace Sciences Meeting, 2016, http://dx.doi.org/10.2514/6.2016-1027.
[26] M. Drela, Development of the D8 transport configuration, in: 29th AIAA Applied Aerodynamics Conference 2011, June, 2011, http://dx.doi.org/10.2514/6.2011-3970.
[27] L. Wiart, O. Atinault, B. Paluch, D. Hue, R. Grenon, Development of NOVA aircraft configurations for large engine integration studies, in: 33rd AIAA Applied Aerodynamics Conference, American Institute of Aeronautics and Astronautics, 2015, http://dx.doi.org/10.2514/6.2015-2254.
[28] J.L. Felder, H. Dae Kim, G.V. Brown, Turboelectric distributed propulsion engine cycle analysis for hybrid-wing-body aircraft, in: 47th AIAA Aerospace Sciences Meeting Including the New Horizons Forum and Aerospace Exposition, American Institute of Aeronautics and Astronautics, Orlando, Florida, USA, 2009, http://dx.doi.org/10.2514/6.2009-1132.
[29] MIDAP Study Group, Guide to In-Flight Thrust Measurement of Turbojets and Fan Engines, Technical Report AGARD-AG-237, 1979, p. 212.
[30] SAE Committee E-33, In-Flight Thrust Determination, Technical Report AIR1703, 1985.
[31] D.S. Sanders, Boundary Layer Ingestion Performance Assessments with Application to Business Jets (Ph.D. thesis), Cranfield University, 2018.
[32] A.L. Habermann, J. Bijewitz, A. Seitz, M. Hornung, Performance bookkeeping for aircraft configurations with fuselage wake-filling propulsion integration, CEAS Aeronaut. J. (2019) 529–551.
[33] M. Drela, Power balance in aerodynamic flows, AIAA J. 47 (7) (2009) 1761–1771.
[34] S. Sato, The Power Balance Method For Aerodynamic Performance Assessment (Ph.D. thesis), Massachusetts Institute of Technology, 2012.
[35] A. Arntz, O. Atinault, A. Merlen, Exergy-based formulation for aircraft aeropropulsive performance assessment: Theoretical development, AIAA J. 53 (6) (2015) 1627–1639.
[36] D.K. Hall, M. Lieu, M. Drela, Aerodynamic performance accounting for ultra-integrated air vehicle configurations, in: AIAA SciTech 2019 Forum, American Institute of Aeronautics and Astronautics, San Diego, California, USA, 2019, http://dx.doi.org/10.2514/6.2019-1310.
[37] I. Lamprakis, D.S. Sanders, P. Laskaridis, Energy-based thermo-aero-propulsive flight vehicle performance assessment, 2023, (Unpublished).
[38] N.G.M. Moirou, D.S. Sanders, P. Laskaridis, Hybrid aero-propulsive performance evaluation approach on novel aircraft, 2023, (Unpublished).
[39] A.M. Ferrar, W.F. O'Brien, Progress in boundary layer ingesting embedded engine research, in: 48th AIAA/ASME/SAE/ASEE Joint Propulsion Conference and Exhibit, American Institute of Aeronautics and Astronautics, Atlanta, Georgia, USA, 2012, http://dx.doi.org/10.2514/6.2012-4283.
[40] P. Okonkwo, H. Smith, Review of evolving trends in blended wing body aircraft design, Prog. Aerosp. Sci. 82 (2016) 1–23.
[41] H.D. Kim, A.T. Perry, P.J. Ansell, A review of distributed electric propulsion concepts for air vehicle technology, in: AIAA Propulsion and Energy 2018 Forum, American Institute of Aeronautics and Astronautics, Cincinnati, Ohio, USA, 2018, http://dx.doi.org/10.2514/6.2018-4998.
[42] E.S. Hendricks, A Review of Boundary Layer Ingestion Modeling Approaches for Use in Conceptual Design, Technical Report, NASA, 2018.
[43] L. Menegozzo, E. Benini, Boundary layer ingestion propulsion: a review on numerical modelling, J. Eng. Gas Turbines Power (c) (2020).
[44] D.E. Diamantidou, M.L. Hosain, K.G. Kyprianidis, Recent advances in boundary layer ingestion technology of evolving powertrain systems, Sustainability 14 (3) (2022).
[45] D.D. Baals, W.R. Corliss, Wind Tunnels of NASA, National Aeronautics and Space Administration, Washington, D.C., USA, 1981.
[46] J.G. Marvin, Wind Tunnel Requirements for Computational Fluid Dynamics Code Verification, Technical Report, NASA, 1987.
[47] A.P. Plas, M.A. Sargeant, V. Madani, D. Crichton, E.M. Greitzer, T.P. Hynes, C.A. Hall, Performance of a boundary layer ingesting (BLI) propulsion system, in: 45th AIAA Aerospace Sciences Meeting and Exhibit, American Institute of Aeronautics and Astronautics, Reno, Nevada, USA, 2007, pp. 5368–5388, http://dx.doi.org/10.2514/6.2007-450.
[48] A. Seitz, C. Gologan, Parametric design studies for propulsive fuselage aircraft concepts, CEAS Aeronaut. J. 6 (1) (2015) 69–82.
[49] A.T. Isikveren, A. Seitz, J. Bijewitz, A. Mirzoyan, A. Isyanov, R. Grenon, O. Atinault, J.L. Godard, S. Stückl, Distributed propulsion and ultra-high by-pass rotor study at aircraft level, Aeronaut. J. 119 (1221) (2015) 1327–1376.
[50] D. Destarac, J.V.D. Vooren, Drag/thrust analysis of jet-propelled transonic transport aircraft: Definition of physical drag components, Aerosp. Sci. Technol. 8 (2004) 545–556.
[51] L.L. Kang, L. Russo, R. Tognaccini, J.Z. Wu, W.D. Su, Aerodynamic force breakdown in reversible and irreversible components by vortex force theory, AIAA J. 57 (11) (2019) 4623–4638.
[52] J.D. Anderson, Aerodynamics: Some fundamental principles and equations, in: Fundamentals of Aerodynamics, sixth ed., Mc Graw Hill Education, New York, USA, 2017, pp. 125–134.
[53] J.D. Anderson, The governing equations of fluid dynamics: Their derivation, a discussion of their physical meaning, and a presentation of forms particularly suitable to CFD, in: Computational Fluid Dynamics: The Basics with Applications, second ed., Mc Graw Hill Education, Singapore, 1995, pp. 49–79.
[54] J.D. Anderson, Compressible flow: Some preliminary aspects, in: Fundamentals of Aerodynamics, sixth ed., Mc Graw Hill Education, New York, USA, 2017, pp. 527–560.
[55] L. Paparone, R. Tognaccini, Computational fluid dynamics-based drag prediction and decomposition, AIAA J. 41 (2003) 1647–1657.
[56] W. Yamazaki, K. Matsushima, K. Nakahashi, Aerodynamic design optimization using the drag-decomposition method, AIAA J. 46 (2008) 1096–1106.
[57] M. Méheut, D. Bailly, Drag-breakdown methods from wake measurements, AIAA J. 46 (2008) 847–862.
[58] T.P. Stańkowski, D.G. MacManus, M. Robinson, C.T. Sheaf, Aerodynamic effects of propulsion integration for high bypass ratio engines, J. Aircr. 54 (2017) 2270–2284.
[59] MIDAP Study Group, Special Course on Subsonic/Transonic Aerodynamic Interference for Aircraft, Technical Report AGARD-R-712, 1983.
[60] T.P. Stańkowski, D.G. MacManus, C.T. Sheaf, N. Grech, Aerodynamic interference for aero-engine installations, in: 54th AIAA Aerospace Sciences Meeting, American Institute of Aeronautics and Astronautics, San Diego, California, USA, 2016, http://dx.doi.org/10.2514/6.2016-0766.

[61] J. Matesanz-García, R. Christie, F. Tejero, D.G. MacManus, A. Heidebrecht, An automated approach for the aerodynamic design of close-coupled propulsion/airframe configurations, in: Aerospace Europe Conference, Bordeaux, France, 2020.

[62] J.S. Gray, Design Optimization of a Boundary Layer Ingestion Propulsor Using a Coupled Aeropropulsive Model (Ph.D. thesis), 2018.

[63] R.T. Kawai, D.M. Friedman, L. Serrano, Blended Wing Body (BWB) Boundary Layer Ingestion (BLI) Inlet Configuration and System Studies, Technical Report, NASA, 2006.

[64] S.S. Ochs, G. Tillman, J. Joo, D.M. Voytovych, CFD-based analysis of boundary layer ingesting propulsion, in: 51st AIAA/SAE/ASEE Joint Propulsion Conference, American Institute of Aeronautics and Astronautics, Orlando, Florida, USA, 2015, http://dx.doi.org/10.2514/6.2015-3800.

[65] W.K. Lord, G. Tillman, S.S. Ochs, X. Cai, B. Moffitt, A performance methodology for ducted boundary layer ingesting propulsion, in: AIAA SciTech 2019 Forum, American Institute of Aeronautics and Astronautics, San Diego, California, USA, 2019, http://dx.doi.org/10.2514/6.2019-1450.

[66] Y. Maldonado, P. Giannakakis, B. Rodriguez, N. Tantot, Book-keeping investigations for BLI aircraft, in: AIAA Propulsion and Energy 2020 Forum, American Institute of Aeronautics and Astronautics, Virtual Event, 2020, http://dx.doi.org/10.2514/6.2020-3521.

[67] M.J. Moran, E. Sciubba, Exergy analysis: Principles and practice, J. Eng. Gas Turbines Power 116 (2) (1994) 285–290.

[68] A. Arntz, Civil Aircraft Aero-Thermo-Propulsive Performance Assessment by an Exergy Analysis of High-Fidelity CFD-RANS Flow Solutions (Ph.D. thesis), Lille University, 2014, p. 234.

[69] I. Lamprakis, D.S. Sanders, P. Laskaridis, Energy-based aerodynamic loss and recovery characteristics of adiabatic and heated fuselages, 2023, (Unpublished).

[70] A. Arntz, O. Atinault, D. Destarac, Numerical airframe aerodynamic performance prediction: An exergy point of view, in: 49th International Symposium of Applied Aerodynamics, La Société Savante de l'Aéronautique et de l'Espace (3AF), Lille, France, 2014.

[71] A. Arntz, D. Hue, Exergy-based performance assessment of the NASA common research model, AIAA J. 54 (1) (2016) 88–100.

[72] A. Arntz, O. Atinault, Exergy-based performance assessment of a blended wing-body with boundary-layer ingestion, AIAA J. 53 (12) (2015) 3766–3776.

[73] M.A. Aguirre, S. Duplaa, X. Carbonneau, A. Turnbull, A. Arntz, A better assessment of the recoverable energy behind a body by the exergy method, in: Aerospace Europe Conference, Bordeaux, France, 2020.

[74] J. Kurzke, Effects of inlet flow distortion on the performance of aircraft gas turbines, J. Eng. Gas Turbines Power 130 (4) (2008) 041201.

[75] S-16 Turbine Engine Inlet Flow Distortion Committee, Gas Turbine Eninge Inlet Flow Distortion Guidelines, Technical Report, SAE International, 1978, http://dx.doi.org/10.4271/ARP1420.

[76] D.K. Hall, E.M. Greitzer, A. Uranga, M. Drela, S.A. Pandya, Inlet flow distortion in an advanced civil transport boundary layer ingesting engine installation, J. Turbomach. 144 (10) (2022).

[77] J.P. Longley, E.M. Greitzer, Inlet distortion effects in aircraft propulsion system integration, in: Steady and Transient Performance Prediction of Gas Turbine Engines, in: AGARD Lecture Series, vol. 183, Neuilly sur Seine, France, 1992.

[78] D.G. MacManus, N. Chiereghin, D.G. Prieto, P. Zachos, Complex aero-engine intake ducts and dynamic distortion, in: 33rd AIAA Applied Aerodynamics Conference, American Institute of Aeronautics and Astronautics, Dallas, Texas, USA, 2015, http://dx.doi.org/10.2514/6.2015-3304.

[79] N.C. Bissinger, T. Breuer, Basic principles: Gas turbine compatibility – Intake aerodynamic aspects, Encycl. Aerosp. Eng. (2010).

[80] H.J. Steiner, A. Seitz, K. Wieczorek, K. Plötner, A.T. Isikveren, M. Hornung, Multi-disciplinary design and feasibility study of distributed propulsion systems, in: 28th International Congress of the Aeronautical Sciences, Brisbane, Australia, 2012.

[81] E.A. Valencia, Investigation of Propulsion Architectures for Advanced Distributed Propulsion Systems (Ph.D. thesis), Cranfield University, 2014.

[82] B.T. Blumenthal, A.A. Elmiligui, K.A. Geiselhart, R.L. Campbell, M.D. Maughmer, S. Schmitz, Computational investigation of a boundary-layer-ingestion propulsion system, J. Aircr. 55 (3) (2018) 1141–1153.

[83] A. Uranga, M. Drela, E.M. Greitzer, N.A. Titchener, M.K. Lieu, N.M. Siu, A.C. Huang, G.M. Gatlin, J.A. Hannon, Preliminary experimental assessment of the boundary layer ingestion benefit for the D8 aircraft, in: 52nd Aerospace Sciences Meeting, American Institute of Aeronautics and Astronautics, National Harbor, Maryland, USA, 2014, http://dx.doi.org/10.2514/6.2014-0906.

[84] P. Baskaran, B.D. Corte, M. van Sluis, A. Gangoli Rao, Aeropropulsive performance analysis of axisymmetric fuselage bodies for boundary-layer ingestion applications, AIAA J. 60 (3) (2022) 1592–1611.

[85] N.E. Mutangara, L. Smith, K.J. Craig, D.S. Sanders, Potential for energy recovery of unpowered configurations using power balance method computations, J. Aircr. 58 (6) (2021) 1364–1374.

[86] D.K. Hall, A.C. Huang, A. Uranga, E.M. Greitzer, M. Drela, S. Sato, Boundary layer ingestion propulsion benefit for transport aircraft, J. Propuls. Power 33 (5) (2017) 1118–1129.

[87] M. Drela, TASOPT 2.00 Transport Aircraft System OPTimization, Technical Report, Massachusetts Institute of Technology, 2010.

[88] B.J. Brelje, J.R. Martins, Electric, hybrid, and turboelectric fixed-wing aircraft: A review of concepts, models, and design approaches, Prog. Aerosp. Sci. 104 (2019) 1–19.

[89] S. Sahoo, X. Zhao, K. Kyprianidis, A review of concepts, benefits, and challenges for future electrical propulsion-based aircraft, Aerospace 7 (4) (2020).

[90] Y. Xie, A. Savvarisal, A. Tsourdos, D. Zhang, J. Gu, Review of hybrid electric powered aircraft, its conceptual design and energy management methodologies, Chin. J. Aeronaut. 34 (4) (2021) 432–450.

[91] J.I. Hileman, J.B. Katz, J.G. Mantilla, G. Fleming, Payload fuel energy efficiency as a metric for aviation environmental performance, in: 26th International Congress of the Aeronautical Sciences, 2008.

[92] M. Drela, Considerations in aerodynamic force decomposition, in: AIAA Aviation 2021 Forum, American Institute of Aeronautics and Astronautics, Virtual Event, 2021, http://dx.doi.org/10.2514/6.2021-2552.

[93] S. Schmitz, Drag decomposition using partial-pressure fields in the compressible Navier-Stokes equations, AIAA J. 57 (5) (2019) 2030–2038.

[94] P.L. Hart, S. Schmitz, Drag decomposition using partial-pressure fields – ONERA M6 wing, in: AIAA Aviation 2021 Forum, Vol. 57, American Institute of Aeronautics and Astronautics, 2021, http://dx.doi.org/10.2514/6.2021-2555.

[95] P.L. Hart, S. Schmitz, Partial pressure field for airfoil wave drag, AIAA J. 60 (10) (2022) 5791–5804.

[96] M.A. Aguirre, S. Duplaa, X. Carbonneau, A. Turnbull, Velocity decomposition method for exergy-based drag prediction, AIAA J. 58 (11) (2020) 4686–4701.

[97] N.E. Mutangara, D.S. Sanders, P. Laskaridis, P.L. Hart, S. Schmitz, A unified partial pressure field and velocity decomposition approach toward improved energetic aerodynamic force decompositions, in: 57th 3AF International Conference on Applied Aerodynamics, Bordeaux, France, 2023.

[98] W.K. Lord, G.L. Suciu, K.L. Hasel, J.M. Chandler, Engine architecture for high efficiency at small core size, in: 53rd AIAA Aerospace Sciences Meeting, American Institute of Aeronautics and Astronautics, Kissimmee, Florida, USA, 2015, http://dx.doi.org/10.2514/6.2015-0071.

[99] M.B. Giles, R.M. Cummings, Wake integration for three-dimensional flowfield computations: Theoretical development, J. Aircr. 36 (1999) 357–365.

[100] F. Nicolosi, P. Della Vecchia, D. Ciliberti, V. Cusati, Fuselage aerodynamic drag prediction method by CFD, in: 5th CEAS Air & Space Conference, 2015.

[101] P.R. Spalart, On the far wake and induced drag of aircraft, J. Fluid Mech. 603 (2008) 413–430.

[102] M. Méheut, F. Sartor, M. Vergez, M. Laban, R. Schnell, A. Stuermer, G. Lefevre, Assessment of fan/airframe aerodynamic performance using 360° uRANS computations: Code-to-code comparison between ONERA, DLR, NLR and Airbus, in: AIAA SciTech 2019 Forum, American Institute of Aeronautics and Astronautics, San Diego, California, USA, 2019, http://dx.doi.org/10.2514/6.2019-0582.

[103] M.A. Aguirre, S. Duplaa, Exergetic drag characteristic curves, AIAA J. 57 (7) (2019) 2746–2757.

[104] C. Goldberg, D. Nalianda, D.G. MacManus, P. Pilidis, J. Felder, Installed performance assessment of a boundary layer ingesting distributed propulsion system at design point, in: 52nd AIAA/SAE/ASEE Joint Propulsion Conference, American Institute of Aeronautics and Astronautics, Salt Lake City, Utah, USA, 2016, http://dx.doi.org/10.2514/6.2016-4800.

[105] B.S. Stratford, G.S. Beavers, The Calculation of the Compressible Turbulent Boundary Layer in an Arbitrary Pressure Gradient - A Correlation of certain previous Methods, Technical Report, Aeronautical Research Council, 1959.

[106] C. Goldberg, D. Nalianda, P. Laskaridis, P. Pilidis, Performance assessment of a boundary layer ingesting distributed propulsion system at off-design, in: 53rd AIAA/SAE/ASEE Joint Propulsion Conference, American Institute of Aeronautics and Astronautics, Atlanta, Georgia, USA, 2017, http://dx.doi.org/10.2514/6.2017-5055.

[107] C. Goldberg, D. Nalianda, D.G. MacManus, P. Pilidis, J. Felder, Method for simulating the performance of a boundary layer ingesting propulsion system at design and off-design, Aerosp. Sci. Technol. 78 (2018) 312–319.

[108] A. Turnbull, H. Jouan, P. Giannakakis, A.T. Isikveren, Modeling boundary layer ingestion at the conceptual level, in: 23rd International Society for Air Breathing Engines Conference, 2017.

[109] M.K. Lieu, Quantification of the Boundary Layer Ingestion Benefit for the D8-Series Aircraft Using a Pressure Rake System (Ph.D. thesis), Massachusetts Institute of Technology, 2015, pp. 1–142.

[110] S. Kaiser, R. Grenon, J. Bijewitz, A. Prendinger, A.T. Isikveren, M. Hornung, Quasi-analytical aerodynamic methods for propulsive fuselage concepts, in: 29th Congress of the International Council of the Aeronautical Sciences, 2014.

[111] D. Lovely, Boundary Layer and Shock Detection in CFD Solutions (Master's thesis), Massachusetts Institute of Technology, 2000.

[112] L. Baskett, R. Haimes, Feature extraction of shear layers, in: 15th AIAA Computation Fluid Dynamics Conference, American Institute of Aeronautics and Astronautics, Anaheim, California, USA, 2001, http://dx.doi.org/10.2514/6.2001-2665.

[113] D. Lovely, R. Hairnes, Shock detection from computational fluid dynamics results, in: 14th Computational Fluid Dynamics Conference, American Institute of Aeronautics and Astronautics, 1999, pp. 296–304, http://dx.doi.org/10.2514/6.1999-3285.

[114] E. Saetta, R. Tognaccini, Identification of flow field regions by machine learning, in: AIAA SciTech 2022 Forum, AIAA International, San Diego, California, USA, 2022, http://dx.doi.org/10.2514/6.2022-0457.

[115] R. Soto-Valle, S. Cioni, S. Bartholomay, M. Manolesos, N. Nayeri, A. Bianchini, C.O. Paschereit, Vortex identification methods applied to wind turbine tip vortices, Wind Energy Sci. Discuss. (2021) 1–28.

[116] L. Graftieaux, M. Michard, G. Nathalie, Combining PIV, POD and vortex identification algorithms for the study of unsteady turbulent swirling flows, Meas. Sci. Technol. 12 (9) (2001) 1422–1429.

[117] J.C.R. Hunt, A.A. Wray, P. Moin, Eddies, streams, and convergence zones in turbulent flows, in: Proceedings of the Summer Program, 1988, pp. 193–208.

[118] V. Kolář, Vortex identification: New requirements and limitations, Int. J. Heat Fluid Flow 28 (4) (2007) 638–652.

[119] V. Holmén, Methods for Vortex Identification (Master's thesis), Lund University, Lund, Sweden, 2012.

[120] W.-W. Zhao, J.-H. Wang, D.-C. Wan, Vortex identification methods in marine hydrodynamics, J. Hydrodyn. 32 (2020) 286–295.

[121] J.I. Hileman, Z.S. Spakovszky, M. Drela, M.A. Sargeant, A. Jones, Airframe design for silent fuel-efficient aircraft, J. Aircr. 47 (3) (2010) 956–969.

[122] R.V. Florea, C. Matalanis, L.W. Hardin, M. Stucky, A. Shabbir, Parametric analysis and design for embedded engine inlets, in: 48th AIAA/ASME/SAE/ASEE Joint Propulsion Conference and Exhibit, American Institute of Aeronautics and Astronautics, Atlanta, Georgia, USA, 2012, http://dx.doi.org/10.2514/6.2012-3994.

[123] J. Bijewitz, A. Seitz, M. Hornung, Power plant pre-design exploration for a turbo-electric propulsive fuselage concept, in: 2018 Joint Propulsion Conference, American Institute of Aeronautics and Astronautics, Cincinnati, Ohio, USA, 2018, http://dx.doi.org/10.2514/6.2018-4402.

[124] T.V. Marien, J.R. Welstead, S.M. Jones, Vehicle-level system impact of boundary layer ingestion for the NASA D8 concept aircraft, in: AIAA Aerospace Sciences Meeting, American Institute of Aeronautics and Astronautics, Kissimmee, Florida, USA, 2018, http://dx.doi.org/10.2514/6.2018-0271.

[125] D.K. Hall, A.P. Dowdle, J.J. Gonzalez, L. Trollinger, W. Thalheimer, Assessment of a boundary layer ingesting turboelectric aircraft configuration using signomial programming, in: 2018 Aviation Technology, Integration and Operations Conference, American Institute of Aeronautics and Astronautics, Atlanta, Georgia, USA, 2018, http://dx.doi.org/10.2514/6.2018-3973.

[126] C. Liu, G. Doulgeris, P. Laskaridis, R. Singh, Turboelectric distributed propulsion system modelling for hybrid-wing-body aircraft, in: 48th AIAA/ASME/SAE/ASEE Joint Propulsion Conference and Exhibit, American Institute of Aeronautics and Astronautics, Atlanta, Georgia, USA, 2012, http://dx.doi.org/10.2514/6.2012-3700.

[127] C. Liu, D. Ihiabe, P. Laskaridis, R. Singh, A preliminary method to estimate impacts of inlet flow distortion on boundary layer ingesting propulsion system design point performance, Proc. Inst. Mech. Eng. G 228 (9) (2014) 1528–1539.

[128] E.A. Valencia, C. Liu, P. Laskaridis, R. Singh, D. Nalianda, Propulsion system analysis using a parametric and the parallel compressor approach to model distortion in boundary layer ingestion systems, in: 51st AIAA/SAE/ASEE Joint Propulsion Conference, American Institute of Aeronautics and Astronautics, Orlando, Florida, USA, 2015, http://dx.doi.org/10.2514/6.2015-3801.

[129] E.A. Valencia, D. Nalianda, P. Laskaridis, R. Singh, Methodology to assess the performance of an aircraft concept with distributed propulsion and boundary layer ingestion using a parametric approach, Proc. Inst. Mech. Eng. G 229 (4) (2015) 682–693.

[130] S.A. Pandya, External aerodynamics simulations for the MIT D8 "double-bubble" aircraft design, in: 7th International Conference on Computation Fluid Dynamics, Big Island, Hawaii, USA, 2012.

[131] J. Ahuja, D.N. Mavris, Sensitivity of boundary layer ingestion effects to tube and wing airframe design features, in: AIAA SciTech 2020 Forum, American Institute of Aeronautics and Astronautics, Orlando, Florida, USA, 2020, http://dx.doi.org/10.2514/6.2020-1523.

[132] R.H. Liebeck, Design of the blended wing body subsonic transport, J. Aircr. 41 (1) (2004) 10–25.

[133] J.I. Hileman, Z.S. Spakovszky, M. Drela, M.A. Sargeant, Airframe design for "silent aircraft", in: 45th AIAA Aerospace Sciences Meeting and Exhibit, American Institute of Aeronautics and Astronautics, Reno, Nevada, USA, 2007, http://dx.doi.org/10.2514/6.2007-453.

[134] P. Schmollgruber, C. Döll, J. Hermetz, R. Liaboeuf, M. Ridel, I. Cafarelli, O. Atinault, C. François, B. Paluch, Multidisciplinary exploration of DRAGON: an ONERA hybrid electric distributed propulsion concept, in: AIAA SciTech 2019 Forum, American Institute of Aeronautics and Astronautics, San Diego, California, USA, 2019, http://dx.doi.org/10.2514/6.2019-1585.

[135] B.T. Schiltgen, J.L. Freeman, D.W. Hall, Aeropropulsive interaction and thermal system integration within the ECO-150: A turboelectric distributed propulsion airliner with conventional electric machines, in: 16th AIAA Aviation Technology, Integration and Operations Conference, American Institute of Aeronautics and Astronautics, Washington, D.C., USA, 2016, http://dx.doi.org/10.2514/6.2016-4064.

[136] J.L. Freeman, B.T. Schiltgen, ECO-150-300 design and performance: A tube-and-wing distributed electric propulsion airliner, in: AIAA SciTech 2019 Forum, American Institute of Aeronautics and Astronautics, San Diego, California, USA, 2019, http://dx.doi.org/10.2514/6.2019-1808.

[137] D. Crichton, L. Xu, C.A. Hall, Preliminary fan design for a silent aircraft, J. Turbomach. 129 (1) (2007) 184–191.

[138] B. Yutko, N. Titchener, C. Courtin, M. Lieu, L. Wirsing, J. Tylko, J. Chambers, T. Roberts, C. Church, Conceptual design of a D8 commercial aircraft, in: 17th AIAA Aviation Technology, Integration and Operations Conference, American Institute of Aeronautics and Astronautics, Denver, Colorado, USA, 2017, http://dx.doi.org/10.2514/6.2017-3590.

[139] D. Silberhorn, C. Hollmann, M. Mennicken, F. Wolters, F. Eichner, M. Staggat, Overall design and assessment of aircraft concepts with boundary layer ingesting engines, in: Deutscher Luft- und Raumfahrtkongress 2019, Deutsche Gesellschaft für Luft- und Raumfahrt, Darmstadt, Germany, 2019.

[140] C.H. Hall, D. Crichton, Engine design studies for a silent aircraft, J. Turbomach. 129 (3) (2007) 479–487.

[141] C. Goldberg, D. Nalianda, P. Laskaridis, P. Pilidis, Installed performance assessment of an array of distributed propulsors ingesting boundary layer flow, J. Eng. Gas Turbines Power 140 (7) (2018).

[142] I. Ordaz, S.K. Rallabhandi, E.J. Nielsen, B. Diskin, Mitigation of engine inlet distortion through adjoint-based design, in: 35th AIAA Applied Aerodynamics Conference, 2017, American Institute of Aeronautics and Astronautics, 2017, http://dx.doi.org/10.2514/6.2017-3410.

[143] J.S. Gray, C.A. Mader, G.K. Kenway, J.R. Martins, Approach to modeling boundary layer ingestion using a fully coupled propulsion-RANS model, in: 58th AIAA/ASCE/AHS/ASC Structures, Structural Dynamics, and Materials Conference, 2017, 2017, http://dx.doi.org/10.2514/6.2017-1753.

[144] J.S. Gray, C.A. Mader, G.K. Kenway, J.R. Martins, Modeling boundary layer ingestion using a coupled aeropropulsive analysis, J. Aircr. 55 (3) (2018) 1191–1199.

[145] J.S. Gray, J.R. Martins, Coupled aeropropulsive design optimisation of a boundary-layer ingestion propulsor, Aeronaut. J. 123 (1259) (2019) 121–137.

[146] M. Pokhrel, M. Shi, J. Ahuja, J. Gladin, D.N. Mavris, Conceptual design of a BLI propulsor capturing aero-propulsive coupling and distortion impacts, in: AIAA SciTech 2019 Forum, January, American Institute of Aeronautics and Astronautics, 2019, http://dx.doi.org/10.2514/6.2019-1588.

[147] P. Giannakakis, Y.-B. Maldonado, N. Tantot, C. Frantz, M. Belleville, Fuel burn evaluation of a turbo-electric propulsive fuselage aircraft, in: AIAA Propulsion and Energy 2019 Forum, American Institute of Aeronautics and Astronautics, 2019, http://dx.doi.org/10.2514/6.2019-4181.

[148] J. Bijewitz, A. Seitz, M. Hornung, Extended design studies for a mechanically driven propulsive fuselage aircraft concept, in: AIAA Aerospace Sciences Meeting, 2018, American Institute of Aeronautics and Astronautics, Kissimmee, Florida, USA, 2018, http://dx.doi.org/10.2514/6.2018-0408.

[149] L. López de Vega, G. Dufour, N. García Rosa, Fully coupled body force-engine performance methodology for boundary layer ingestion, J. Propuls. Power 37 (2) (2021) 192–201.

[150] J.L. Felder, G.V. Brown, H.D. Kim, J. Chu, Turboelectric distributed propulsion in a hybrid wing body aircraft, in: 20th International Society for Air Breathing Engines Conference, Gothenburg; Sweden, 2011.

[151] J.L. Felder, H.D. Kim, G.V. Brown, J. Chu, An examination of the effect of boundary layer ingestion on turboelectric distributed propulsion systems, in: 49th AIAA Aerospace Sciences Meeting Including the New Horizons Forum and Aerospace Exposition, American Institute of Aeronautics and Astronautics, Orlando, Florida, USA, 2011, http://dx.doi.org/10.2514/6.2011-300.

[152] L.W. Hardin, G. Tillman, O.P. Sharma, J. Berton, D.J. Arend, Aircraft system study of boundary layer ingesting propulsion, in: 48th AIAA/ASME/SAE/ASEE Joint Propulsion Conference and Exhibit, American Institute of Aeronautics and Astronautics, Atlanta, Georgia, USA, 2012, http://dx.doi.org/10.2514/6.2012-3993.

[153] D.L. Rodriguez, A multidisciplinary optimization method for designing boundary layer ingesting inlets, in: 9th AIAA/ISSMO Symposium on Multidisciplinary Analysis and Optimization, American Institute of Aeronautics and Astronautics, Atlanta, Georgia, USA, 2002, http://dx.doi.org/10.2514/6.2002-5665.

[154] D.L. Rodriguez, Multidisciplinary optimization method for designing boundary-layer-ingesting inlets, J. Aircr. 46 (3) (2009) 883–894.

[155] A.L. Habermann, R. Zahn, A. Seitz, M. Hornung, Multidimensional parametric study of a propulsive fuselage concept using OpenFOAM, in: AIAA Aviation 2020 Forum, American Institute of Aeronautics and Astronautics, Virtual Event, 2020, http://dx.doi.org/10.2514/6.2020-2754.

[156] J. Ahuja, D.N. Mavris, Assessment of propulsor on-design and off-design impacts on BLI effects, in: AIAA SciTech 2021 Forum, January, American Institute of Aeronautics and Astronautics, Virtual Event, 2021, http://dx.doi.org/10.2514/6.2021-0605.

[157] A.L. Habermann, A. Gokhale, M. Hornung, Numerical investigation of the effects of fuselage upsweep in a propulsive fuselage concept, CEAS Aeronaut. J. 12 (2021) 173–189.

[158] A.T. Isikveren, A. Seitz, J. Bijewitz, M. Hornung, A. Mirzoyan, A. Isyanov, J.-L. Godard, S. Stückl, J. Van Toor, Recent advances in airframe-propulsion concepts with distributed propulsion, in: 29th Congress of the International Council of the Aeronautical Sciences, 2014.

[159] A. Battiston, R. Ponza, E. Benini, Design exploration for an axisymmetric rear BLI propulsor, in: AIAA Propulsion and Energy Forum, American Institute of Aeronautics and Astronautics, Virtual Event, 2021, http://dx.doi.org/10.2514/6.2021-3470.

[160] M. Lorteau, L. Wiart, V. Kopiev, S. Denisov, Numerical study, with experimental validation, of fan noise installation effects in over-wing nacelle configuration using the immersed boundary method, in: 25th AIAA/CEAS Aeroacoustics Conference, American Institute of Aeronautics and Astronautics, Delft, The Netherlands, 2019, http://dx.doi.org/10.2514/6.2019-2519.

[161] G.K. Kenway, C. Kiris, Aerodynamic shape optimization of the STARC-ABL concept for minimal inlet distortion, in: AIAA/ASCE/AHS/ASC Structures, Structural Dynamics, and Materials Conference, 2018, American Institute of Aeronautics and Astronautics, Kissimmee, Florida, USA, 2018, http://dx.doi.org/10.2514/6.2018-1912.

[162] A. Seitz, A.L. Habermann, M. van Sluis, Optimality considerations for propulsive fuselage power savings, Proc. Inst. Mech. Eng. G 235 (1) (2020) 22–39.

[163] J. Bijewitz, A. Seitz, M. Hornung, Multi-disciplinary design investigation of propulsive fuselage aircraft concepts, Aircr. Eng. Aerosp. Technol. J. 88 (2) (2016) 257–267.

[164] J. Bijewitz, A. Seitz, M. Hornung, A.T. Isikveren, Progress in optimizing the propulsive fuselage aircraft concept, J. Aircr. 54 (5) (2017) 1979–1989.

[165] O. Atinault, G. Carrier, R. Grenon, C. Verbecke, P. Viscat, Numerical and experimental aerodynamic investigations of boundary layer ingestion for improving propulsion efficiency of future air transport, in: 31st AIAA Applied Aerodynamics Conference, American Institute of Aeronautics and Astronautics, San Diego, California, USA, 2013, http://dx.doi.org/10.2514/6.2013-2406.

[166] B.T. Blumenthal, A.A. Elmiligui, K.A. Geiselhart, R.L. Campbell, M.D. Maughmer, S. Schmitz, Computational investigation of a boundary-layer ingesting propulsion system for the common research model, in: 46th AIAA Fluid Dynamics Conference, Washington, D.C., USA, 2016, http://dx.doi.org/10.2514/6.2016-3812.

[167] P. Schmollgruber, D. Donjat, M. Ridel, I. Cafarelli, O. Atinault, C. François, B. Paluch, Multidisciplinary design and performance of the ONERA hybrid electric distributed propulsion concept (DRAGON), in: AIAA SciTech 2020 Forum, American Institute of Aeronautics and Astronautics, Orlando, Florida, USA, 2020, http://dx.doi.org/10.2514/6.2020-0501.

[168] J. Matesanz-García, T. Piovesan, D.G. MacManus, Aerodynamic optimization of the exhaust system of an aft-mounted boundary layer ingestion propulsor, Internat. J. Numer. Methods Heat Fluid Flow (2022).

[169] J.S. Gray, G.K. Kenway, C.A. Mader, J.R. Martins, Aeropropulsive design optimization of a turboelectric boundary layer ingestion propulsion system, in: 2018 Aviation Technology, Integration, and Operations Conference, 2018, http://dx.doi.org/10.2514/6.2018-3976.

[170] J.S. Gray, C. Mader, G. Kenway, J. Martins, Coupled aeropropulsive optimization of a three-dimensional boundary-layer ingestion propulsor considering inlet distortion, J. Aircr. 57 (6) (2020) 1014–1025.

[171] B.J. Lee, M.-F. Liou, M.-S. Liou, Conceptual aerodynamic design of a tail-cone thruster system under axi-symmetric inlet distortion, in: Proceedings of ASME Turbo Expo 2018 Turbomachinery Technical Conference and Exposition GT2018, Oslo, Norway, 2018, http://dx.doi.org/10.1115/GT2018-75861.

[172] B.J. Lee, M.-F. Liou, M.-S. Liou, Aerodynamic conceptual design of boundary layer ingestion propulsor system: A Quasi-2D through flow analysis method and multi-fidelity propulsor design framework, in: Proceedings of ASME Turbo Expo 2018 Turbomachinery Technical Conference and Exposition GT2018, 2018.

[173] A. Yildirim, J.S. Gray, C.A. Mader, J.R. Martins, Aeropropulsive design optimization of a boundary layer ingestion system, in: AIAA Aviation 2019 Forum, June, American Institute of Aeronautics and Astronautics, 2019, http://dx.doi.org/10.2514/6.2019-3455.

[174] A. Yildirim, J.S. Gray, C.A. Mader, J.R.R.A. Martins, Boundary-layer ingestion benefit for the STARC-ABL concept, J. Aircr. 59 (2022).

[175] L. Wiart, C. Negulescu, Exploration of the airbus "Nautilius" engine integration concept, in: 31st Congress of the International Council of the Aeronautical Sciences, Belo Horizonte, Brazil, 2018.

[176] H. Kim, M.-S. Liou, Flow simulation of N3-X hybrid wing-body configuration, in: 51st AIAA Aerospace Sciences Meeting Including the New Horizons Forum and Aerospace Exposition, American Institute of Aeronautics and Astronautics, Grapevine, Texas, USA, 2013, http://dx.doi.org/10.2514/6.2013-221.

[177] O. Petit, F. Costa, C. Bringhenti, J. Tomita, Aerodynamic influence of airframe boundary layer on propeller performance, in: 24th International Society for Air Breathing Engines Conference, 2019.

[178] A. Castillo Pardo, C.A. Hall, Aerodynamics of boundary layer ingesting fuselage fans, in: 24th International Society for Air Breathing Engines Conference, Canberra, Australia, 2019.

[179] A. Castillo Pardo, C.A. Hall, Design of a transonic boundary layer ingesting fuselage fan, in: Global Power and Propulsion Society, GPPS, Chania, Greece, 2020, http://dx.doi.org/10.33737/gpps20-tc-42.

[180] B. Della Corte, M. van Sluis, L.L.M. Veldhuis, A. Gangoli Rao, Power balance analysis experiments on an axisymmetric fuselage with an integrated boundary-layer-ingesting fan, AIAA J. 59 (12) (2021) 5211–5224.

[181] T.S. Tse, C.A. Hall, Flow field and power balance of a distributed aft-fuselage boundary layer ingesting aircraft, in: AIAA Propulsion and Energy 2020 Forum, American Institute of Aeronautics and Astronautics, Virtual Event, 2020, http://dx.doi.org/10.2514/6.2020-3779.

[182] G. Romani, Q. Ye, F. Avallone, D. Ragni, D. Casalino, Fan noise boundary layer ingestion installation effects for NOVA aircraft configuration, in: 25th AIAA/CEAS Aeroacoustics Conference, 2019, American Institute of Aeronautics and Astronautics, Delft, The Netherlands, 2019, http://dx.doi.org/10.2514/6.2019-2429.

[183] G. Romani, Q. Ye, F. Avallone, D. Ragni, D. Casalino, Numerical analysis of fan noise for the NOVA boundary-layer ingestion configuration, Aerosp. Sci. Technol. 96 (2020) 105532.

[184] A. Uranga, M. Drela, D.K. Hall, E.M. Greitzer, Analysis of the aerodynamic benefit from boundary layer ingestion for transport aircraft, AIAA J. 56 (11) (2018) 4271–4281.

[185] B. Godard, C. Negulescu, Fan design investigation on the nautilus engine integration concept, in: AMSE Turbo Expo 2020, American Society of Mechanical Engineers, Virtual Event, 2020, http://dx.doi.org/10.1115/GT2020-14628.

[186] R.V. Florea, D. Voytovych, G. Tillman, M. Stucky, A. Shabbir, O. Sharma, D.J. Arend, Aerodynamic analysis of a boundary-layer-ingesting distortion-tolerant fan, in: ASME Turbo Expo 2013: Turbine Technical Conference and Exposition, American Society of Mechanical Engineers, San Antonio, Texas, USA, 2013, http://dx.doi.org/10.1115/GT2013-94656.

[187] R.V. Florea, C. Matalanis, L.W. Hardin, M. Stucky, A. Shabbir, Parametric analysis and design for embedded engine inlets, J. Propuls. Power 31 (3) (2015) 843–850.

[188] J.H. Bell, R.D. Mehta, Contraction Design for Small Low-Speed Wind Tunnels, Technical Report, Stanford University, Stanford, California, USA, 1988.

[189] R. Christie, A. Heidebrecht, D.G. MacManus, An automated approach to nacelle parameterization using intuitive class shape transformation curves, J. Eng. Gas Turbines Power 139 (6) (2017) 062601.

[190] A.S. Hahn, Vehicle sketch pad: A parametric geometry modeler for conceptual aircraft design, in: 48th AIAA Aerospace Sciences Meeting Including the New Horizons Forum and Aerospace Exposition, January, American Institute of Aeronautics and Astronautics, 2010, http://dx.doi.org/10.2514/6.2010-657.

[191] N.R. Secco, J.P. Jasa, G.K.W. Kenway, J.R.R.A. Martins, Component-based geometry manipulation for aerodynamic shape optimization with overset meshes, AIAA J. 56 (9) (2018) 3667–3679.

[192] Pointwise, Inc., Mesh and grid generation software for CFD: Pointwise, 2014, URL: https://http://www.pointwise.com/.

[193] STAR-CCM+ 11.0 User's Guide, CD-adapco, Inc, 2016.

[194] A. Diedrich, J. Hileman, D. Tan, K. Willcox, Z. Spakovszky, Multidisciplinary design and optimization of the silent aircraft, in: 44th AIAA Aerospace Sciences Meeting and Exhibit, American Institute of Aeronautics and Astronautics, Reno, Nevada, USA, 2006, http://dx.doi.org/10.2514/6.2006-1323.

[195] Ansys® ICEM CFD Release 18.1, ANSYS, Inc., 2018.

[196] Ansys® ICEM CFD Release 20.2, ANSYS, Inc., 2020.

[197] M. Nemec, M.J. Aftosmis, M. Wintzer, Adjoint-based adaptive mesh refinement for complex geometries, in: 46th AIAA Aerospace Sciences Meeting and Exhibit, American Institute of Aeronautics and Astronautics, Reno, Nevada, USA, 2008, http://dx.doi.org/10.2514/6.2008-725.

[198] W.M. Chan, Overset grid technology development at NASA ames research center, Comput. & Fluids 38 (3) (2009) 496–503.

[199] AutoGrid5™, Cadence Design Systems, Inc., 2016.

[200] C. Geuzaine, J.-F. Remacle, GSMH: a 3-D finite element mesh generator with build-in pre- and post-processign facilities, Internat. J. Numer. Methods Engrg. 79 (11) (2009) 1309–1331.

[201] I.B. Celik, U. Ghia, P.J. Roache, C.J. Freitas, H. Coleman, P.E. Raad, Procedure for estimation and reporting of uncertainty due to discretization in CFD applications, J. Fluids Eng. 130 (7) (2008).

[202] Ansys® Fluent Release 20.2, ANSYS, Inc., 2020.

[203] OpenFOAM User's Guide: snappyHexMesh, OpenFOAM, 2012, URL: https://www.openfoam.com/documentation/guides/latest/doc/guide-meshing-snappyhexmesh.html.

[204] L. Cambier, S. Heib, S. Plot, The onera elsa CFD software: Input from research and feedback from industry, Mech. Ind. 14 (3) (2013) 159–174.

[205] D. Schwamborn, T. Gerhold, R. Heinrich, The DLR TAU-code: Recent applications in research and industry, in: European Conference on Computational Fluid Dynamics, Egmond aan Zee, The Netherlands, 2006.

[206] Ansys® CFX Release 18.1, ANSYS, Inc., 2018.

[207] C.A. Mader, J.R. Martins, J.J. Alonso, E.D. Van Weide, ADjoint: An approach for the rapid development of discrete adjoint solvers, AIAA J. 46 (4) (2008) 863–873.

[208] J. Kurzke, I. Halliwell, Propulsion and Power: An Exploration of Gas Turbine Performance Modeling, Springer International Publishing, 2018, p. 755.

[209] J. Lytle, G. Follen, C. Naiman, A. Evans, J. Veres, K. Owen, I. Lopez, Numerical Propulsion System Simulation (NPSS) 1999 Industry Review, Technical Report, NASA, Cleveland, Ohio, USA, 2000.

[210] D.-C. Mincu, T. Le Garrec, S. Péron, M. Terracol, Immersed boundary conditions for high order CAA solvers - Aeroacoustics installation effects assessment, in: 23rd AIAA/CEAS Aeroacoustics Conference, American Institute of Aeronautics and Astronautics, Denver, Colorado, USA, 2017, http://dx.doi.org/10.2514/6.2017-3504.

[211] S. Péron, T. Renaud, M. Terracol, C. Benoit, I. Mary, An immersed boundary method for preliminary design aerodynamic studies of complex configurations, in: 23rd AIAA Computational Fluid Dynamics Conference, American Institute of Aeronautics and Astronautics, Denver, Colorado, USA, 2017, http://dx.doi.org/10.2514/6.2017-3623.

[212] A. Seitz, F. Peter, J. Bijewitz, A. Habermann, Concept validation study for fuselage wake-filling propulsion integration, in: 31st Congress of International Council of the Aeronautical Sciences, Belo Horizonte, Brazil, 2018.

[213] A. Castillo Pardo, C.A. Hall, Effects of sideslip direction on a rear fuselage boundary layer ingesting fan, J. Turbomach. 144 (12) (2022).

[214] A.R. Kulkarni, G.L. Rocca, L.L.M. Veldhuis, G. Eitelberg, Sub-scale flight test model design: Developments, challenges and opportunities, Prog. Aerosp. Sci. 130 (2022).

[215] D.M. Bushnell, Scaling: Wind tunnel to flight, Annu. Rev. Fluid Mech. 38 (2006) 111–128.

[216] P.R. Spalart, Direct simulation of a turbulent boundary layer up to R_θ= 1410, J. Fluid Mech. 187 (1988) 61–98.

[217] A. Elsenaar, T.W. Binion, E. Stanewsky, Reynolds Number Effects in Transonic Flow, Technical Report, AGARD, 1988.

[218] A.B. Haines, Scale Effects on Aircraft and Weapon Aerodynamics, Technical Report, AGARD, 1994.

[219] A.B. Haines, Prediction of scale effects at transonic speeds: Current practice and a gaze into the future, Aeronaut. J. 104 (1039) (2000) 421–431.

[220] P. Lv, D. Ragni, T. Hartuc, L. Veldhuis, A.G. Rao, Experimental investigation of the flow mechanisms associated with a wake-ingesting propulsor, AIAA J. 55 (4) (2017) 1332–1342.

[221] L.L. Kob, J.J. Doherty, D.M. Birch, Experimental and Computational Investigation for In-Line Boundary Layer Ingestion, June, AIAA Aviation Forum, 2019, http://dx.doi.org/10.2514/6.2019-3037.

[222] C.P. Coutinho, A.J. Baptista, J. Dias Rodrigues, Reduced scale models based on similitude theory: A review up to 2015, Eng. Struct. 119 (2016) 81–94.

[223] M.M. Curtin, D.R. Bogue, D. Om, S.M.B. Rivers, O.C. Pendergraft, R.A. Wahls, Investigation of transonic Reynolds number scaling on a twin-engine transport, in: 40th AIAA Aerospace Sciences Meeting and Exhibit, American Institute of Aeronautics and Astronautics, Reno, Nevada, USA, 2002, http://dx.doi.org/10.2514/6.2002-420.

[224] W.G. Tomek, R.A. Wahls, L.R. Owens, A.B. Burner, S.S. Graves, J.M. Luckring, Investigation of aerodynamic scale effects for a generic fighter configuration in the national transonic facility, in: 41st AIAA Aerospace Sciences Meeting and Exhibit, American Institute of Aeronautics and Astronautics, Reno, Nevada, USA, 2003, http://dx.doi.org/10.2514/6.2003-751.

[225] J.J. Peterson, M. Mann, R. Sorrells, W. Sawyer, D. Fuller, Wind-Tunnel/Flight Correlation Study of Aerodynamic Characteristics of a Large Flexible Supersonic Cruise Airplane (XB-701) II - Extrapolation of Wind-Tunnel Data to Full-Scale Conditions, Technical Report, NASA, 1980.

[226] H. Arnaiz, J.J. Peterson, J. Daugherty, Wind-Tunnel/Flight Correlation Study of Aerodynamic Characteristics of a Large Flexible Supersonic Cruise Airplane (XB-701) III - A Comparison Between Characteristics Predicted from Wind-Tunnel Measurements and those Measured in Flight, Technical Report, NASA, 1980.

[227] B. Della Corte, M. van Sluis, A. Gangoli Rao, L.L.M. Veldhuis, L. Orsini, Experimental investigation of the flow past an axisymmetric body at low speed, in: 24th International Society for Air Breathing Engines Conference, Canberra, Australia, 2019.

[228] W.Z. Shen, R. Mikkelsen, J.N. Sørensen, C. Bak, Tip loss corrections for wind turbine computations, Wind Energy 8 (4) (2005) 457–475.

[229] C.E. Robinson, G.D. Smith, R.J. Matz, D. Smith, R.J. Matz, Evaluation of an ejector-powered engine simulator at transonic mach numbers, in: 15th AIAA/SAE/ASME Joint Propulsion Conference, American Institute of Aeronautics and Astronautics, Las Vegas, Nevada, USA, 1979, http://dx.doi.org/10.2514/6.1979-1165.

[230] Z. Rongping, W. Xunnian, J. Rongchao, Development in ejector nacelle simulation testing in low speed wind tunnel, ACTA Aerodyn. Sin. 34 (6) (2016) 756–761.

[231] SUBLIME Project, SUBLIME - The test, 2022, URL: http://sublime-cleansky.com/the-test/.

[232] K. Sabo, M. Drela, Benefits of boundary layer ingestion propulsion, in: 53rd AIAA Aerospace Sciences Meeting, American Institute of Aeronautics and Astronautics, Kissimmee, Florida, USA, 2015, http://dx.doi.org/10.2514/6.2015-1667.

[233] J.D. Wolter, D.J. Arend, S.M. Hirt, J.A. Gazzaniga, Development of a rotating rake array for boundary-layer-ingesting fan-stage measurements, in: 53rd AIAA/SAE/ASEE Joint Propulsion Conference, American Institute of Aeronautics and Astronautics, Atlanta, GA, USA, 2017, http://dx.doi.org/10.2514/6.2017-4636.

[234] E. Vardaki, N.P. Stokes, S.D. Fonov, J.W. Crafton, Pressure sensitive paint measurements at the ARA transonic wind tunnel, in: 27th AIAA Aerodynamic Measurement Technology and Ground Testing Conference, American Institute of Aeronautics and Astronautics, Chicago, Illinois, USA, 2010, http://dx.doi.org/10.2514/6.2010-4796.

[235] D.A. Roberts, N.P. Stokes, M.K. Quinn, J.H. Coppin, T.J. Birch, Evaluation of dynamic pressure-sensitive paint for improved analysis of cavity flows and CFD validation, in: 54th AIAA Aerospace Sciences Meeting, American Institute of Aeronautics and Astronautics, San Diego, California, USA, 2016, http://dx.doi.org/10.2514/6.2016-0311.

[236] M.R. Abdulwahab, Y.H. Ali, F.J. Habeeb, A.A. Borhana, A.M. Abdelrhman, S.M. Ali Al-Obaidi, A review in particle image velocimetry techniques (developments and applications), J. Adv. Res. Fluid Mech. Therm. Sci. 65 (2) (2020) 213–229.

[237] S. Crowder, C. Delker, E. Forrest, N. Martin, Monte Carlo methods for the propagation of uncertainties, in: Introduction to Statistics in Metrology, Springer, 2020, pp. 153–180, http://dx.doi.org/10.1007/978-3-030-53329-8_8.

[238] NASA Illustration, NASA armstrong hosts convergent aeronautics solutions showcase, 2018, URL: https://www.nasa.gov/centers/armstrong/features/CAS_showcase.html.

[239] J.J. Berton, W.J. Haller, A noise and emissions assessment of the N3-X transport, in: 52nd Aerospace Sciences Meeting, American Institute of Aeronautics and Astronautics, National Harbor, Maryland, USA, 2014, http://dx.doi.org/10.2514/6.2014-0594.

[240] S.A. Pandya, A. Huang, A. Espitia, A. Uranga, Computational assessment of the boundary layer ingesting nacelle design of the D8 aircraft, in: 52 Aerospace Sciences Meeting, American Institute of Aeronautics and Astronautics, National Harbor, Maryland, USA, 2014, http://dx.doi.org/10.2514/6.2014-0907.

[241] A. Isyanov, A. Lukovnikov, A. Mirzoyan, Development challenges of distributive propulsion systems for advanced aeroplanes, Aircr. Eng. Aerosp. Technol. J. 86 (6) (2014) 459–463.

[242] A. Mirzoyan, A. Isyanov, A.T. Isikveren, Comparative efficiency analysis of distributed propulsion systems for propulsive fuselage and hybrid wing body concepts in FP7 project "DisPURSAL", in: 30th Congress of the International Council of the Aeronautical Sciences, Daejon, Korea, 2016.

[243] A. Dowling, T. Hynes, Towards a silent aircraft, Aeronaut. J. 110 (1110) (2006) 487–494.

[244] C.A. Hall, D. Crichton, Engine and installation configurations for a silent aircraft, in: 17th International Society for Air Breathing Engines Conference, Munich, Germany, 2005.

[245] D. Crichton, E. de la Blanco Rosa, T.R. Law, J.I. Hileman, Design and operation for ultra low noise take-off, in: 45th AIAA Aerospace Sciences Meeting and Exhibit, American Institute of Aeronautics and Astronautics, Reno, Nevada, USA, 2007, http://dx.doi.org/10.2514/6.2007-456.

[246] R. Kirner, L. Raffaelli, A. Rolt, P. Laskaridis, G. Doulgeris, R. Singh, An assessment of distributed propulsion: Advanced propulsion system architectures for conventional aircraft configurations, Aerosp. Sci. Technol. 46 (2015) 42–50.

[247] R. Kirner, L. Raffaelli, A. Rolt, P. Laskaridis, G. Doulgeris, R. Singh, An assessment of distributed propulsion: Part B - Advanced propulsion system architectures for blended wing body aircraft configurations, Aerosp. Sci. Technol. 50 (2016) 212–219.

[248] P. Laskaridis, E. Valencia, R. Kirner, J.W. Tan, Assessment of distributed propulsion systems used with different aircraft configurations, in: 51st AIAA/SAE/ASEE Joint Propulsion Conference, American Institute of Aeronautics and Astronautics, Orlando, Florida, USA, 2015, http://dx.doi.org/10.2514/6.2015-4029.

[249] P. Giannakakis, C. Pornet, A. Turnbull, Turbo-electric propulsive fuselage aircraft BLI benefits: A design space exploration using an analytical method, Aeronaut. J. 124 (1280) (2020) 1523–1544.

[250] R.H. Jansen, M.L. Celestina, H.D. Kim, Electrical propulsive fuselage concept for transonic transport aircraft, in: 24th International Society for Air Breathing Engines Conference, Canberra, Australia, 2019.

[251] F. Troeltsch, J. Bijewitz, A. Seitz, Design trade studies for turbo-electric propulsive fuselage integration, in: 24th International Society for Air Breathing Engines Conference, Canberra, Australia, 2019.

[252] R. Burzaco, Las Alas de Perón - Aeronáutica Argentina 1945/1960, Da Vinci, 1995.

[253] D.P. Wells, B.L. Horvath, L.A. McCullers, The Flight Optimization System Weight Estimation Method, Technical Report, NASA, 2017.

[254] M.K. Bradley, C.K. Droney, Subsonic Ultra Green Aircraft Research: Phase I Final Report, Technical Report, NASA, 2011.

[255] M.K. Bradley, C.K. Droney, Subsonic Ultra Green Aircraft Research: Phase II Advanced Concept Development, Technical Report, NASA, 2012.

[256] M.K. Bradley, T.J. Allen, C.K. Droney, Subsonic Ultra Green Aircraft Research: Phase II - Volume II - Hybrid Electric Design Exploration, Technical Report, NASA, 2015.

[257] M.K. Bradley, T.J. Allen, C.K. Droney, Subsonic Ultra Green Aircraft Research: Phase II - Volume III - Truss Braced Wing Design Exploration, Technical Report, NASA, 2015.

[258] A. Yildirim, Robust Methods for Aeropropulsive Design Optimization (Ph.D. thesis), University of Michigan, 2021.

[259] Z. Goraj, B. Goliszek, M. Kowalski, A. Seitz, F. Peter, F. Meller, Strategy and implementation of a parametric CAD model for R2035 aircraft structure and external configuration, in: 31st Congress of the International Council of the Aeronautical Sciences, Belo Horizonte, Brazil, 2018.

[260] S. Stückl, J. Bijewitz, A. Seitz, A.T. Isikveren, J.-L. Godard, A. Mirzoyan, D1.2 – Report on the Technology Roadmap for 2035, Technical Report, 2015.

[261] S. Pirzadeh, Progress toward a user-oriented unstructured viscous grid generator, in: 34th AIAA Aerospace Sciences Meeting and Exhibit, Vol. 34, American Institute of Aeronautics and Astronautics, Reno, Nevada, USA, 1996, http://dx.doi.org/10.2514/6.1996-31.

[262] N.T. Frink, Assessment of an unstructured-grid method for predicting 3-D turbulent viscous flows, in: 34th Aerospace Sciences Meeting and Exhibit, American Institute of Aeronautics and Astronautics, Reno, Nevada, USA, 1996, http://dx.doi.org/10.2514/6.1996-292.

[263] R.L. Campbell, Efficient viscous design of realistic aircraft configurations, in: 29th AIAA Fluid Dynamics Conference, American Institute of Aeronautics and Astronautics, Albuquerque, New Mexico, USA, 1998, http://dx.doi.org/10.2514/6.1998-2539.

[264] E.M. Greitzer, P.A. Bonnefoy, E. de la Rosa Blanco, C.S. Dorbian, M. Drela, D.K. Hall, R.J. Hansman, J.I. Hileman, R.H. Liebeck, J. Lovegren, P. Mody, J.A. Pertuze, S. Sato, Z.S. Spakovszky, C.S. Tan, J.S. Hollman, J.E. Duda, N. Fitzgerald, J. Houghton, J.L. Kerrebrock, G.F. Kiwada, D. Kordonowy, J.C. Parrish, J. Tylko, E.A. Wen, W. Lord, N+3 Aircraft Concept Designs and Trade Studies, Final Report Vol. 1, Technical Report, 1, 2010.

[265] I.A. Clark, R.H. Thomas, Y. Guo, Aircraft system noise assessment of the NASA D8 subsonic transport concept, in: AIAA/CEAS Aeroacoustics Conference, American Institute of Aeronautics and Astronautics, Atlanta, Georgia, USA, 2018, http://dx.doi.org/10.2514/6.2018-3124.

[266] I.A. Clark, R.H. Thomas, Y. Guo, Aircraft system noise of the NASA D8 subsonic transport concept, J. Aircr. 58 (5) (2021) 1106–1120.

[267] I.A. Clark, R.H. Thomas, Y. Guo, Far term noise reduction roadmap for the NASA D8 and single-aisle tube-and-wing aircraft concepts, in: AIAA/CEAS Aeroacoustics Conference, American Institute of Aeronautics and Astronautics, Delft, The Netherlands, 2019, http://dx.doi.org/10.2514/6.2019-2427.

[268] E. de la Rosa Blanco, C.A. Hall, D. Crichton, Challenges in the silent aircraft engine design, in: 45th AIAA Aerospace Sciences Meeting and Exhibit, American Institute of Aeronautics and Astronautics, Reno, Nevada, USA, 2007, http://dx.doi.org/10.2514/6.2007-454.

[269] J.I. Hileman, T.G. Reynolds, E. de la Blanco Rosa, T.R. Law, S. Thomas, Development of approach procedures for silent aircraft, in: 45th AIAA Aerospace Sciences Meeting and Exhibit, American Institute of Aeronautics and Astronautics, Reno, Nevada, USA, 2007, http://dx.doi.org/10.2514/6.2007-451.

[270] M.-S. Liou, H. Kim, M.-F. Liou, Challenges and Progress in Aerodynamic Design of Hybrid Wingbody Aircraft With Embedded Engines, Technical Report, NASA, 2016.

[271] H.D. Kim, J.J. Berton, S.M. Jones, Low noise cruise efficient short take-off and landing transport vehicle study, in: 6th AIAA Aviation Technology, Integration and Operations Conference, ATIO, American Institute of Aeronautics and Astronautics, Wichita, Kansas, USA, 2006, http://dx.doi.org/10.2514/6.2006-7738.

[272] J.R. Stone, E.A. Krejsa, J.A. Berton, H.D. Kim, Initial noise assessment of an embedded-wing-propulsion concept vehicle, in: 42nd AIAA/ASME/SAE/ASEE Joint Propulsion Conference and Exhibit, American Institute of Aeronautics and Astronautics, Sacramento, California, USA, 2006, http://dx.doi.org/10.2514/6.2006-4979.

[273] R.T. Kawai, Acoustic Prediction Methodology and Test Validation for an Efficient Low-Noise Hybrid Wing Body Subsonic Transport, Technical Report, The Boeing Company, 2011.

[274] M.A. Bakhle, T.S.R. Reddy, G.P. Herrick, A. Shabbir, R.V. Florea, Aeromechanics analysis of a boundary layer ingesting fan, in: 48th AIAA/ASME/SAE/ASEE Joint Propulsion Conference and Exhibit, American Institute of Aeronautics and Astronautics, Atlanta, Georgia, USA, 2012, http://dx.doi.org/10.2514/6.2012-3995.

[275] D. Friedman, Aerodynamic Prediction Methodology and Test Validation for an Efficient Low-Noise Hybrid Wing Body Subsonic Transport, Technical Report, The Boeing Company, 2010.

[276] R. Kirner, An Investigation into the Benefits of Distributed Propulsion on Advanced Aircraft Configurations (Ph.D. thesis), Cranfield University, 2013.

[277] H. Smith, P. Laskaridis, Airframe integration for LH2 fuelled distributed propulsion systems, in: 22nd International Society for Air Breathing Engines Conference, Phoenix, Arizona, USA, 2015.

[278] H. Smith, Airframe integration for an LH2 hybrid-electric propulsion system, Aircr. Eng. Aerosp. Technol. J. 86 (6) (2014) 562–567.

[279] P. Rompokos, A. Rolt, D. Nalianda, A.T. Isikveren, C. Senné, T. Grönstedt, H. Abedi, Synergistic technology combinations for future commercial aircraft using liquid hydrogen, J. Eng. Gas Turbines Power 143 (7) (2021).

[280] D. Chandel, J.D. Reband, D.K. Hall, T. Balachandran, J. Xiao, K.S. Haran, E.M. Greitzer, Conceptual design of distributed electrified boundary layer ingesting propulsors for the CHEETA aircraft concept, in: AIAA Propulsion and Energy 2021 Forum, American Institute of Aeronautics and Astronautics, Virtual Event, 2021, http://dx.doi.org/10.2514/6.2021-3287.

[281] J. Hermetz, M. Ridel, C. Döll, Distributed electric propulsion for small business aircraft: a concept-plane for key-technologies investigations, in: 30th Congress of the International Council of the Aeronautical Sciences, Daejon, Korea, 2016.

[282] A. Sgueglia, P. Schmollgruber, N. Bartoli, O. Atinault, E. Benard, J. Morlier, Exploration and sizing of a large passenger aircraft with distributed ducted electric fans, in: AIAA Aerospace Sciences Meeting, American Institute of Aeronautics and Astronautics, Kissimmee, Florida, USA, 2018, http://dx.doi.org/10.2514/6.2018-1745.

[283] R.A. Danis, J.L. Freeman, B.T. Schiltgen, Applications for hybrid electric power and energy supplementation on a single-aisle airliner, in: AIAA Propulsion and Energy 2018 Forum, American Institute of Aeronautics and Astronautics, Cincinnati, Ohio, USA, 2018, http://dx.doi.org/10.2514/6.2018-5021.

[284] G.T. Klunk, J.L. Freeman, B.T. Schiltgen, Vertical tail area reduction for aircraft with spanwise distributed electric propulsion, in: AIAA Propulsion and Energy 2018 Forum, American Institute of Aeronautics and Astronautics, Cincinnati, Ohio, USA, 2018, http://dx.doi.org/10.2514/6.2018-5022.

[285] M.A. Aguirre, R. Bracco, F. Milanese, M. Meroniuc, Design of an external six-component wind tunnel balance with floating frame, Int. J. Aerodyn. 7 (2) (2021) 105–126.



https://dspace.org/

Advancements and prospects of boundary layer ingestion propulsion concepts

Moirou, Nicolas G. M.; Sanders, Drewan S.; Laskaridis, Panagiotis

2023-04-01
Elsevier
https://doi.org/10.1016/j.paerosci.2023.100897
Moirou NGM, Sanders DS, Laskaridis P. (2023) Advancements and prospects of boundary layer ingestion propulsion concepts. Progress in Aerospace Sciences, Volume 138, April 2023, Article number 100897

Downloaded from a DSpace repository. https://dspace.org/